Supporting Information

Crystallographic Evidence of a Trinuclear (salen)Manganese(IV/III/IV)-*μ*-Oxo Formed during Catalytic C(sp^3)–H Oxidation Reactions

Bhaswati Paul,[a] Kusalvin Dabare,[a,b] Joshua D. Bocarsly,[a,b] and L. Reginald Mills[a]*

[a]*Department of Chemistry, University of Houston, Houston, TX 77204-5003*

[b]*Texas Center for Superconductivity, University of Houston, Houston, TX 77204*

*lrmills2@uh.edu

Table of Contents

I. General Experimental Considerations

Unless otherwise mentioned, all air- and moisture-sensitive manipulations were performed on an N_2- or Ar-filled Schlenk line using standard Schlenk techniques. Glassware for air- and moisture-sensitive manipulations was oven-dried (100 ºC) prior to use. DHA-d_4 was prepared from natural abundance 9,10-dihydroanthracene (DHA) in the presence of DMSO-d_6 and D_2O.[1] All other chemicals and solvents were purchased from commercial suppliers and used as received.

^1H, and ^{19}F spectra were recorded on JEOL ECX-400P and JEOL ECA-500 spectrometers. All ^1H NMR chemical shifts are reported in ppm relative to $SiMe_4$, which was referenced using known chemical shifts of residual solvent. ^1H NMR data for paramagnetic compounds are reported as follows: chemical shift, peak width at half height (Hz), integration. FTIR spectra were recorded on a Thermo Nicolet Summit Pro with Everest ZnSe ATR; peaks are reported in wavenumbers (cm^{-1}). UV-Vis spectroscopy data were recorded in a Cary 50 Bio UV-Vis spectrophotometer. GC-MS data were obtained on a Shimadzu GCMS-QP2020NX SE. Continuous wave EPR spectra were recorded on an X-band Bruker EMXnano spectrometer. Solution magnetic moments were determined using Evans's method (n = 3; error = std. dev.).[2] Cyclic voltammograms were recorded using a BASi EC Epsilon electrochemical workstation employing a glassy carbon working electrode, Pt-wire counter electrode, and Ag/Ag^+ reference electrode. All scans were performed using the open circuit potential as starting point; potentials are reported versus Cp_2Fe/Fc^+ internal standard. CHN combustion analyses were performed by Robertson Microlit Laboratories (Ledgewood, NJ).

Data collection for single crystal X-ray structure analysis was performed in a Bruker D8 Venture diffractometer, equipped with INCOATEC IμS 3.0 microfocus sealed tube X-ray source for Cu K_α (λ = 1.5406 Å) and Mo $K\alpha$ (λ = 0.71073 Å) radiation, and Photon-III_C7 detector. The crystals were analyzed under a polarized optical microscope and mounted using MiTeGen loops. Cell parameters were estimated from a pre-experiment run and complete data sets collected at 100K (± 0.2 K). Diffraction data were collected and processed with the Bruker Apex III software suite incorporated with multiple tools such as Cell Now and RLATT for determining the unit cell, SAINT-plus for data reduction, and SADABS for absorption correction. The structure solutions were performed with SHELXT, and the full-matrix least-squares refinements were performed with the SHELXL suite of programs incorporated in the Apex version 6 suite and Olex2. All non-hydrogen atoms were anisotropically refined.[3,4,5]

Magnetic measurements for the two samples were performed using a Quantum Design Magnetic Property Measurement System (MPMS3) with DC measurements. Approximately 6 - 10 mg of the dried powder samples were loaded into propylene carbonate (PC) capsules and were secured in plastic straw type sample holders. Zero-field-cooled (ZFC) and field-cooled (FC) temperature-dependent magnetization (moment vs. temperature) measurements were carried out between 1.8 K and 300 K under an applied magnetic field of 200 Oe, using a temperature sweep rate of 3 K/min. Magnetic susceptibility data were corrected for diamagnetism of the ligands using Pascal's constants. This data was fit to a model Hamiltonian using the PHI program.[6] Field-dependent magnetization (moment vs. field) measurements were collected at 300 K and 1.8 K at stabilized fields between 5 T and -5T, with a field sweep rate of 700 Oe/s between points.

Photo-electrons were collected on a Physical Electronics Model 5700 XPS instrument. These were produced via a monochromatic Al-ka x-ray source (1486.6 eV) operated at 350 W. The analyzed area, collection solid cone and take off angle were set at 800 mm, 5^{o} and 45^{o} respectively. Analyzer pass energy is 23.5 eV. All spectra were acquired once vacuum of $5x10^{-9}$ torr or better was attained. Data processing was carried out using the Multipak^{TM} software package. A Shirley background subtraction routine had been applied throughout. The samples were pressed into In foil prior to analysis since this provided effective support and enhanced charge neutralization. Concentrations of all elements present were derived from the survey spectra following background removal. Chemical state information was extracted from the recorded binding energy values.

II. Synthesis and Characterization of Manganese Compounds

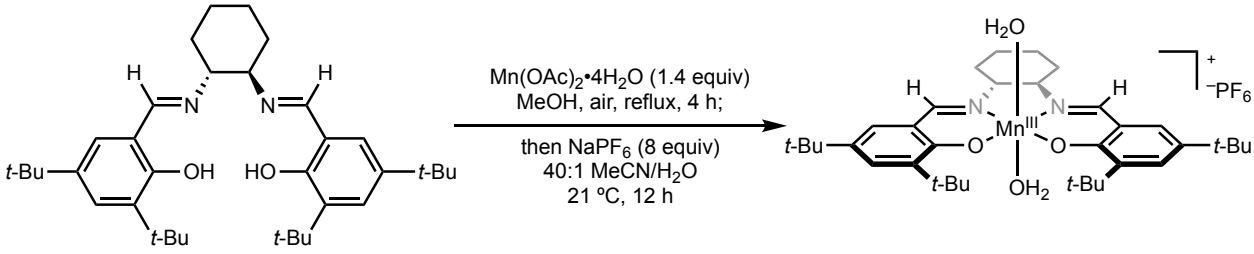

(salen)Mn(H_2O)$_2$(PF_6) (1a): The compound was made following a literature procedure.[7,8] On benchtop, a 250 mL round-bottom flask with a stir bar was sequentially charged with salen ligand (3.8 g, 7.0 mmol, 1.0 equiv), $Mn(OAc)_2$•$4H_2O$ (2.5 g, 10 mmol, 1.4 equiv), and MeOH (100 mL, 0.070 M). The flask was fitted with a condenser, and the mixture was stirred at reflux under air for 4 h. After 4 h, the dark brown solution was filtered over a pad of Celite, and the Celite cake was washed with additional MeOH (10 mL). The filtrates were combined and concentrated under vacuum, forming a brown solid concentrate. In a 250-mL round-bottom flask, the brown solid was dissolved in MeCN (80 mL). In a separate vial, $NaPF_6$ (9.0 g, 56 mmol) was dissolved in HPLC-grade water (2.0 mL), then was added to the brown MeCN solution. The solution was stirred at ambient temperature (21 ºC) for 12 h, then was filtered over Celite. The Celite cake was washed with additional MeCN (10 mL) and filtered, and the filtrates were combined and concentrated under reduced pressure. The solid residue was dissolved in CH_2Cl_2 (30 mL), and the organic solution was washed with H_2O (1×10 mL) and concentrated under reduced pressure, yielding the desired compound as a dark brown solid (3.1 g, 4.0 mmol, 57% yield). The analytical data were consistent with those reported in the literature.[8] **^{1}H NMR** (400 MHz, CD_3CN, 298 K): δ 20.89 (br s, $\Delta\nu_{1/2}$ = 800 Hz) 18.31 (br s, $\Delta\nu_{1/2}$ = 592 Hz), 7.46 (br s, $\Delta\nu_{1/2}$ = 796 Hz), 2.14 (br s, $\Delta\nu_{1/2}$ = 40 Hz), 1.98 (br s, $\Delta\nu_{1/2}$ = 3 Hz), −30.90 (br s, $\Delta\nu_{1/2}$ = 760 Hz), −32.62 (br s, $\Delta\nu_{1/2}$ = 544 Hz). **IR** (neat, 21 ºC): 3652, 2953, 1618, 1541, 1248, 1172, 1032, 841, 738, 639, 576, 487 cm^{-1}. **Solution μ_{eff}** (CD_3CN, 298 K): 4.9(1) μ_B.

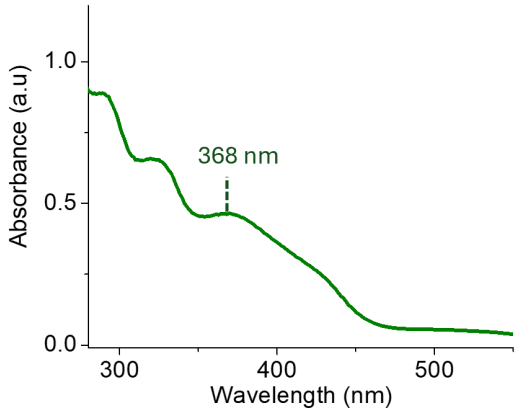

Figure S1. UV-Vis absorption spectrum of (salen)Mn(H_2O)$_2$(PF_6) (**1a**) (MeCN).

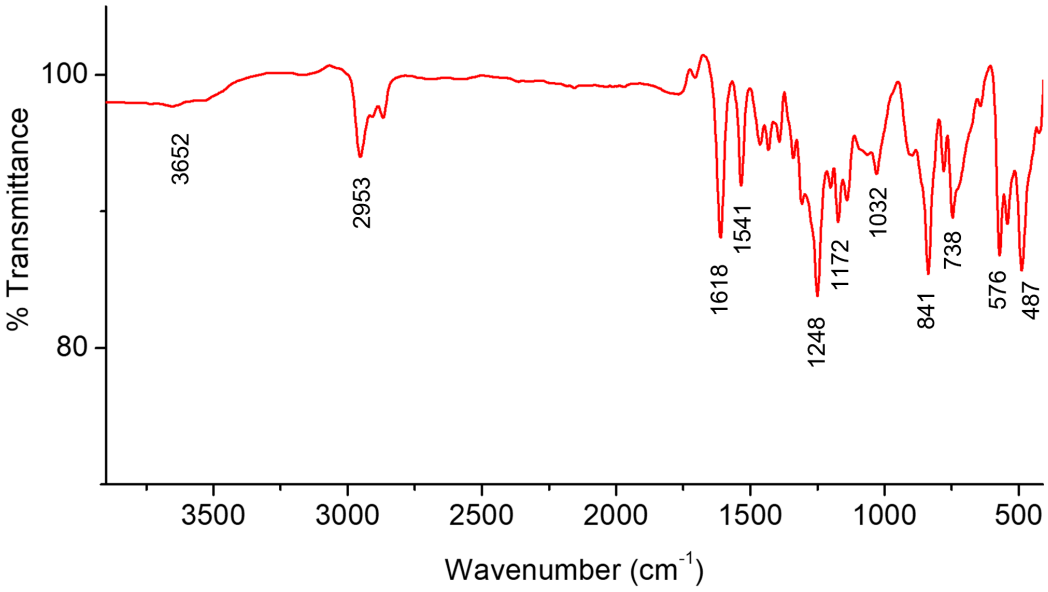

Figure S2. FTIR spectrum of (salen)Mn(H_2O)$_2$(PF_6) (**1a**) (neat, 21 ºC).

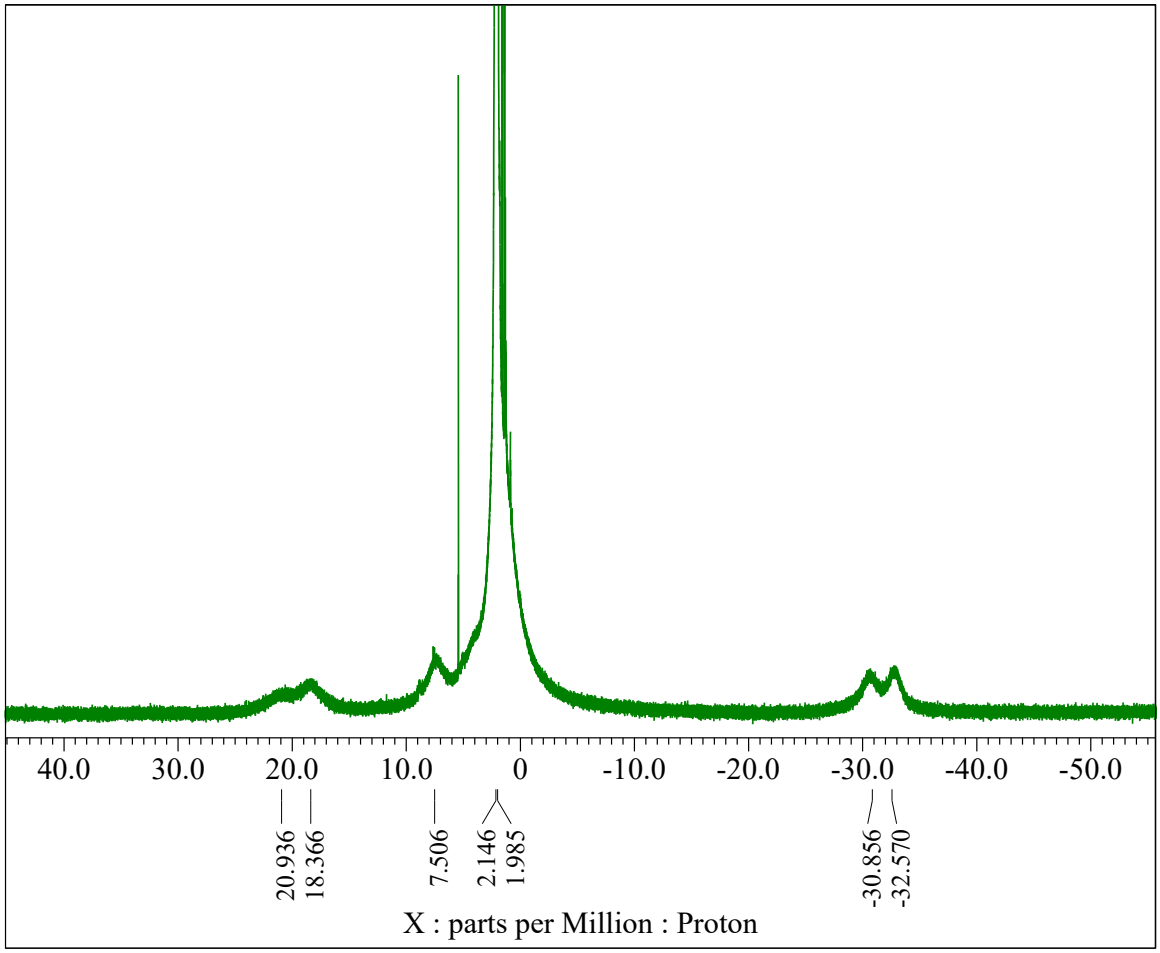

Figure S3. ^{1}H NMR spectrum (CD_3CN; 400 MHz) of (salen)Mn(H_2O)$_2$(PF_6) (**1a**).

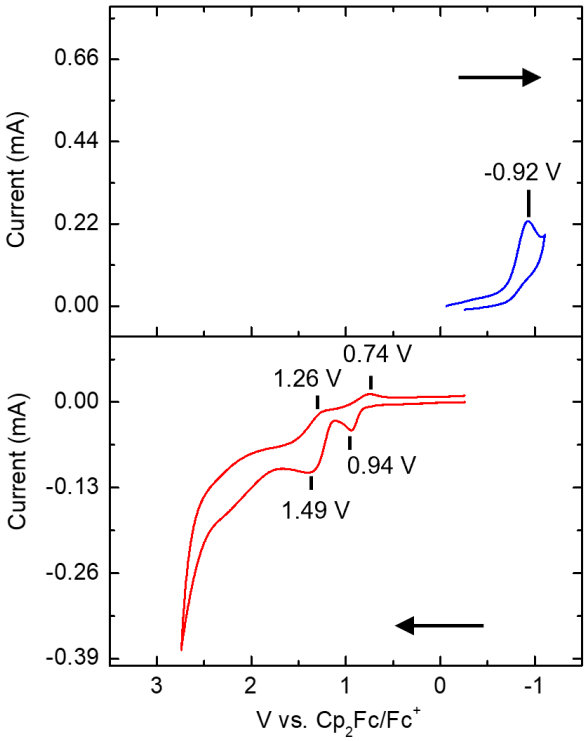

Figure S4. CV of (salen)Mn(H_2O)$_2$(PF_6) **1a** (3 mM) in MeCN at 23 ºC. Electrolyte = 0.2 M $TBAPF_6$, scan rate = 100 mV/s internal standard = $Fc^{0/+}$.

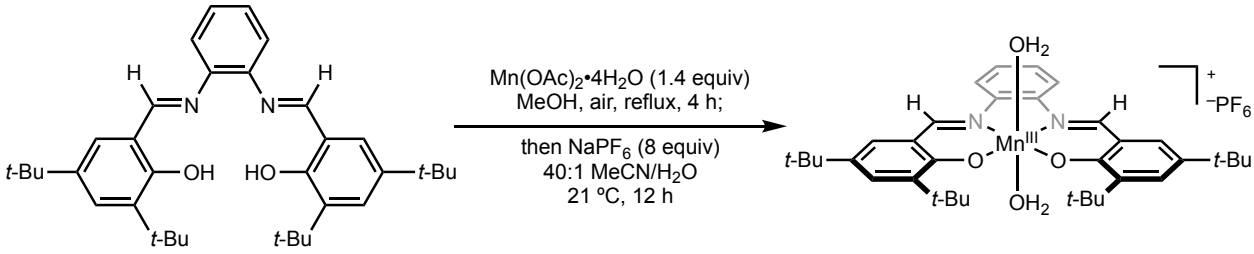

(salophen)Mn(H_2O)$_2$(PF_6) (1b): On benchtop, a 250-mL round-bottom flask was sequentially charged with salophen ligand (3.8 g, 7.0 mmol, 1.0 equiv), $Mn(OAc)_2$•$4H_2O$ (2.5 g, 10 mmol, 1.4 equiv), and MeOH (120 mL, 0.058 M). The flask was fitted with a reflux condenser, and the mixture was stirred under air at reflux for 4 h. After 4 h, the dark brown solution was cooled to ambient temperature and filtered over Celite. The Celite cake was washed with additional MeOH (8.0 mL) and filtered, and the filtrates were combined and concentrated. The resulting brown concentrate was dissolved in MeCN (100 mL) in a 250 mL round-bottom flask. In a separate vial, $NaPF_6$ (9.0 g, 56 mmol) was dissolved in HPLC-grade water (2.0 mL), which was added to the brown MeCN solution. The solution was stirred at ambient temperature (21 ºC) for 12 h, then was filtered over Celite. The Celite cake was washed with additional MeCN (10 mL), and the filtrates were combined and concentrated under reduced pressure. The solid residue was dissolved in CH_2Cl_2 (40 mL), and the organic solution was washed with H_2O (1×10 mL) and concentrated under reduced pressure, yielding the desired compound as a dark brown solid (4.1 g, 5.3 mmol, 76%). The analytical data were consistent with those reported in the literature.[9] **^{1}H NMR** (400 MHz, CD_3CN, 298 K): δ 25.49 (br s, $\Delta\nu_{1/2}$ = 904 Hz), 17.18 (br s, $\Delta\nu_{1/2}$ = 1780 Hz), 2.08 (obsc br s), 1.87 (obsc br s), −20.23 (br s, $\Delta\nu_{1/2}$ = 220 Hz), −33.16 (br s, $\Delta\nu_{1/2}$ = 320 Hz). **IR** (neat, 21 ºC): 3414, 2869, 1595, 1533, 1463, 1357, 1255, 843, 745, 554 cm^{-1}. **Solution μ_{eff}** (CD_3CN, 298 K): 4.5(1) μ_B.

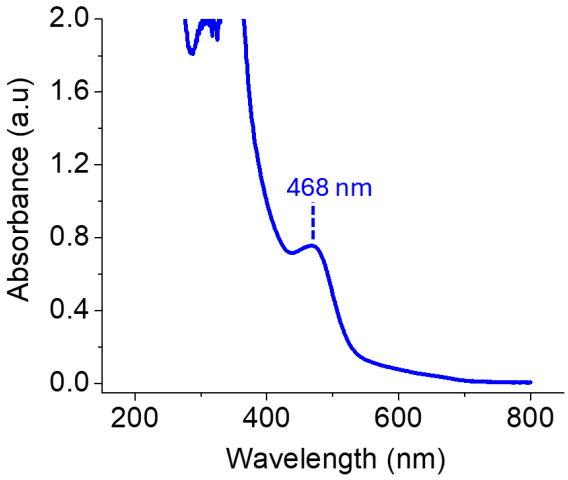

Figure S5. UV-Vis absorption spectrum of (salophen)Mn(H_2O)$_2$(PF_6) (**1b**) in MeCN (21 ºC).

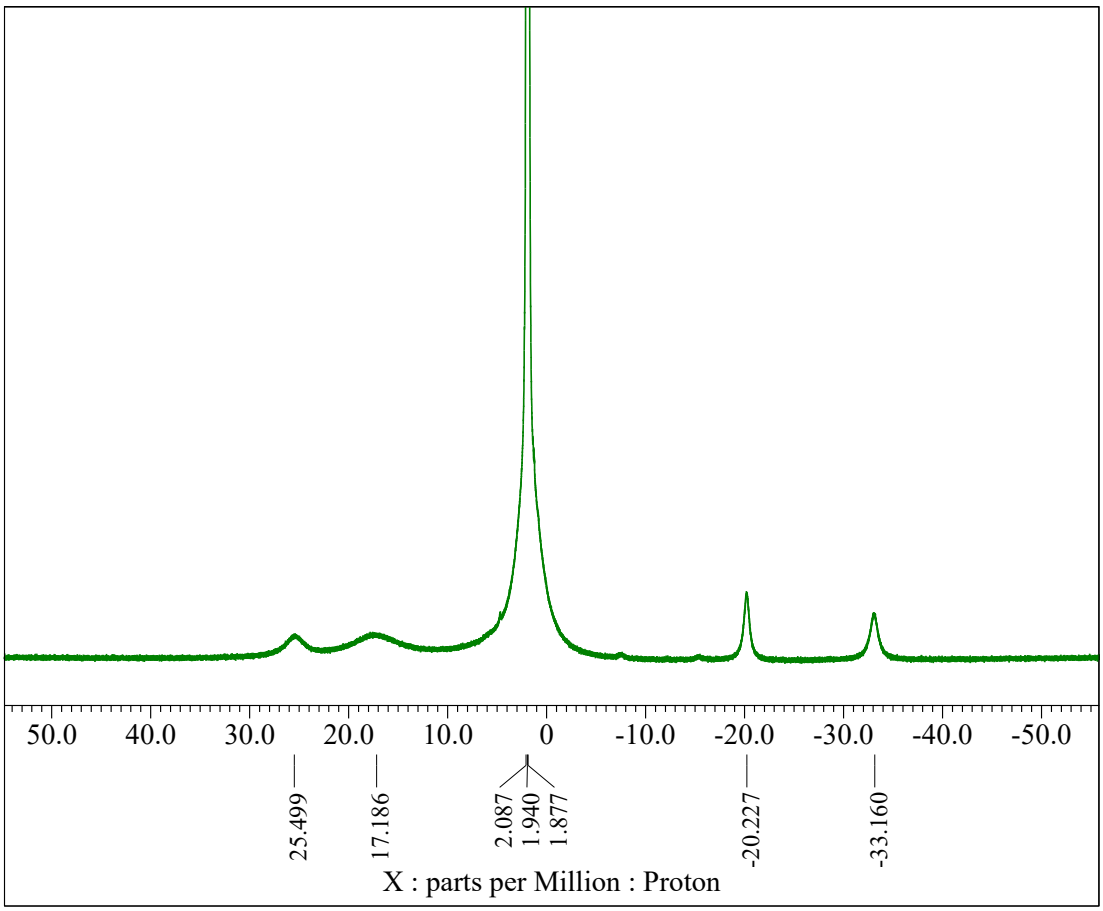

Figure S6. ^{1}H NMR spectrum (CD_3CN; 400 MHz) of (salophen)Mn(H_2O)$_2$(PF_6) (**1b**).

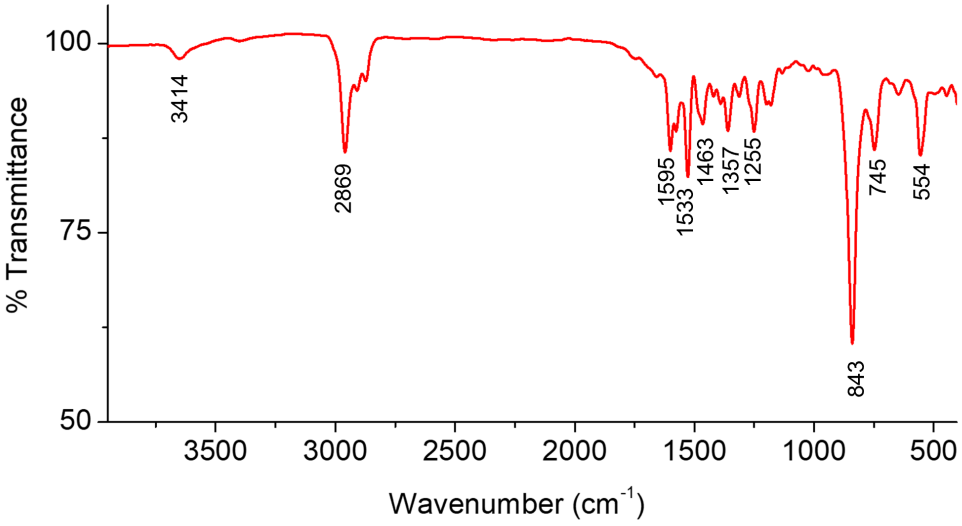

Figure S7. FTIR spectrum of (salophen)Mn(H_2O)$_2$(PF_6) (**1b**).

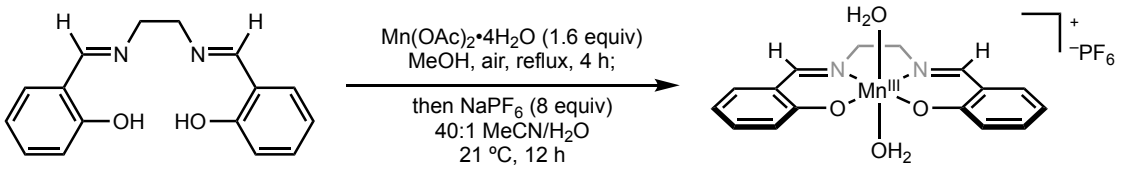

(*N,N′*-Bis(salicylidene)ethylenediamine)Mn(H_2O)$_2$(PF_6):[8] On benchtop, a 50-mL round-bottom flask with a stir bar was sequentially charged with *N,N′*-bis(salicylidene)ethylenediamine (0.25 g, 0.90 mmol, 1.0 equiv), $Mn(OAc)_2$•$4H_2O$ (0.35 g, 1.42 mmol, 1.6 equiv), and MeOH (20 mL, 0.045 M). The flask was fitted with a reflux condenser, and the solution was stirred open to air at reflux for 4 h. After 4 h, the dark brown solution was cooled to ambient temperature and was filtered over Celite. The Celite cake was additionally washed with MeOH (10 mL) and filtered, and the filtrates were combined and concentrated under vacuum. The brown concentrate was dissolved in MeCN (50 mL) in a 100-mL round-bottom flask, and an aqueous solution of $NaPF_6$ (1.2 g, 7.2 mmol in 1.0 mL of H_2O) was added to the solution. The solution was stirred at ambient temperature (21 ºC) for 12 h, then was filtered over Celite. The Celite cake was washed with additional MeCN (2.0 mL) and filtered, and the organic filtrates were combined. The collected MeCN solution was reduced under vacuum to a volume of 30 mL, then was allowed to stand at ambient temperature (21 ºC) in a fumehood over three days while slow evaporation occurred, resulting in formation of red-brown block crystals. The crystalline precipitate was collected in a funnel, which was sequentially washed with MeCN (1×1.0 mL) and with hexanes (5×1.0 mL), and dried under vacuum, yielding the desired compound as a dark brown solid (0.20 g, 0.44 mmol, 51%). Single crystals suitable for X-ray diffraction were obtained by slow evaporation recrystallization at 21 ºC over 24 hours (MeCN). The analytical data were identical to those in the literature.[8] **^{1}H NMR** (400 MHz, CD_3CN, 298 K): δ 40.42 (br s, $\Delta\nu_{1/2}$ = 2205 Hz), 8.61 (br s, $\Delta\nu_{1/2}$ = 704 Hz), 1.23 (obsc br s), −7.03 (br s, $\Delta\nu_{1/2}$ = 960 Hz), −27.15 (br s, $\Delta\nu_{1/2}$ = 370 Hz), −29.59 (br s, $\Delta\nu_{1/2}$ = 370 Hz), −128.11 (br s, $\Delta\nu_{1/2}$ = 6600 Hz).

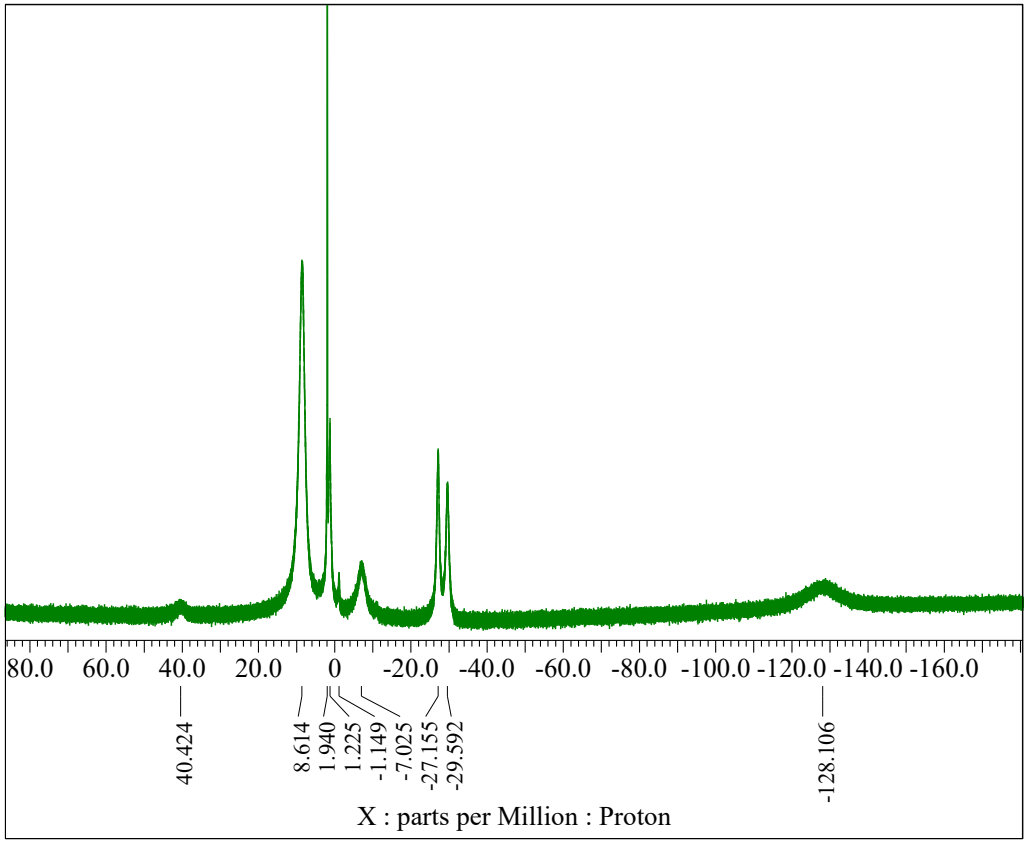

Figure S8. ^{1}H NMR spectrum (CD_3CN; 400 MHz) of (*N,N′*-bis(salicylidene)ethylenediamine)Mn(H_2O)$_2$(PF_6).

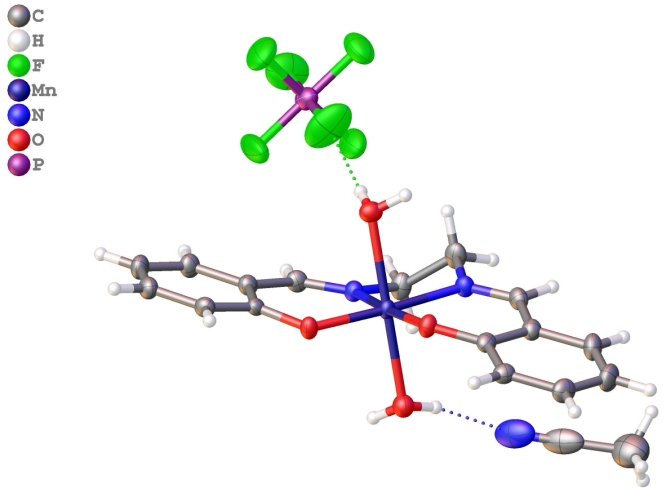

Figure S9. Solid-state molecular structure of (*N,N′*-bis(salicylidene)ethylenediamine)Mn(H_2O)$_2$(PF_6)•MeCN determined by X-ray diffraction.

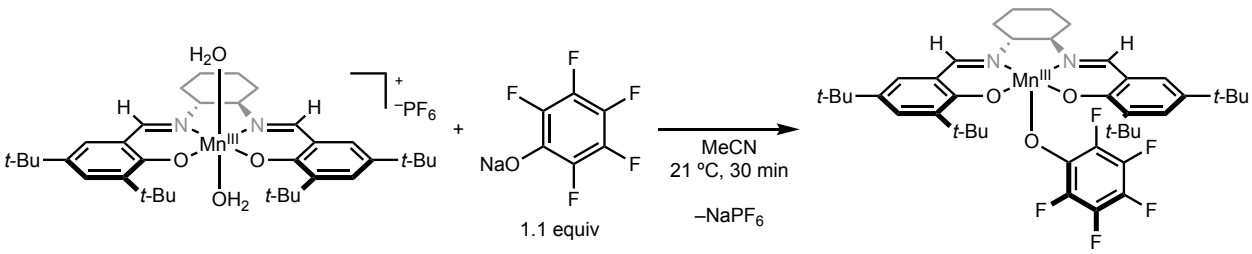

(salen)Mn(OC$_6$F$_5$) (2): In a 25 mL round bottom flask, (salen)Mn(H$_2$O)$_2$(PF$_6$) (**1a**) (100 mg; 0.13 mmol, 1.0 equiv) was dissolved in 8 mL of acetonitrile. To the solution was added sodium 2,3,4,5,6-pentafluorophenolate (30 mg, 0.14 mmol, 1.1 equiv), and the mixture was stirred at ambient temperature (21 ºC) for 30 min, forming a dark brown precipitate. The brown precipitate was collected in a funnel fitted with filter paper, and the precipitate was sequentially washed with MeCN (1×1 mL) and with hexane (1×5 mL). The precipitate was dissolved in benzene (2.0 mL), filtered over Celite, and concentrated, yielding a dark brown crystalline solid (93 mg, 0.119 mmol, 92%). Single crystals suitable for X-ray diffraction were obtained by slow diffusion recrystallization (acetone, 21 ºC). **^{1}H NMR** (400 MHz, benzene-d_6, 298 K): δ 17.52 (br s, $\Delta\nu_{1/2}$ = 800 Hz), 13.19 (br s, $\Delta\nu_{1/2}$ = 640 Hz), 10.12 (br s, $\Delta\nu_{1/2}$ = 900 Hz), −22.82 (br s, $\Delta\nu_{1/2}$ = 428 Hz), −26.21 (br s, $\Delta\nu_{1/2}$ = 868 Hz). **^{19}F NMR** (400 MHz, benzene-d_6, 298 K): δ −161.6 (br s, $\Delta\nu_{1/2}$ = 688 Hz). **IR** (neat, 21 ºC): 2948, 2872, 1612, 1498, 1307, 1256, 1167, 989, 836, 747, 645, 556, 466 cm^{-1}. **Solution μ_{eff}** (Benzene-d_6, 298 K): 4.8(1) μ_B. **Anal. calcd.** for C$_{42}$H$_{52}$F$_5$MnN$_2$O$_3$•(CH$_3$)$_2$CO: C, 64.28; H, 6.95; N, 3.33; found: C, 64.12; H, 6.69; N, 3.32.

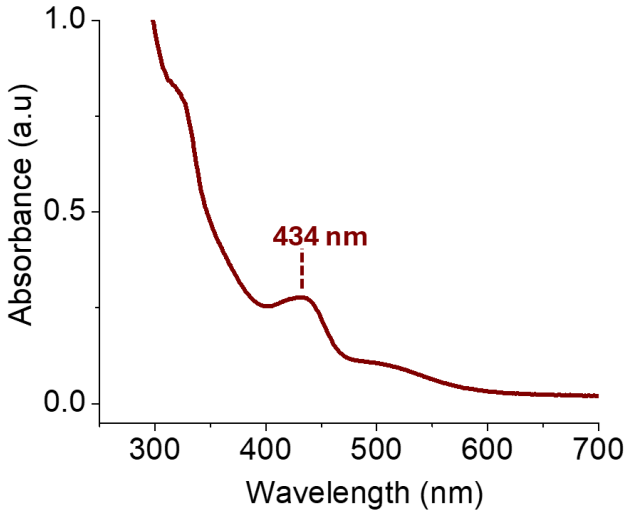

Figure S10. UV-Vis spectrum of (salen)MnOC$_6$F$_5$ (CH$_2$Cl$_2$).

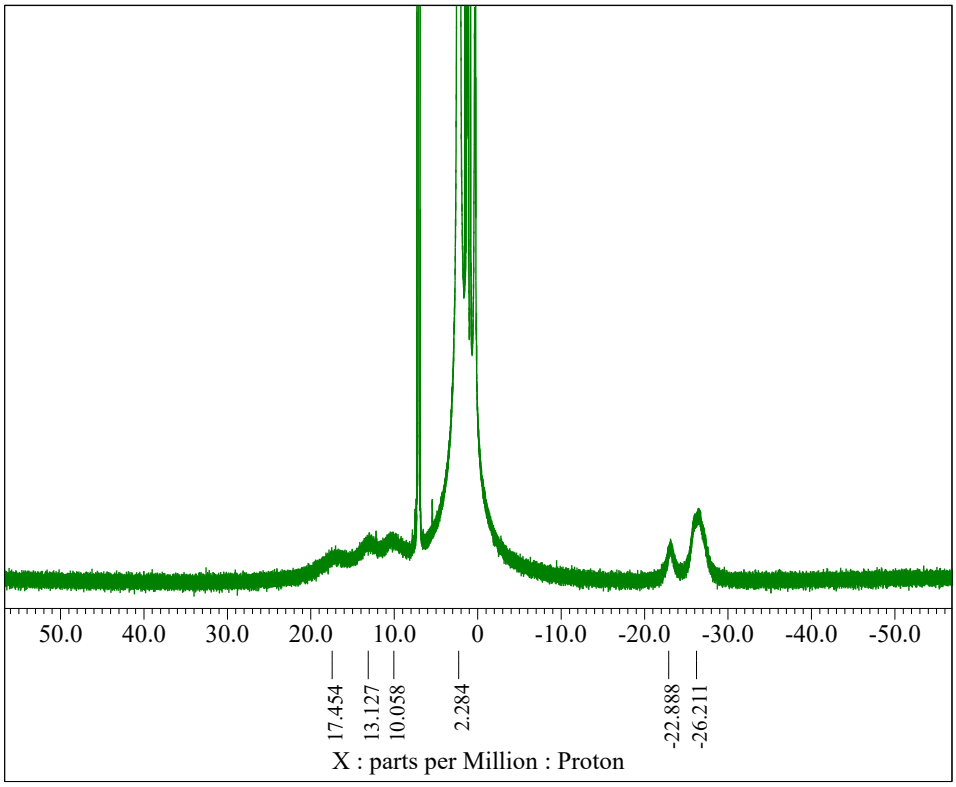

Figure S11. ^{1}H NMR spectrum (400 MHz; benzene-d_6) of (salen)MnOC$_6$F$_5$.

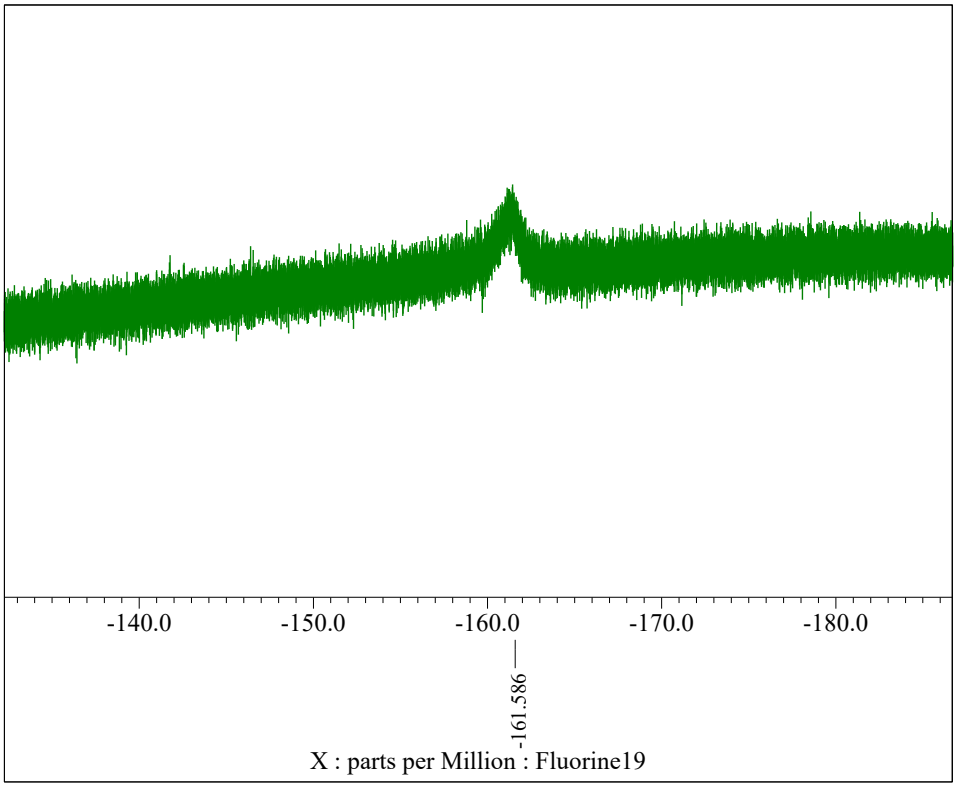

Figure S12. ^{19}F NMR spectrum (400 MHz, benzene-d_6) of (salen)MnOC$_6$F$_5$.

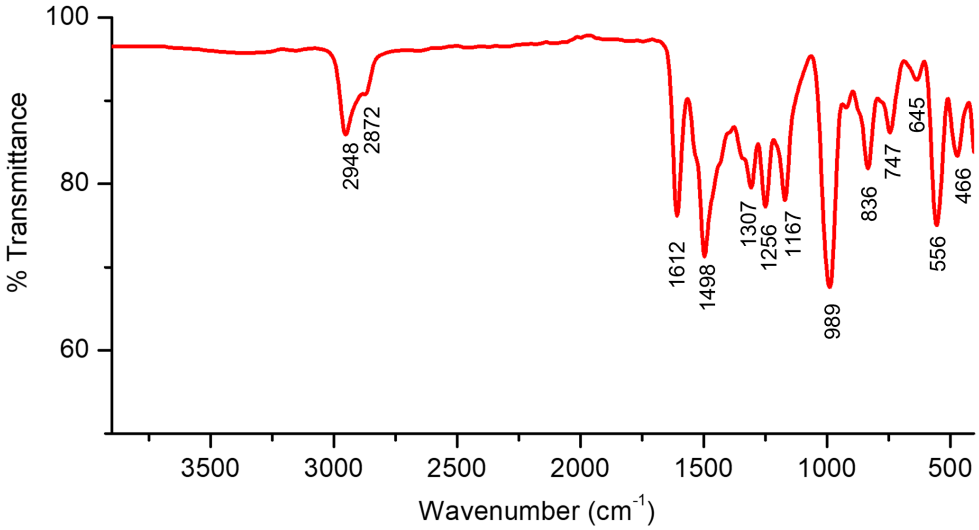

Figure S13. FTIR spectrum of [(salophen)$Mn^{III}(OC_6F_5)$] (**2**).

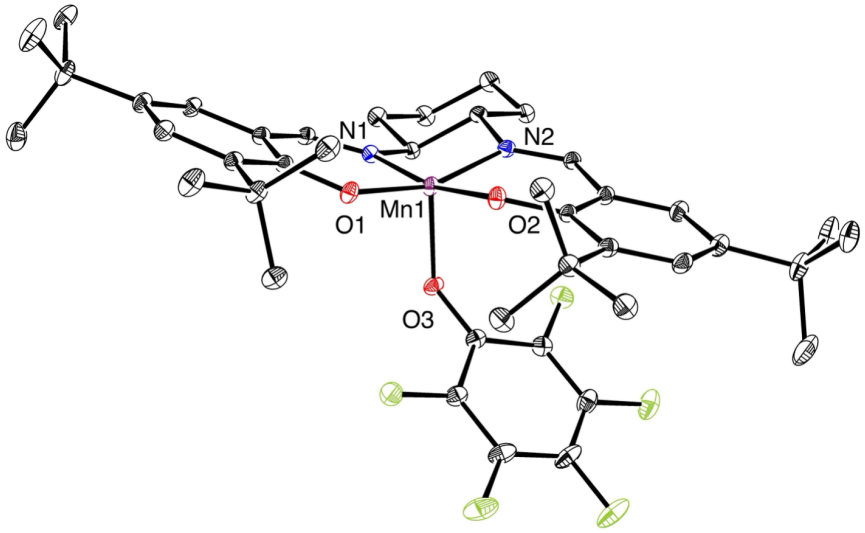

Figure S14. Solid-state molecular structure of (salen)$MnOC_6F_5$ determined by X-ray diffraction (30% probability ellipsoids).

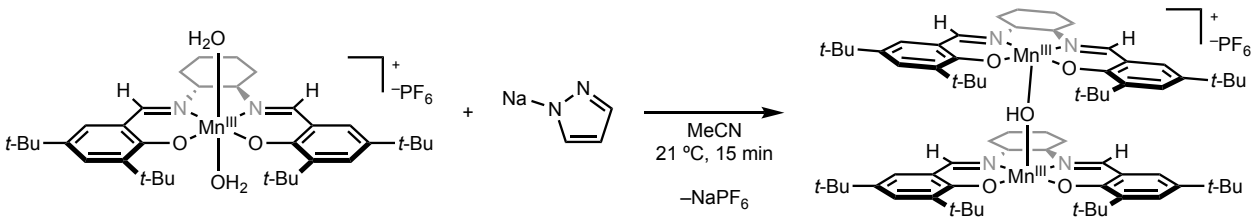

(salen)Mn–μ-OH–(salen)Mn(PF_6) (3a): In a 50-mL round-bottom flask with a stir bar, (salen)Mn(H_2O)$_2$(PF_6) (0.15 g, 0.20 mmol, 1.0 equiv) was dissolved in MeCN (20 mL, 0.010 M). While stirring the solution, sodium pyrazolate (NaPz) (18 mg, 0.20 mmol, 1.0 equiv) was added, and the solution was stirred at ambient temperature for 15 min, over which period the solution changed color from dark brown to red-brown. After 15 min, the solution was concentrated. The red-brown solid was dissolved in benzene (8.0 mL), filtered over Celite, and concentrated. The concentrate was washed with pentane and dried under vacuum, yielding the desired compound as a red-brown solid (0.13 g, 0.95 mmol, 95%). The spectroscopic data were consistent with those reported in the literature for complex (salen)Mn–μ-OH–(salen)Mn(OTf).[10] **^{1}H NMR** (400 MHz, benzene-d_6, 298 K): 10.11 (obsc s), 2.16 (br s), 1.97 (br s), −7.68 (br s, $\Delta\nu_{1/2}$ = 360 Hz), −10.30 (br s, $\Delta\nu_{1/2}$ = 392 Hz), −14.30 (br s, $\Delta\nu_{1/2}$ = 429 Hz). **IR** (neat, 21 ºC): 3433, 2949, 2860, 1613, 1537, 1346, 1308, 1257, 1177, 1113, 1037, 833, 757, 680, 553, 490 cm^{-1}. **Solution μ_{eff}** (benzene-d_6, 298 K): 5.4(1) μ_B. **Anal. calcd.** for $C_{72}H_{105}F_6Mn_2N_4O_5P$: C, 63.52; H, 7.77; N, 4.12; found: C, 62.94; H, 7.52; N, 4.56.

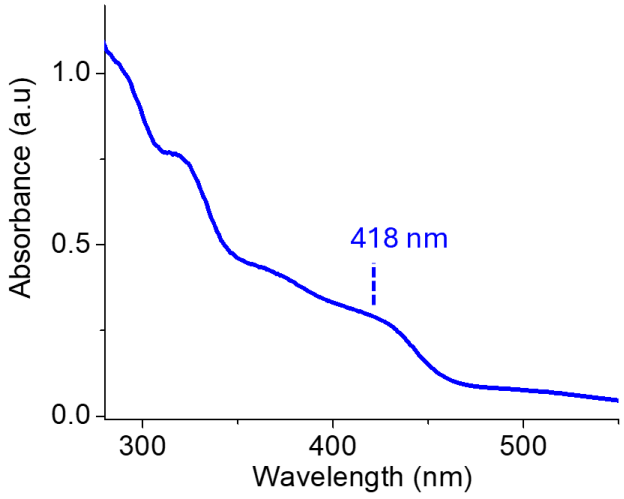

Figure S15. UV-Vis spectrum of (salen)Mn–μ-OH–(salen)Mn(PF_6) (**3a**) in acetonitrile.

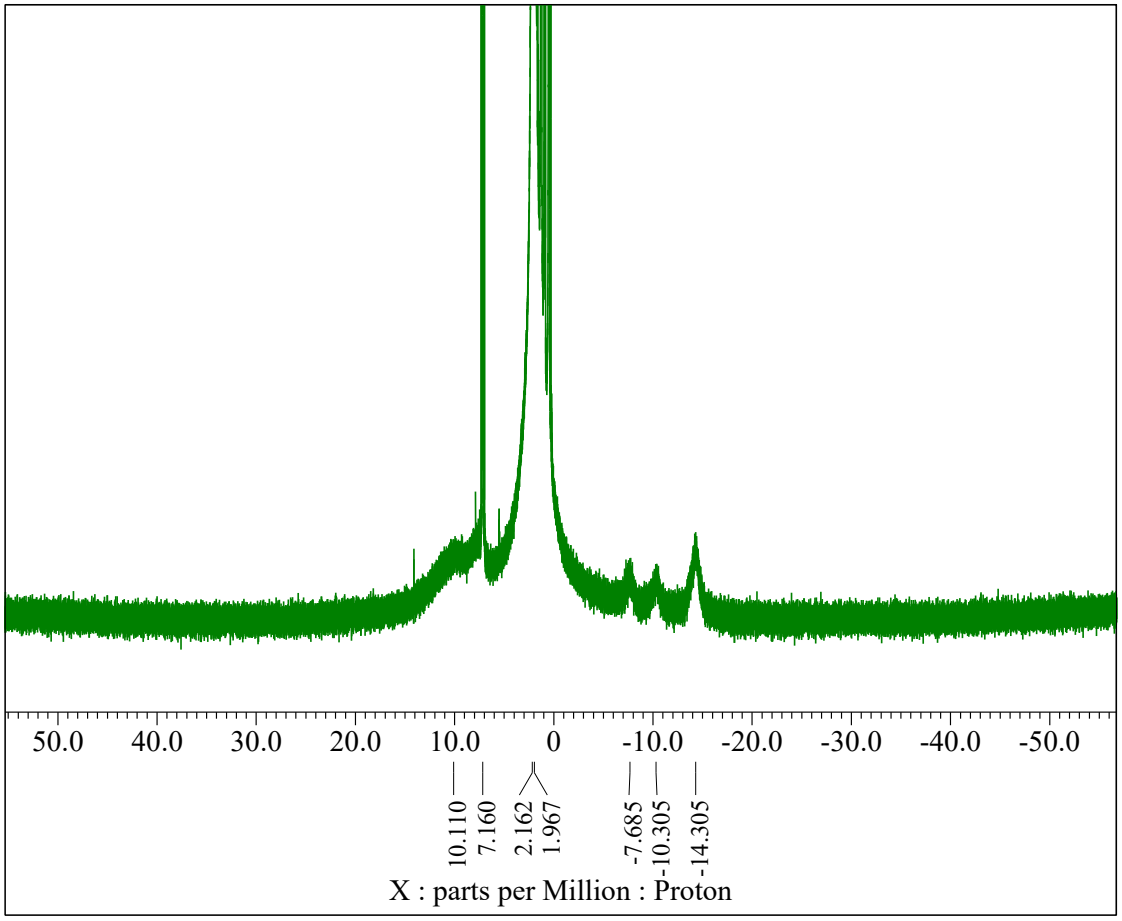

Figure S16. ^{1}H NMR (400 MHz; Benzene-d_6) of (salen)Mn–μ-OH–(salen)Mn(PF_6) (**3a**).

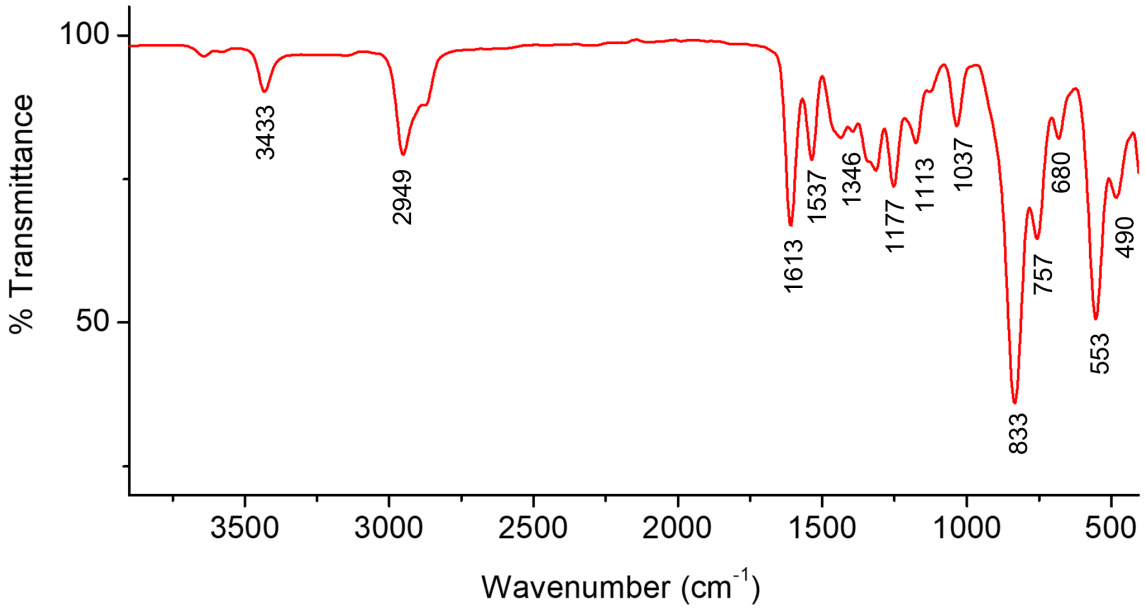

Figure S17. FTIR spectrum of (salen)Mn–μ-OH–(salen)Mn(PF_6) (**3a**).

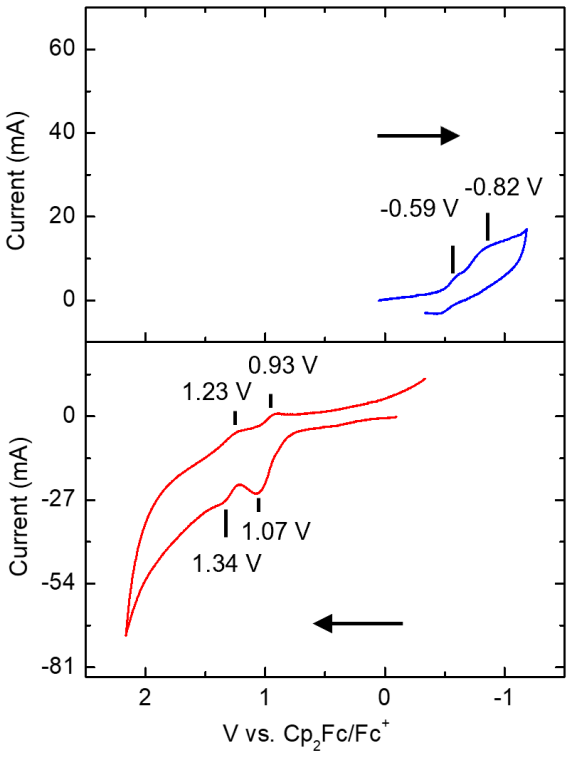

Figure S18. CV of (salen)Mn–μ-OH–(salen)Mn(PF_6) (**3a**) (3 mM) in MeCN at 23 ºC. Scan rate = 100 mV/s, electrolyte = 0.2 M $TBAPF_6$, internal standard = $Fc^{0/+}$.

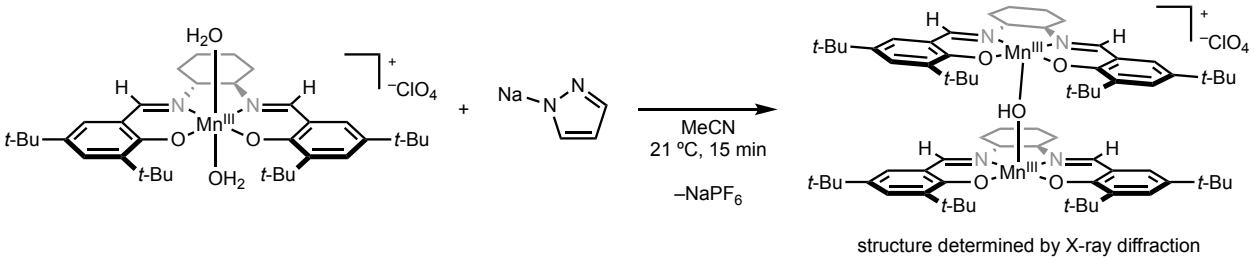

Perchlorate cation (salen)Mn–μ-OH–(salen)Mn(ClO_4) (for determination of the molecular structure): To a 1-dram vial with a stir bar were sequentially added (salen)Mn(H_2O)$_2$(ClO_4)[8] (10 mg, 0.014 mmol, 1.0 equiv), MeCN (1.0 mL), and NaPz (1.2 mg, 0.013 mmol, 0.093 equiv), and the solution was stirred at ambient temperature (21 ºC) for 15 min. After 15 min, the solution was concentrated. The brown residue was redissolved in benzene (1 mL) and it was filtered through Celite. Then the solution was allowed to stand at ambient temperature for 24 h, resulting in formation of reddish-brown crystals suitable for X-ray diffraction.

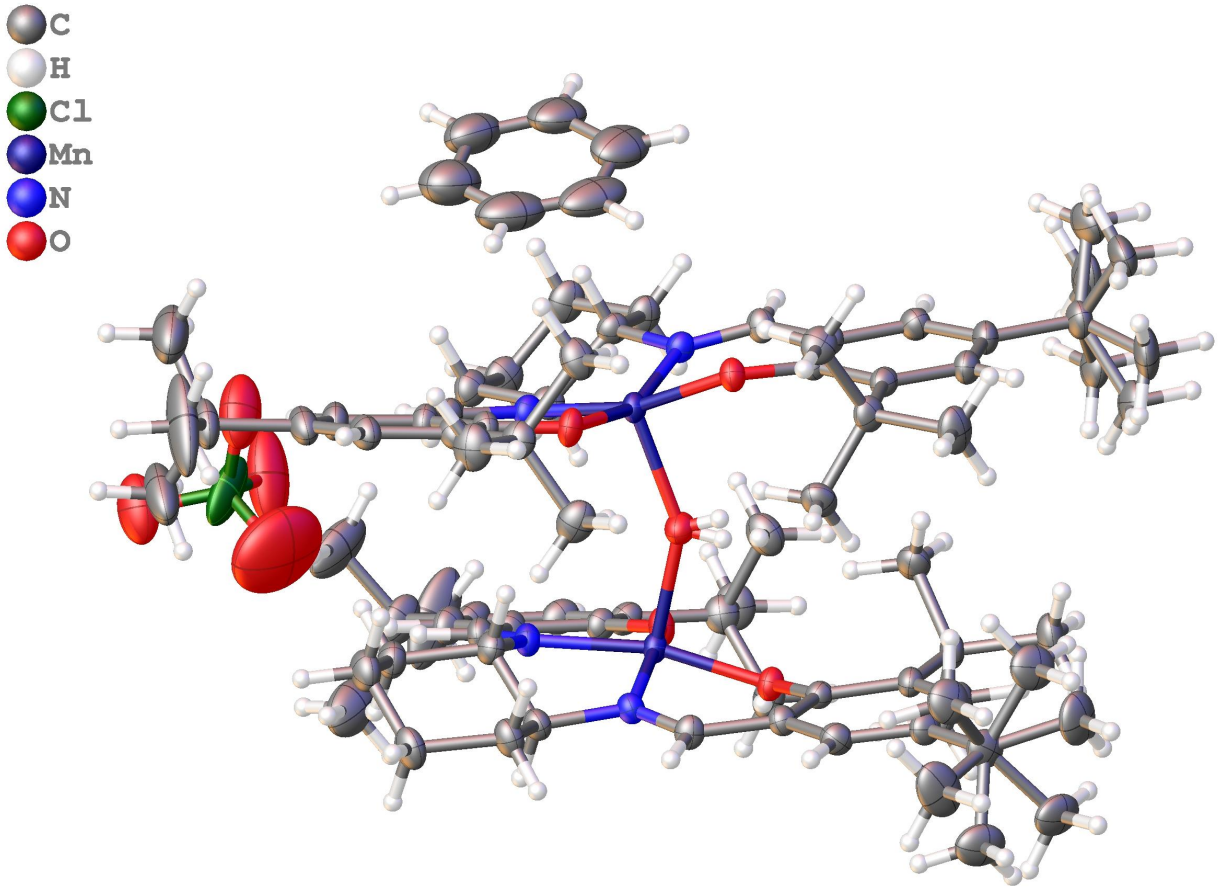

Figure S19. Solid-state molecular structure of (salen)Mn–μ-OH–(salen)Mn(ClO_4) determined by X-ray diffraction.

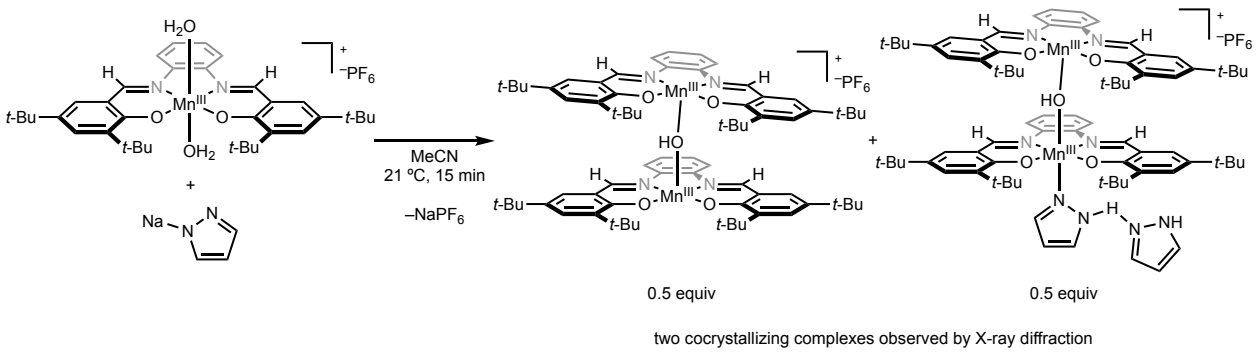

(salophen)Mn–μ-OH–(salophen)Mn(L)(PF_6) (3b) (L = MeCN, PzH): To a 50 mL round-bottom flask with a stir bar were sequentially added (salophen)Mn(H_2O)$_2$(PF_6) (0.15 g mg; 0.20 mmol, 1.0 equiv), MeCN (20 mL), and sodium pyrazolate (NaPz) (18 mg, 0.20 mmol, 1.0 equiv), and the mixture was stirred at ambient temperature (21 ºC) for 15 min, after which time the color changed from dark brown to red-brown. After 15 min, the solution was filtered over Celite and concentrated. The concentrate was dissolved in benzene (8.0 mL), and the benzene solution was filtered over Celite and concentrated. The resulting concentrate was washed with pentane (×1) and dried under vacuum, yielding the desired product as a red-brown solid, which represented a 1:1 mixture of (salophen)Mn–μ-OH–(salophen)Mn(PF_6) and (salophen)Mn–μ-OH–(salophen)Mn(PzH)$_2$(PF_6) (0.14 g, 0.097 mmol, 97%). Single crystals suitable for X-ray diffraction were obtained by slow evaporation recrystallization (MeCN, 21 ºC). **^{1}H NMR** (400 MHz, benzene-d_6, 298 K): δ 16.46 (br s, $\Delta\nu_{1/2}$ = 1280 Hz), 11.40 (br s, $\Delta\nu_{1/2}$ = 430 Hz), 8.26 (obsc br s), 7.54 (obsc br s), 1.97 (obsc br s), 1.89 (obsc br s), −3.45 (br s, $\Delta\nu_{1/2}$ = 220 Hz), −9.59 (br s, $\Delta\nu_{1/2}$ = 540 Hz), −15.89 (br s, $\Delta\nu_{1/2}$ = 720 Hz), −21.71 (br s, $\Delta\nu_{1/2}$ = 580 Hz). **IR** (neat, 21 ºC): 3435, 2952, 2875, 1577, 1526, 1462, 1398, 1357, 1319, 1256, 1179, 1039, 829, 753, 549 cm^{-1}. **Solution μ_{eff}** (benzene-d_6, 298 K): 5.2(1) μ_B. **Anal. calcd.** for $C_{72}H_{93}F_6Mn_2N_4O_5P$•(MeCN)$_2$•pyrazole•$H_2O$: C, 62.52; H, 6.97; N, 7.38; found: C, 61.76; H, 6.48; N, 7.37.

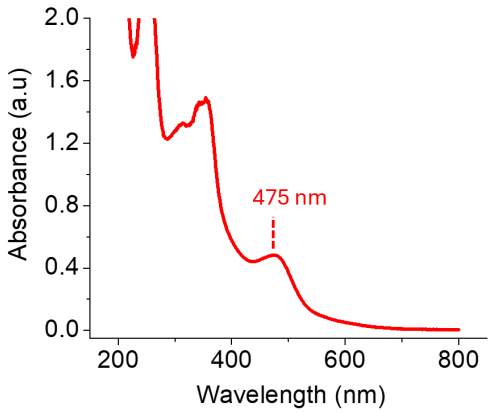

Figure S20. UV-Vis spectrum of (salophen)Mn–μ-OH–(salophen)Mn(PF_6) (**3b**) in acetonitrile.

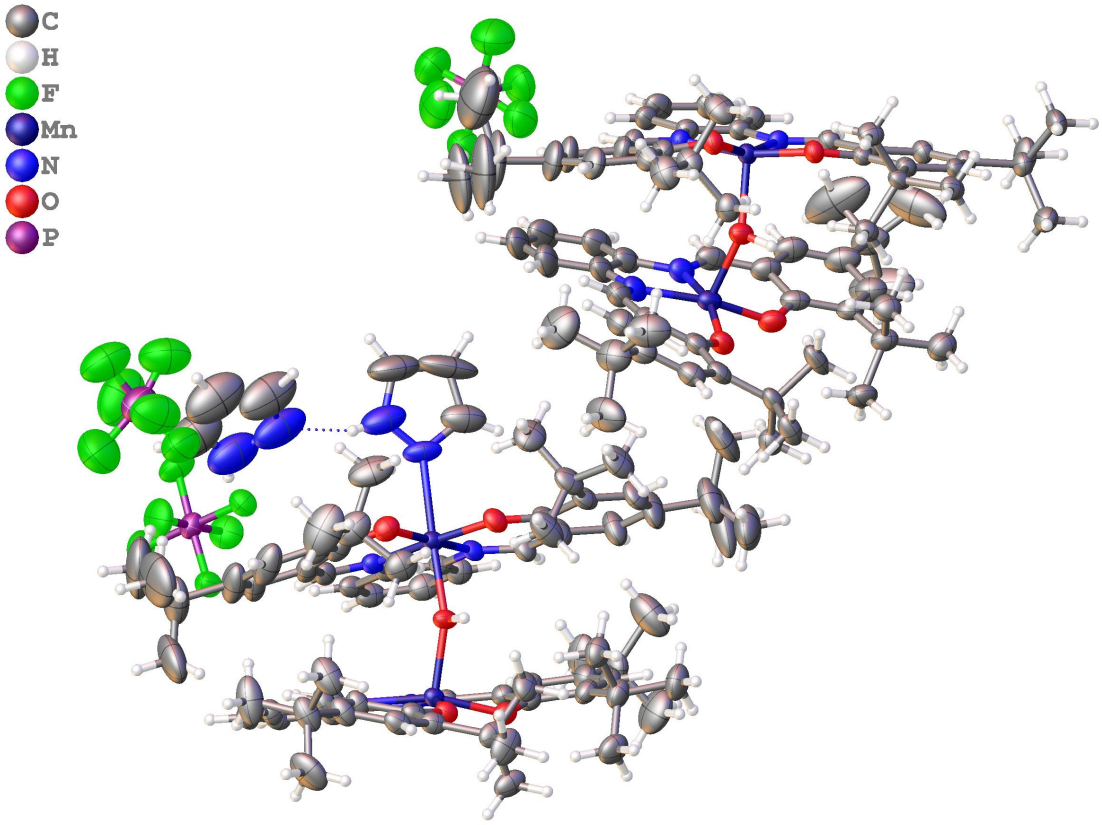

Figure S21. Solid state molecular structures of (salophen)Mn–μ-OH–(salophen)Mn(PF_6) (**3b**) and (salophen)Mn–μ-OH–(salophen)Mn($PzH)_2(PF_6$) (**3b**-PzH_2) determined by X-ray diffraction.

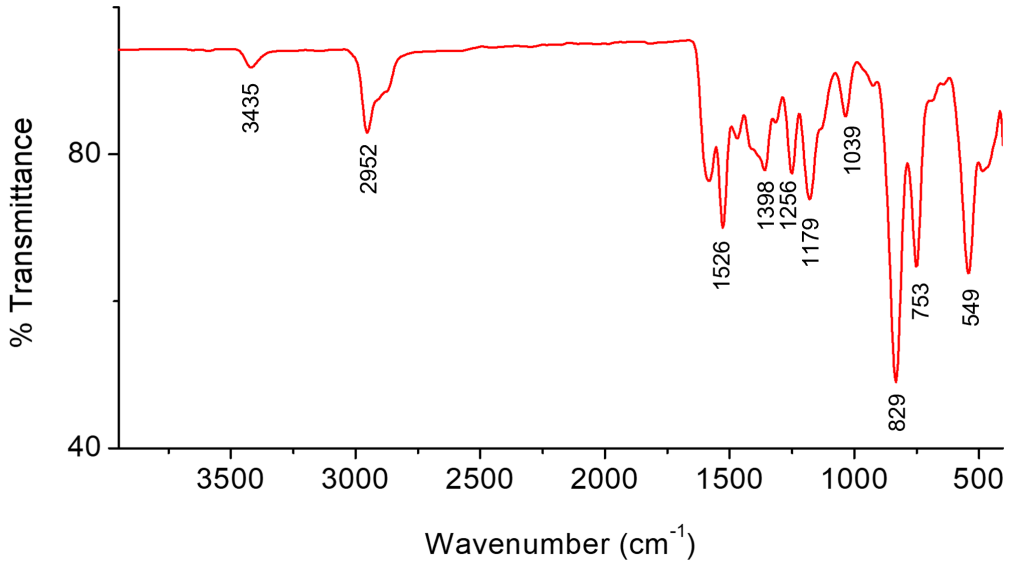

Figure S22. FTIR spectrum of (salophen)Mn–μ-OH–(salophen)Mn(PF_6) (**3b**).

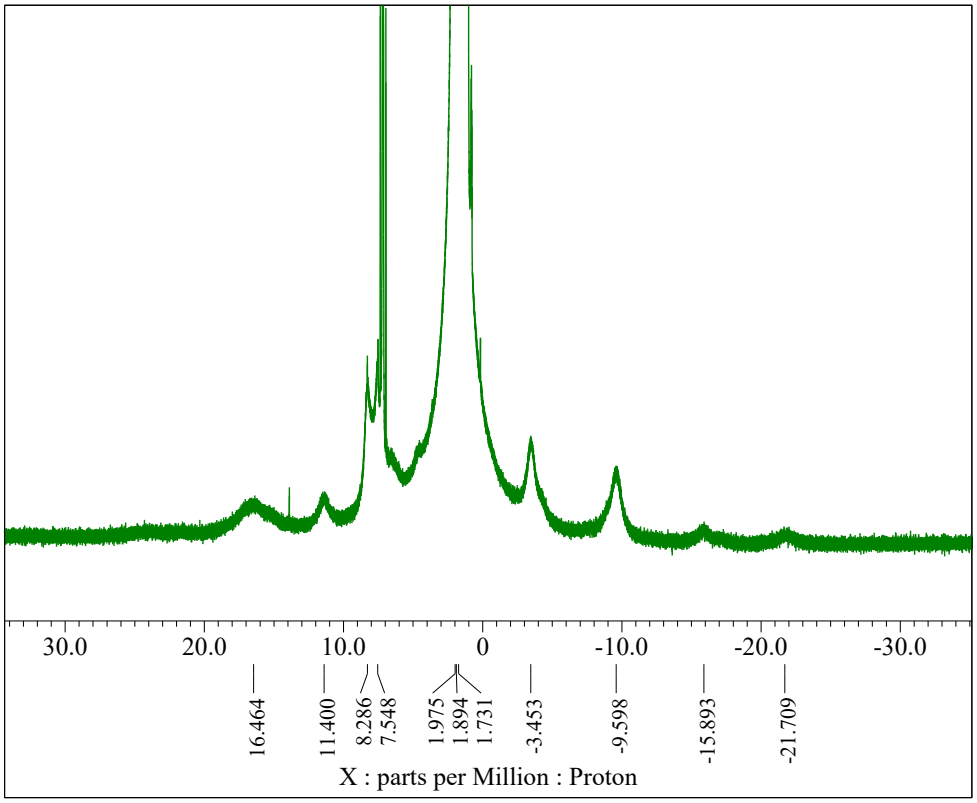

Figure S23. ^{1}H NMR (400 MHz; Benzene-d_6) of (salophen)Mn–μ-OH–(salophen)Mn(PF_6) (**3b**).

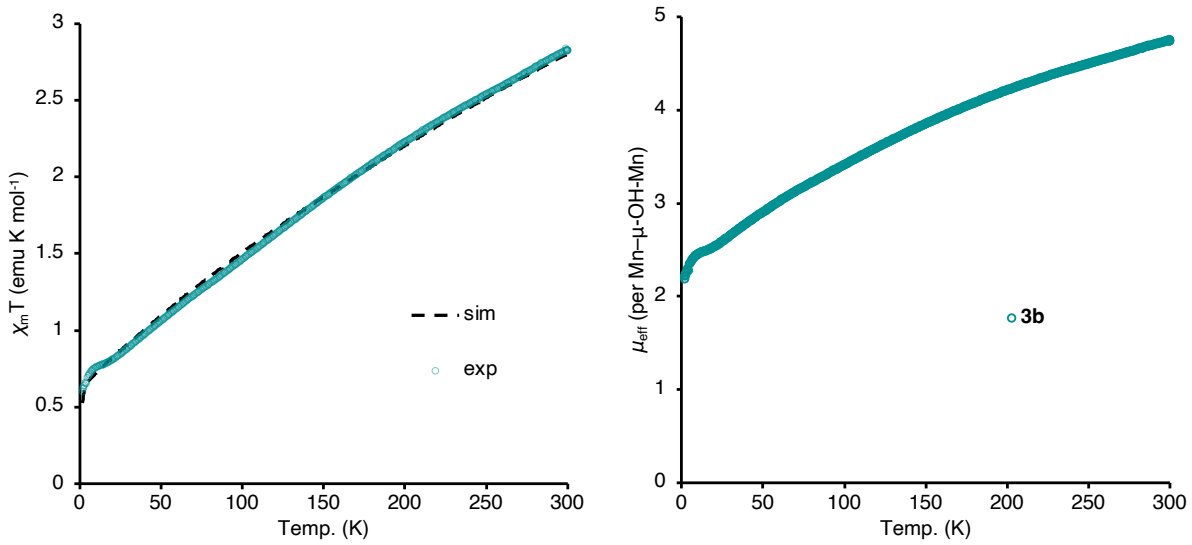

Figure S24. SQUID magnetization for (salophen)Mn–μ-OH–(salophen)Mn(PF_6)•PzH•H_2O•$(MeCN)_2$ (**3b**). Magnetic field = 200 Oe. The major feature was simulated as: g_{iso} = 2.00, J = −28.80(3) cm^{-1}.

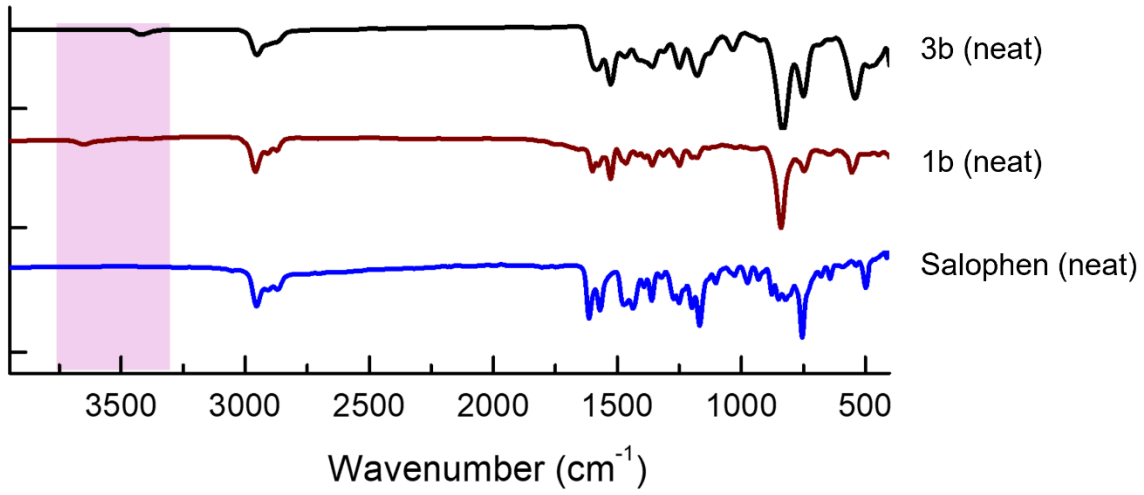

Figure S25. Stacked FTIR spectra of free salophen ligand, compounds **1b** and **3b**, highlighting change in O–H stretching frequency.

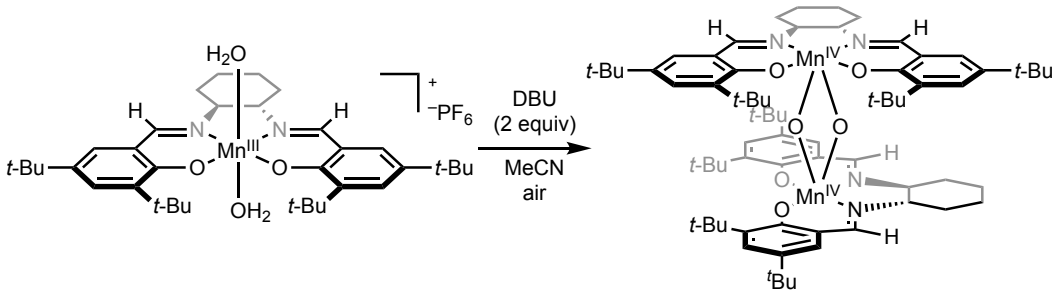

(salen)Mn-(μ-O)$_2$-(salen)Mn (4):[10] On benchtop, to a 8-mL vial with a stir bar were added (salen)Mn(H_2O)$_2$(PF_6) (0.10 g, 0.13 mmol, 1.0 equiv) and MeCN (5.0 mL). To the solution was added DBU (38 µL, 0.26 mmol, 2.0 equiv), and the mixture was stirred at ambient temperature for 30 min, resulting in a color change from dark brown to red-brown. After 30 min, the solution was allowed to stand at ambient temperature (21 ºC), resulting in formation of dark brown crystals that were identical to those previously reported (orthorhombic $C222_1$; a = 12.2207(10) Å, b = 27.657(2) Å, c = 21.0415(16); α = 90° β = 90° γ = 90° ; Volume = 7111.6(10) Å^3).[11] The crystalline solid was collected in a funnel, washed with MeCN (1×1 mL) and pentane (1×10 mL), and dried under vacuum, yielding (salen)Mn-(μ-O)$_2$-(salen)Mn as a red-brown solid (61 mg, 0.050 mmol, 77%). The ^{1}H NMR spectrum was identical to that reported in the literature.[10] **^{1}H NMR** (400 MHz, benzene-d_6, 298 K): δ 8.88 (br, s, $\Delta\nu_{1/2}$ = 156 Hz), 4.52 (br s, $\Delta\nu_{1/2}$ = 92 Hz), 3.0 (obsc br s), 1.63 (br s, $\Delta\nu_{1/2}$ = 4 Hz), 0.70 (br), −0.66 (br s, $\Delta\nu_{1/2}$ = 68 Hz), −1.63 (br s, $\Delta\nu_{1/2}$ = 84 Hz).

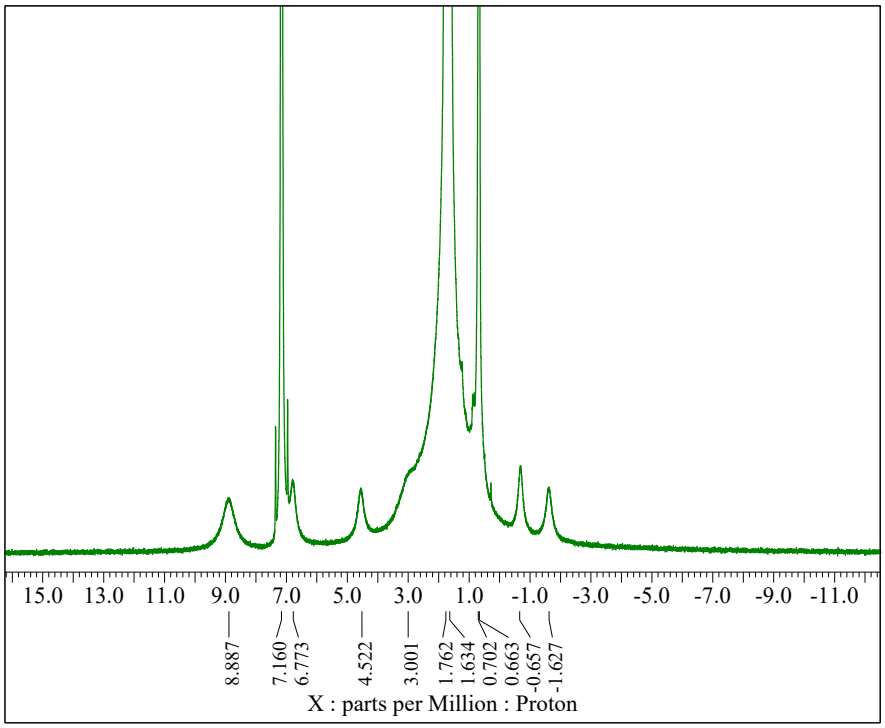

Figure S26. ^{1}H NMR (400 MHz; 9:1 C_6D_6/CD_3CN) of (salen)Mn-(μ-O)$_2$-(salen)Mn (**4**).

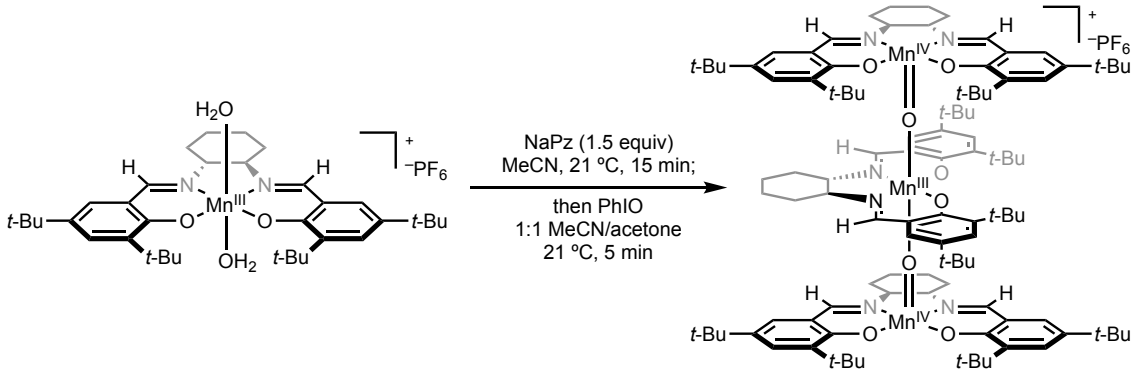

(salen)Mn–*μ*-O–(salen)Mn–*μ*-O–(salen)Mn(PF_6) (5): To a 25-mL round-bottom flask with a stir bar was added (salen)Mn(H_2O)$_2$(PF_6) (0.10 g, 0.13 mmol, 1.0 equiv), followed by MeCN (5.0 mL, 0.026 M). While stirring to the solution was added NaPz (18 mg, 0.20 mmol, 1.5 equiv), and the mixture was stirred at ambient temperature (21 ºC) for 15 min. After 15 min, brown precipitate was apparent in the mixture. Then, to the mixture was added acetone (5.0 mL), which dissolved the brown precipitate, and the resulting mixture was filtered over Celite. The red-brown filtrate was collected in a 100-mL round-bottom flask, and the solution was cooled to 0 ºC. In a separate vial was prepared a suspension of PhIO (28 mg, 0.13 mmol, 1.0 equiv) in H_2O (1.0 mL), which suspension was added to the 100-mL round-bottom flask. The reaction mixture was stirred at 0 ºC for 5 min. After 5 min, the flask was removed from the cooling bath, and the solution was filtered over Celite. The filtrate was collected and concentrated, and the brown concentrate was washed with pentane (×1) and dried under vacuum, yielding the desired compound as a crystalline brown solid (73 mg, 0.037 mmol, 85%). Single crystals suitable for X-ray diffraction were obtained by slow evaporation recrystallization over 48 h (1:1 MeCN/acetone, 21 ºC). **^{1}H NMR** (400 MHz, CD_3CN, 298 K): 11.64 (br s, $\Delta\nu_{1/2}$ = 184 Hz), 8.36 and 7.85 (br d, $\Delta\nu_{1/2}$ = 484 Hz), 2.37 (br s, $\Delta\nu_{1/2}$ = 40 Hz), −9.53 (br s, $\Delta\nu_{1/2}$ = 236 Hz), −14.29 (br s, $\Delta\nu_{1/2}$ = 456 Hz). **IR** (neat, 21 ºC): 2949, 2872, 1607, 1544, 1453, 1306, 1245, 1175, 1028, 838, 749, 560, 478 cm^{-1}. **Solution μ_{eff}** (CD_3CN, 298 K): 5.4(1) μ_B. **Anal. calcd.** for $C_{108}H_{156}F_6Mn_3N_6O_8P$•$(MeCN)_2$•$H_2O$: C, 64.79; H, 7.96; N, 5.40; found: C, 60.41; H, 7.58; N, 4.15. **X-Band EPR:** silent at 77 K in MeCN glass.

Figure S27. Crude GC-MS chromatogram of a crude reaction mixture in synthesis of **3a**, demonstrating iodobenzene formation from oxidation of **3a** with PhIO.

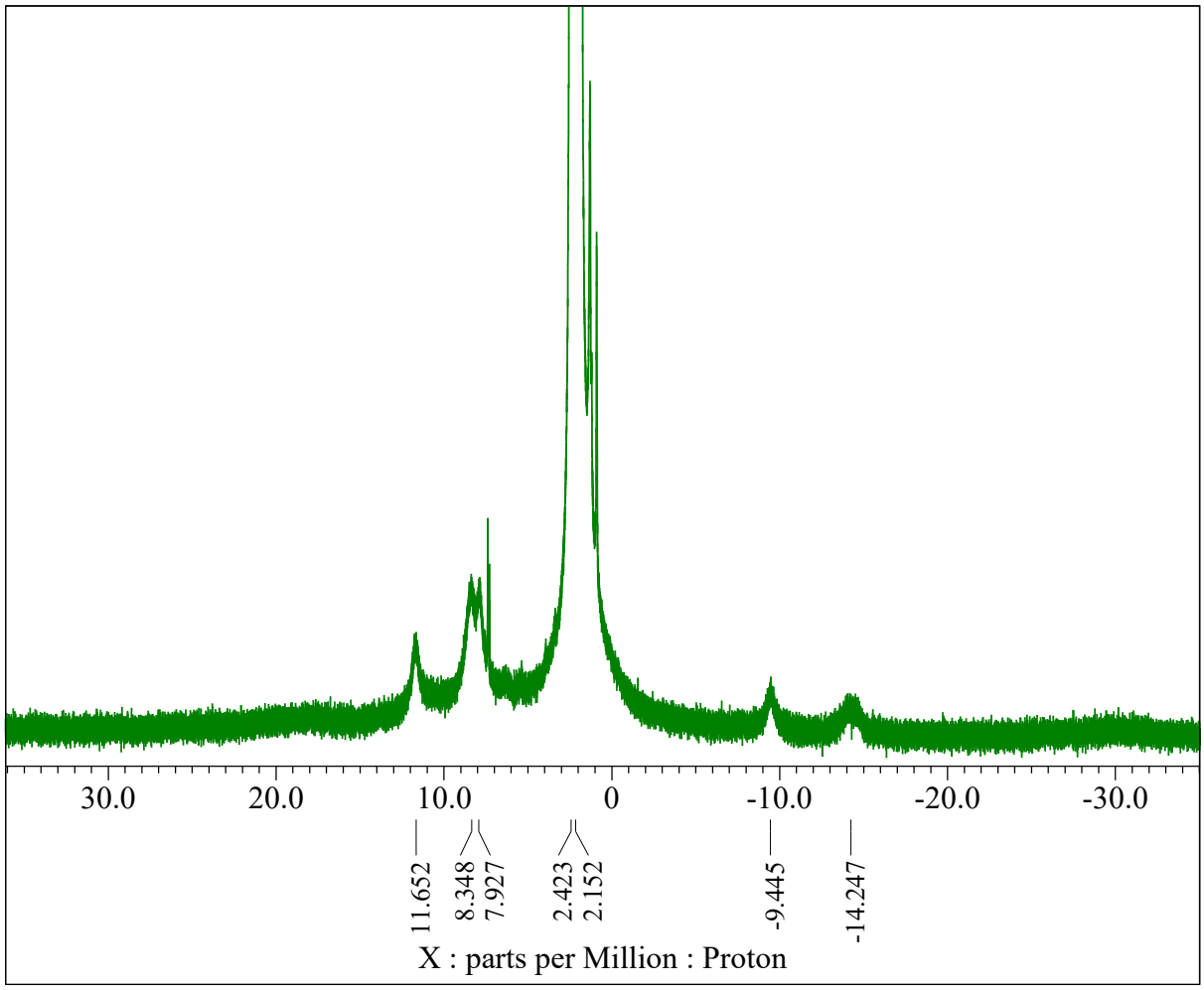

Figure S28. ^{1}H NMR (CD_3CN; 400 MHz) of (salen)Mn–μ-O–(salen)Mn–μ-O–(salen)Mn(PF_6) (**5**).

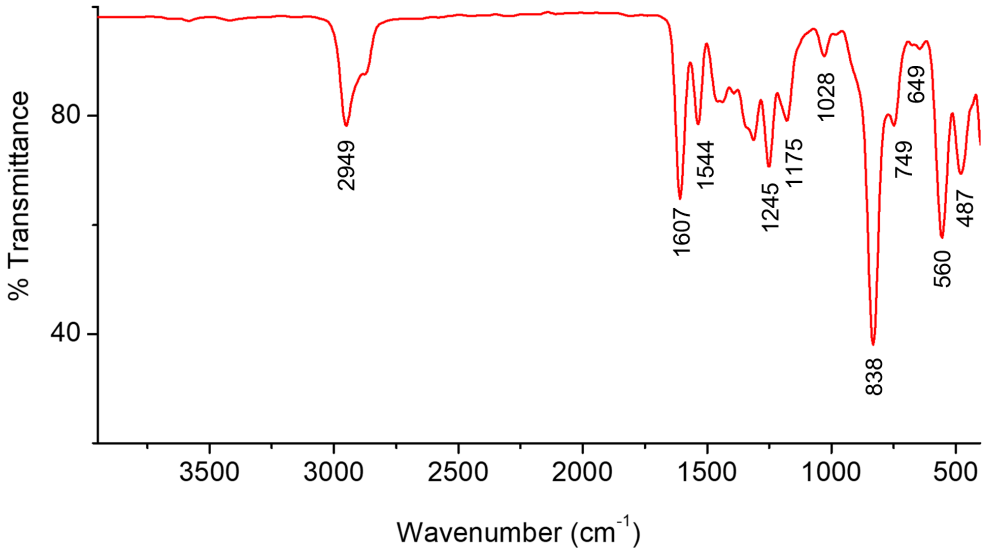

Figure S29. FTIR spectrum of (salen)Mn–μ-O–(salen)Mn–μ-O–(salen)Mn(PF_6) (**5**).

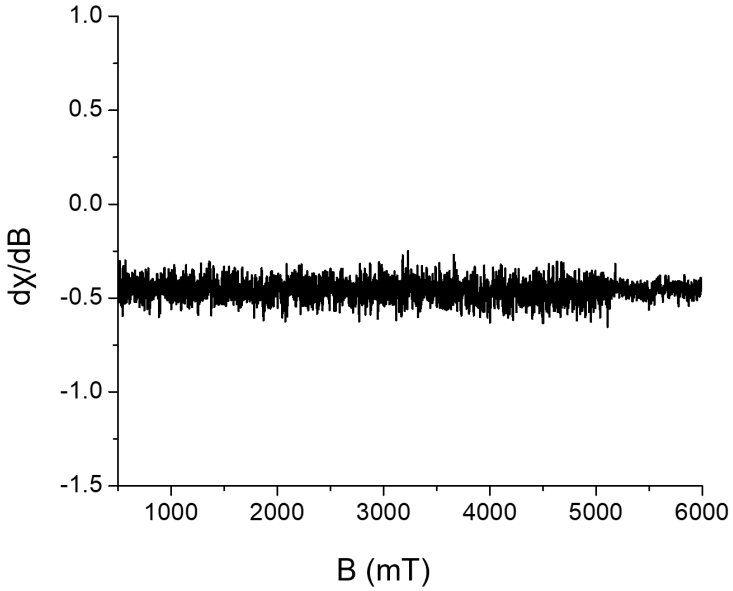

Figure S30. CW X-band EPR spectrum of (salen)Mn–μ-O–(salen)Mn–μ-O–(salen)Mn(PF_6) (**5**) in frozen MeCN at 77 K. Collection parameters: microwave frequency = 9.639764 GHz, power = 0.3162 mW; modAmp = 1 G.

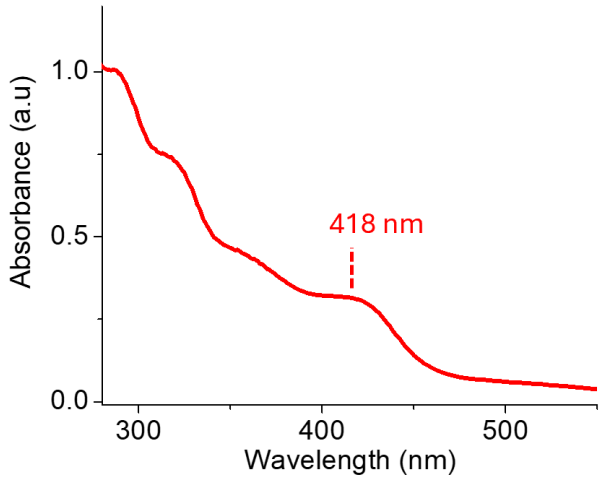

Figure S31. UV-Vis spectrum of (salen)Mn–μ-O–(salen)Mn–μ-O–(salen)Mn(PF_6) (**5**) in acetonitrile.

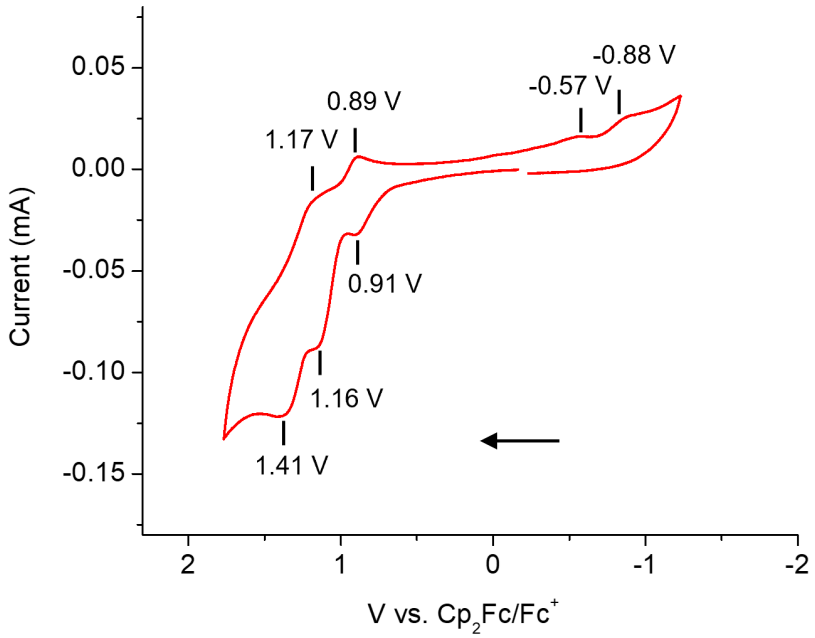

Figure S32. CV of (salen)Mn–μ-O–(salen)Mn–μ-O–(salen)Mn(PF_6) (5) (0.5 mM) in MeCN at 23 ºC. Scan rate = 100 mV/s, electrolyte = 0.2 M $TBAPF_6$, internal standard = $Fc^{0/+}$.

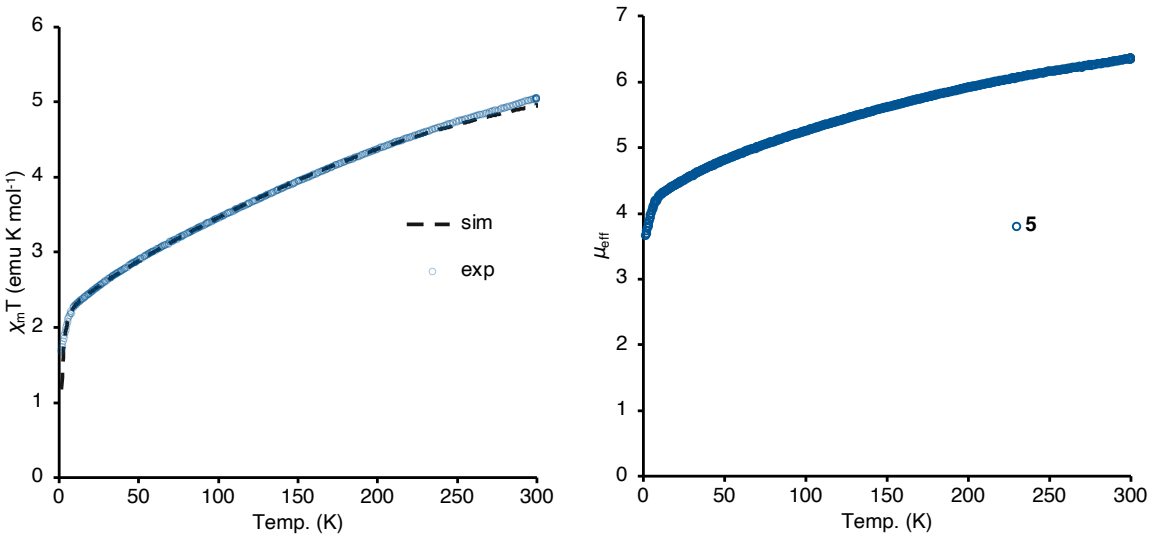

Figure S33. SQUID magnetization for (salen)Mn–μ-O–(salen)Mn–μ-O–(salen)Mn(PF_6)•MeCN•(3,5-di-tBu-salicylaldehyde) (**5**). Magnetic field = 200 Oe. Simulation parameters: Mn(IV/III/IV), J = −61.1(2) cm^{-1}, g_{iso} = 2.00, impurity = 2.6%.

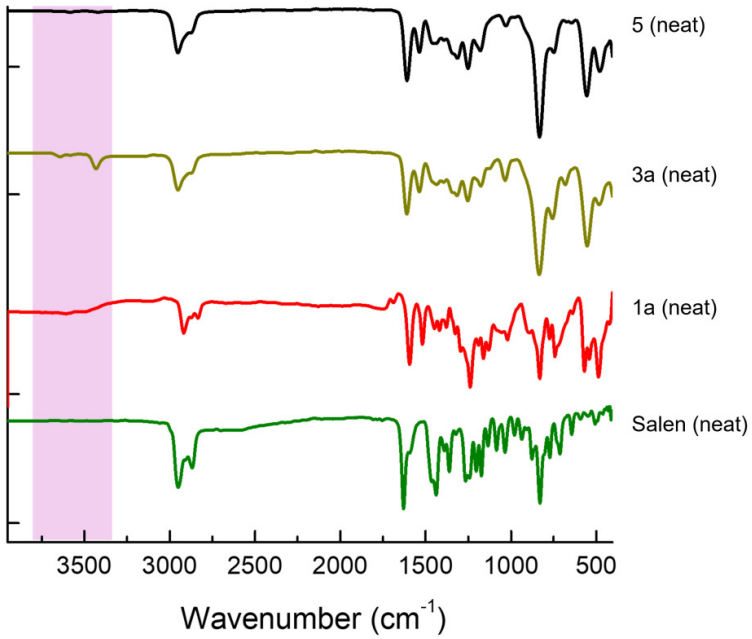

Figure S34. Stacked FTIR spectra of free salen ligand (green), (salen)Mn(OH_2)$_2$(PF_6) (**1a**), (salen)Mn–μ-OH–(salen)Mn(PF_6) (**3a**), and (salen)Mn–μ-O–(salen)Mn–μ-O–(salen)Mn(PF_6) (**5**), highlighting O–H stretching differences.

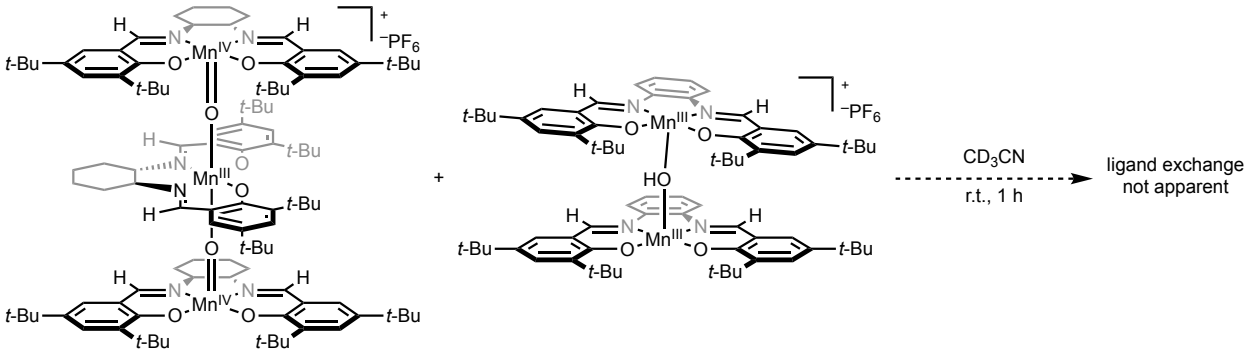

Experiment to determine complex exchange: A 4.0 mL septum-capped vial with a stir bar was charged with compound **3b** (3.9 mg, 2 mmol) and **5** (2.8 mg, 2 mmol). To the vial was added CD_3CN (1.0 mL), and the mixture was stirred for 1 h at ambient temperature and analyzed by ^1H NMR spectroscopy.

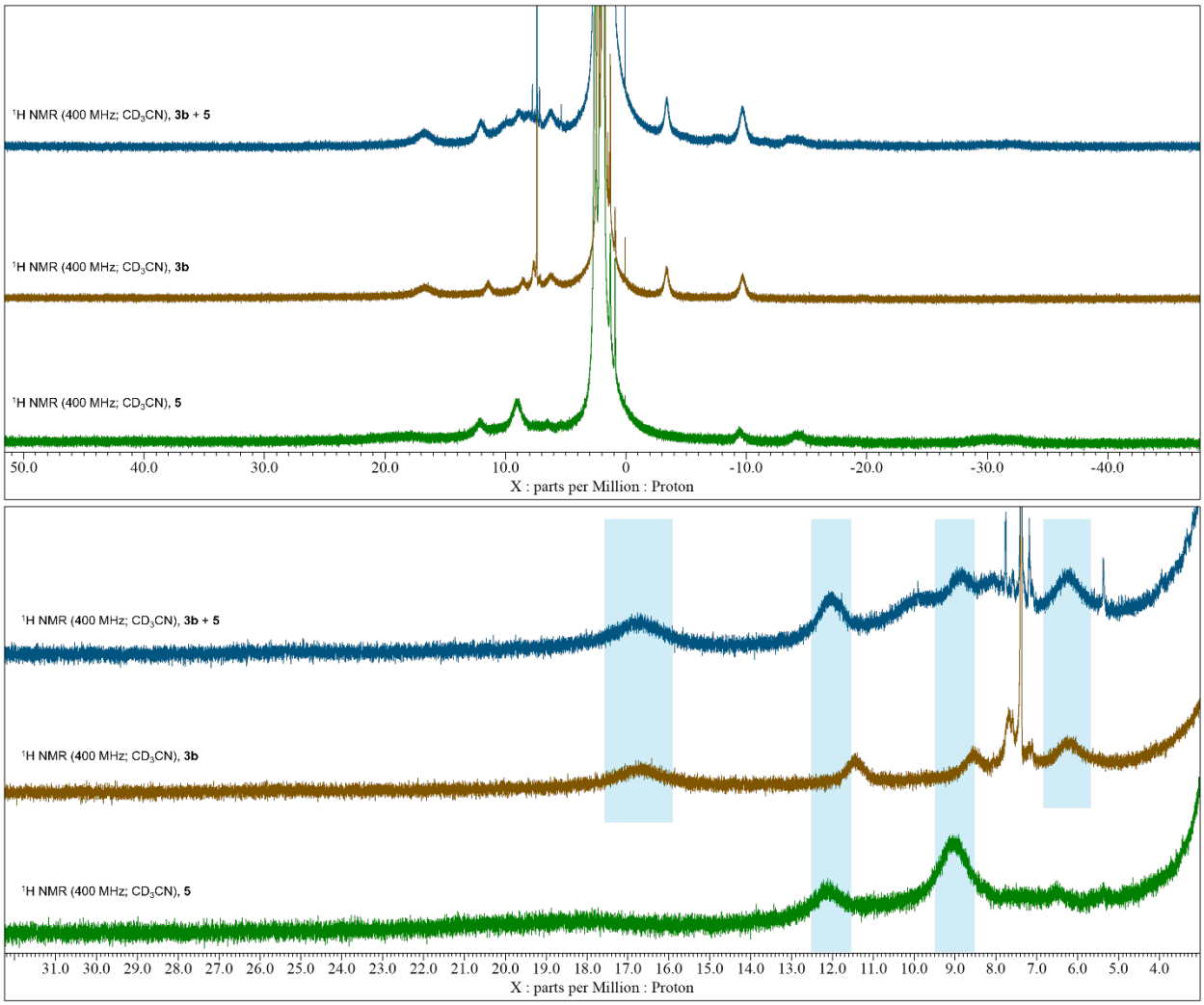

Figure S35. Stacked ^1H NMR (400 MHz; CD_3CN) spectra of **5** (2 mM) (green), **3b** (2 mM) (brown), and the mixture of **5** (2 mM) and **3b** (2 mM) (blue), demonstrating minimal peak broadening (consistent with minimal ligand exchange).

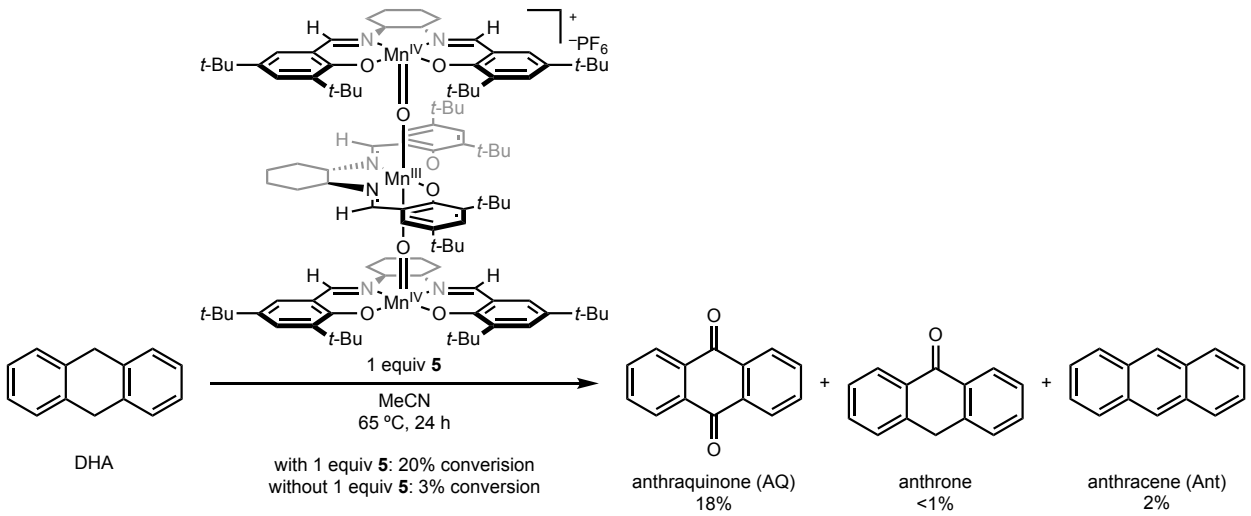

Stoichiometric reaction of trinuclear complex (5) with DHA: A 4.0 mL septum-capped vial with a stir bar was charged with DHA (12.6 mg, 0.07 mmol, 1 equiv), and trinuclear manganese metal complex **5** (138 mg, 0.070 mmol, 1 equiv). Dry MeCN (1 mL) was added to it and the reaction mixture was stirred at 65 °C for 24 hours. The reaction was cooled, diluted with CH_2Cl_2 (2.0 mL), and dodecane (16 μL, 0.070 mmol, 1.0 equiv) was added as internal standard. The organic layer was filtered over a pipette plug of Celite/$MgSO_4$ and analyzed by GC-MS to determine the yield of organic products.

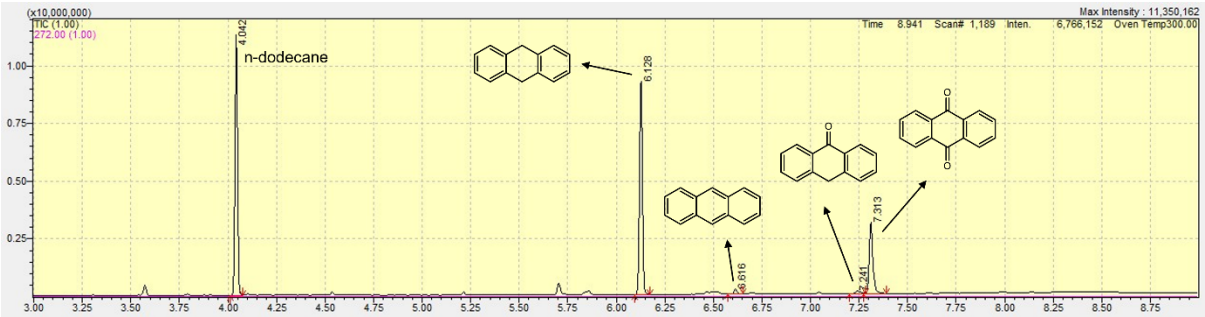

Figure S36. GC-MS chromatogram for DHA oxidation reaction in presence of complex **5**.

III. *In Situ* Oxidation of (salen)Manganese Complexes

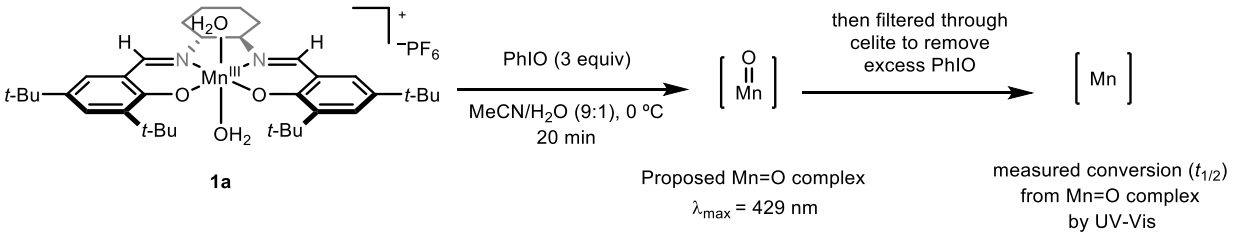

Oxidation of 1a by PhIO: 0.9 mL of the 3 mM stock solution prepared for **1a (**2 mg, 0.003 mmol) in acetonitrile was taken in a 4 mL vial. 0.1 mL of HPLC grade water was added to the solution followed by addition of 3 equiv of PhIO (2 mg, 0.009 mmol). Then the solution was stirred at 0 °C for 20 min. After that, the dark brown solution was filtered through celite to remove the excess solid PhIO. 100 µL of the filtrate was diluted to 3 mL in a cuvette. The UV-Vis spectra were recorded at several intervals of time by keeping the cuvette undisturbed at 21 °C.

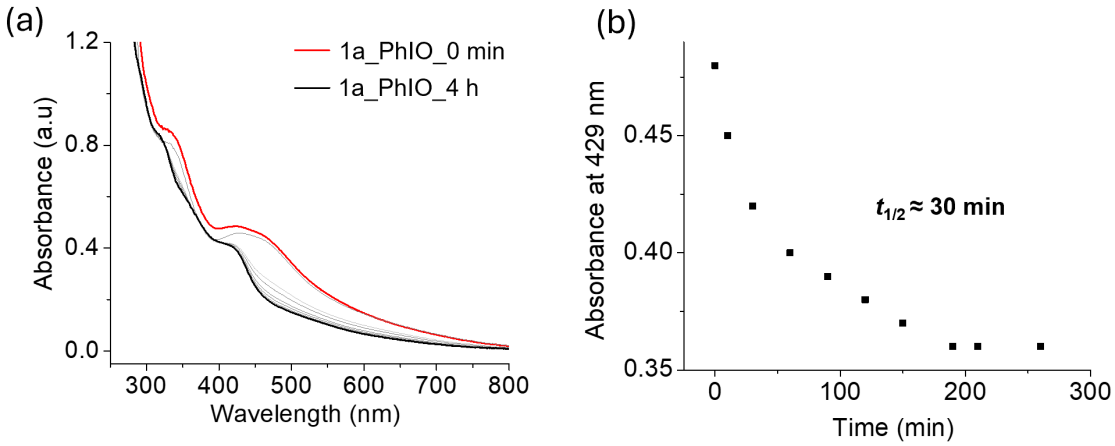

Figure S37. (a) UV-Vis spectra of [Mn(salen)](PF_6) (**1a**) after oxidation with PhIO at different time intervals and (b) the half-life of the oxidized complex in acetonitrile/water (9:1). Data demonstrate instability of putative Mn=O intermediate in the absence of substrate, implying catalyst decomposition and/or challenge of isolation.

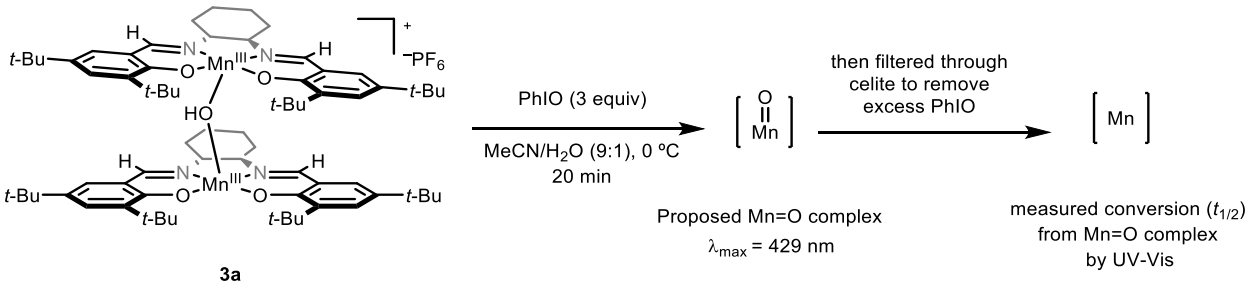

Oxidation of 3a by PhIO: 0.9 mL of the 3 mM stock solution prepared for **3a (**3.67 mg, 0.003 mmol) in acetonitrile was taken in a 4 mL vial. 0.1 mL of HPLC grade water was added to the solution followed by addition of 6 equiv of PhIO (4 mg, 0.018 mmol). Then the solution was stirred at 0 °C for 20 min. After that, the dark brown solution was filtered through celite to remove the excess solid PhIO. 50 µL of the filtrate was diluted to 3 mL in a cuvette. The UV-Vis spectra were recorded at several intervals of time by keeping the cuvette undisturbed at 21 °C.

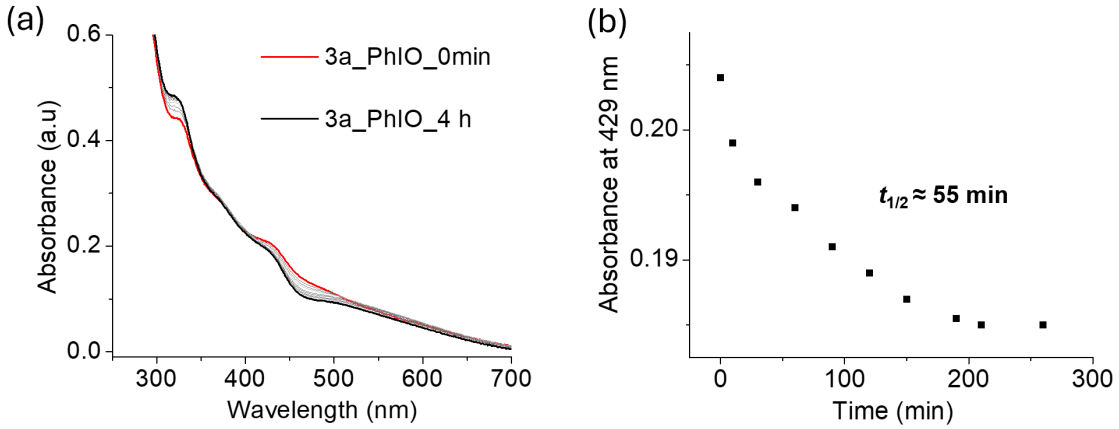

Figure S38. (a) UV-Vis spectra of [(salen)Mn–μ-OH–(salen)Mn](PF_6) (**3a**) after oxidation with PhIO at different time intervals and (b) decay of peak at 429 nm over time. Data demonstrate instability of putative Mn=O intermediate in the absence of substrate, implying catalyst decomposition and/or challenge of isolation.

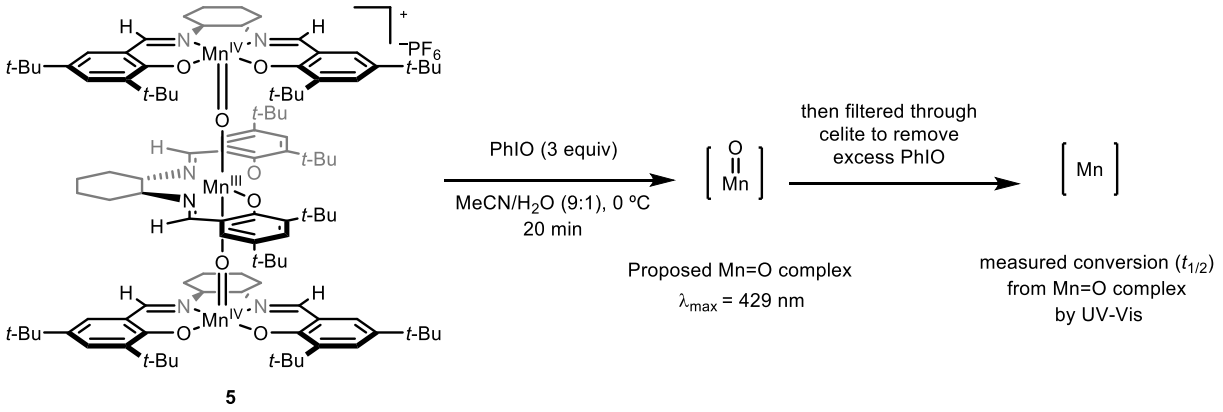

Oxidation of 5 by PhIO: 0.9 mL of the 3 mM stock solution prepared for **5 (**5.3 mg, 0.003 mmol) in acetonitrile was taken in a 4 mL vial. 0.1 mL of HPLC grade water was added to the solution followed by addition of 9 equiv of PhIO (6 mg, 0.027 mmol). Then the solution was stirred at 0 °C for 20 min. After that, the dark brown solution was filtered through celite to remove the excess solid PhIO. 33 µL of the filtrate was diluted to 3 mL in a cuvette. The UV-Vis spectra were recorded at several intervals of time by keeping the cuvette undisturbed at 21 °C.

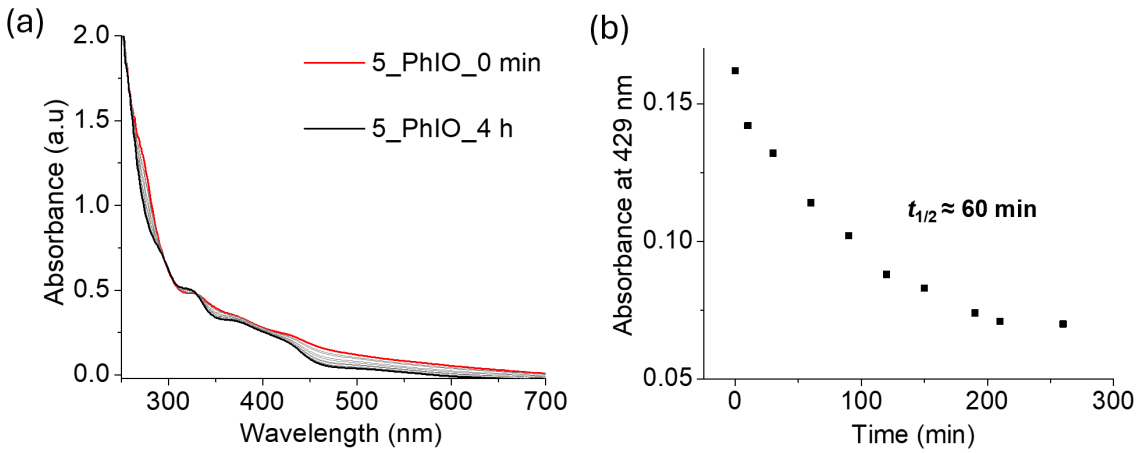

Figure S39. (a) UV-Vis spectra of [(salen)Mn–μ-O–(salen)Mn–μ-O–(salen)Mn](PF$_6$) (**5**) after oxidation with PhIO at different time intervals and (b) decay of peak at 429 nm over time. Data demonstrate instability of putative Mn=O intermediate in the absence of substrate, implying catalyst decomposition and/or challenge of isolation.

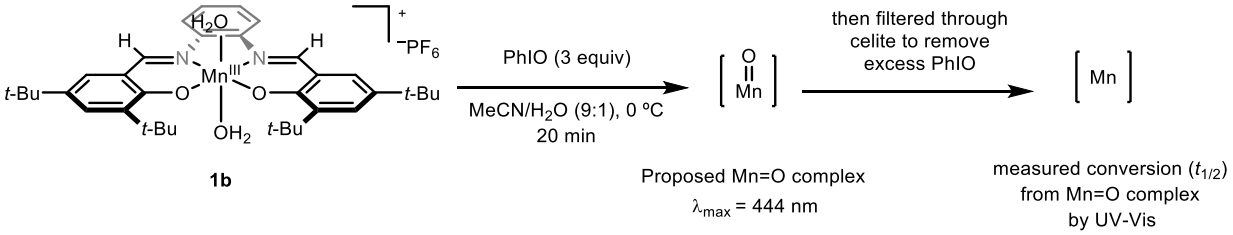

Oxidation of 1b by PhIO: 0.9 mL of the 3 mM stock solution prepared for **1b (**1.99 mg, 0.003 mmol) in acetonitrile was taken in a 4 mL vial. 0.1 mL of HPLC grade water was added to the solution followed by addition of 3 equiv of PhIO (2 mg, 0.009 mmol). Then the solution was stirred at 0 °C for 20 min. After that, the dark brown solution was filtered through celite to remove the excess solid PhIO. 100 µL of the filtrate was diluted to 3 mL in a cuvette. The UV-Vis spectra were recorded at several intervals of time by keeping the cuvette undisturbed at 21 °C.

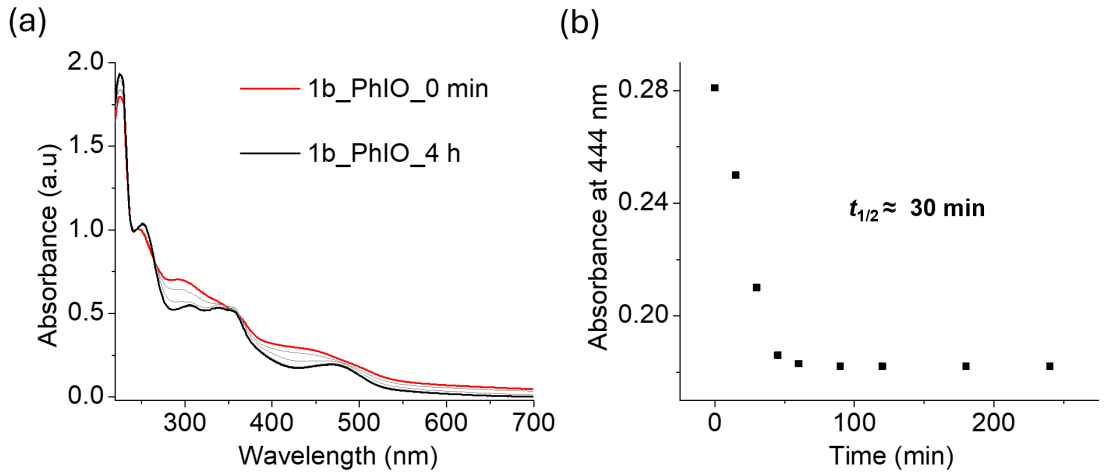

Figure S40. (a) UV-Vis spectra of [Mn(salophen)](PF_6) (**1b**) after oxidation with PhIO at different time intervals and (b) decay of peak at 444 nm over time. Data demonstrate instability of putative Mn=O intermediate in the absence of substrate, implying catalyst decomposition and/or challenge of isolation.

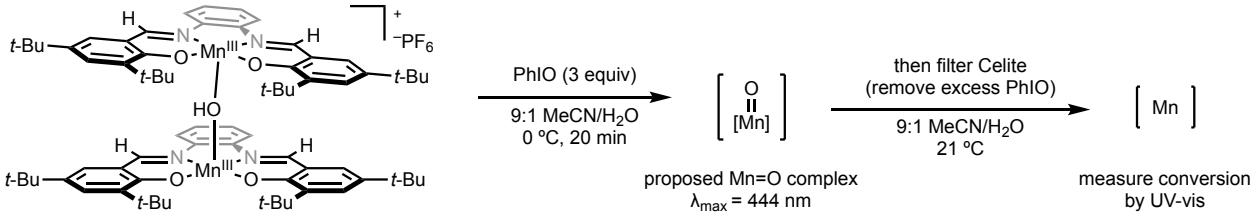

Oxidation of 3b by PhIO: 0.9 mL of the 3.3 mM stock solution prepared for **3b (**3.8 mg, 0.003 mmol) in acetonitrile was taken in a 4 mL vial. 0.1 mL of HPLC grade water was added to the solution followed by addition of 6 equiv of PhIO (4 mg, 0.018 mmol). Then the solution was stirred at 0 °C for 20 min. After that, the dark brown solution was filtered through celite to remove the excess solid PhIO. 50 µL of the filtrate was diluted to 3 mL in a cuvette. The UV-Vis spectra were recorded at several intervals of time by keeping the cuvette undisturbed at 21 °C.

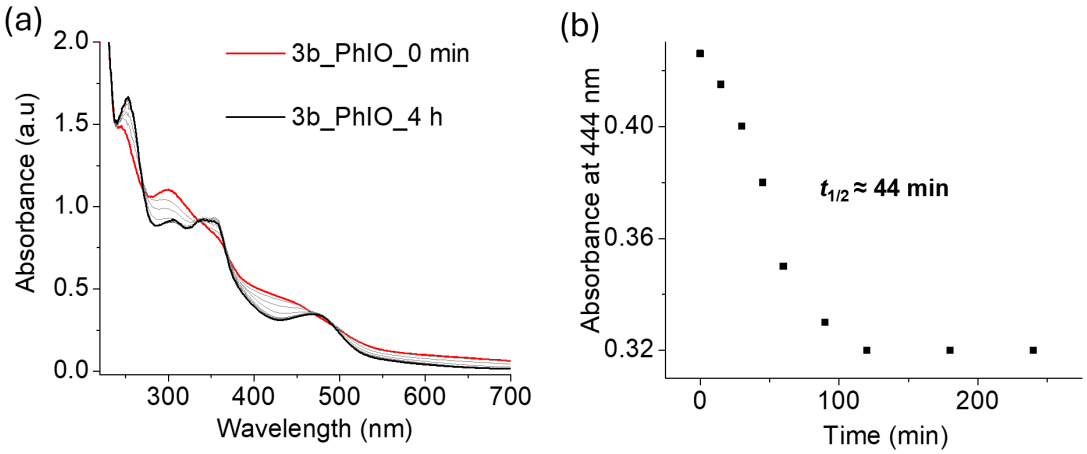

Figure S41. (a) UV-Vis spectra of [(salophen)Mn–μ-OH–(salophen)Mn](PF_6) (**3b**) after oxidation with PhIO at different time intervals and (b) decay of peak at 444 nm over time. Data demonstrate instability of putative Mn=O intermediate in the absence of substrate, implying catalyst decomposition and/or challenge of isolation.

IV. Catalytic C–H Oxidation Reactions

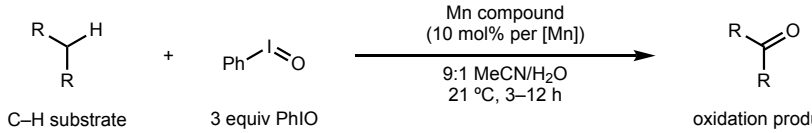

General procedure for catalytic C–H oxidation reactions: On benchtop, a 4.0-mL septum-capped vial with a stir bar was charged with metal complex (3.3–10 mol%), PhIO (92 mg, 0.42 mmol, 3.0 equiv), and substrate (if solid) (0.14 mmol). To the vial was added MeCN (0.90 mL) and H_2O (0.10 mL), followed by substrate (if oil) (0.14 mmol). The reaction mixture was stirred at ambient temperature (21 ºC) for 3–12 h. After the appropriate amount of time, the mixture was diluted with CH_2Cl_2 (3.0 mL), and dodecane (32 μL, 0.14 mmol, 1.0 equiv) was added as internal standard. The organic layer was filtered over a pipette plug of Celite/$MgSO_4$ and analyzed by GC-MS to determine the yield of organic products.

For catalyst characterization by ^1H NMR spectroscopy, the reaction was repeated using CD_3CN (0.90 mL) and H_2O (0.10 mL). After 16 h, the solution was filtered over Celite and analyzed by NMR spectroscopy.

Table S1. Oxidation of DHA according to Mn precatalyst.

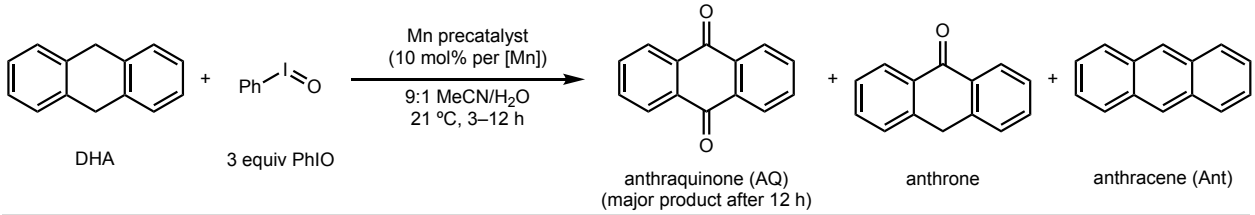

Entry	Precatalyst	DHA conversion	Yield AQ	Yield anthrone	Yield Ant
1	**1a** (10 mol%)	>99%	84%	5%	11%
2	**1b** (10 mol%)	>99%	86%	3%	9%
3	**2** (10 mol%)	>99%	80%	9%	10%
4	**3a** (5 mol%)	>99%	84%	7%	3%
5	**3b** (5 mol%)	>99%	88%	6%	5%
6	**5** (3.3 mol%)	>99%	81%	2%	15%

Yields determined by GC-MS calibrated against *n*-dodecane internal standard.

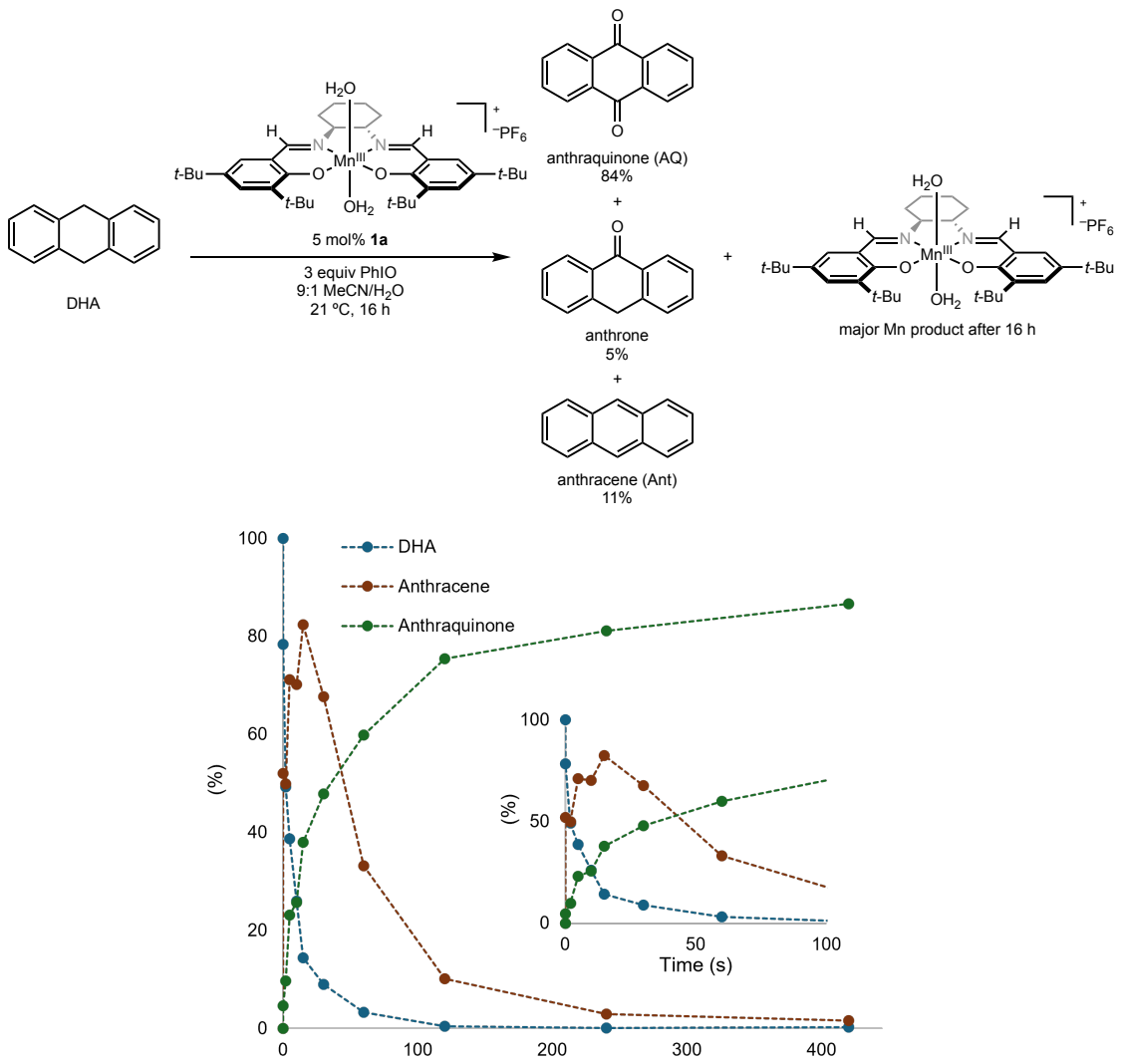

Figure S42. DHA oxidation reaction time course catalysed with the precatalyst **1a** (5 mol%). Yields determined by GC-MS.

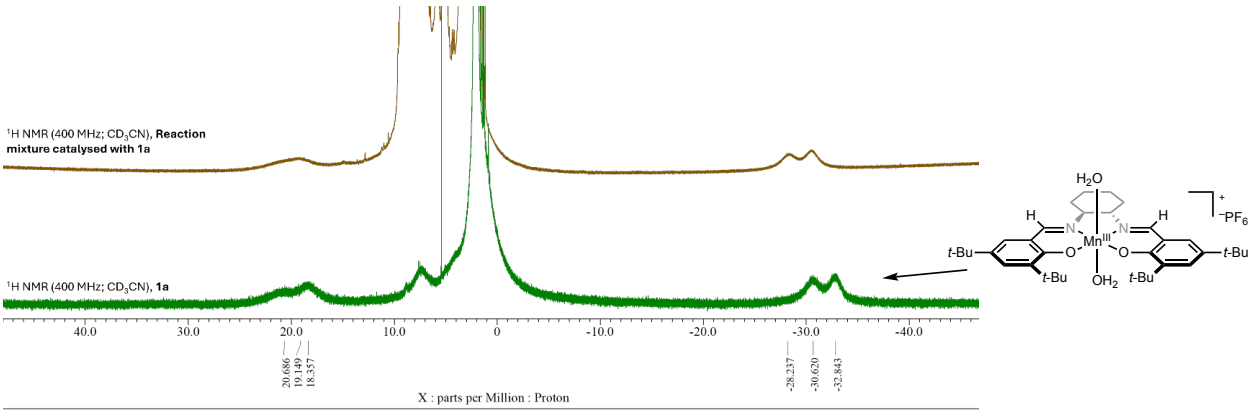

Figure S43. Crude ^{1}H NMR spectrum of the DHA oxidation reaction catalyzed by **3a** after 16 h.

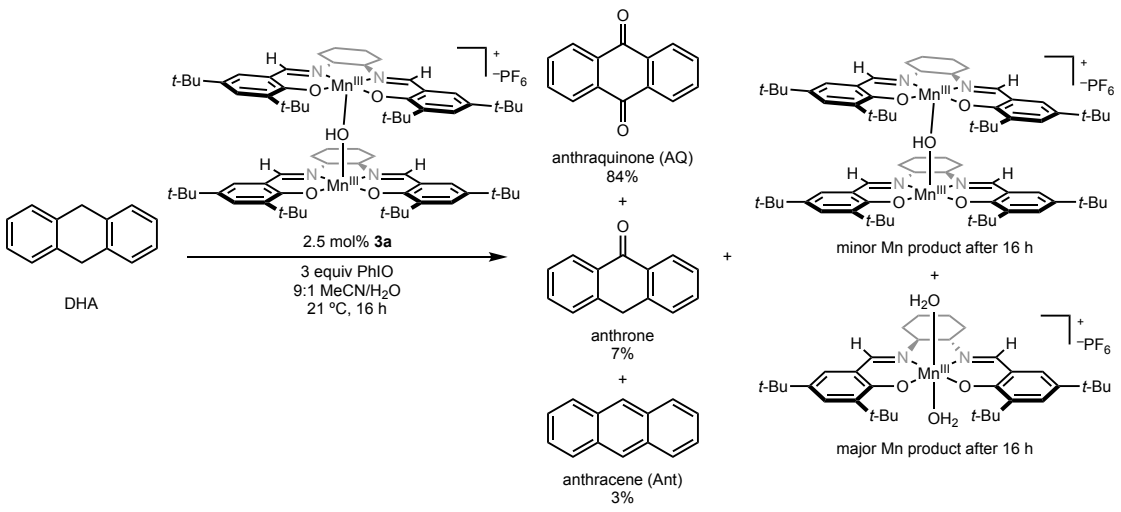

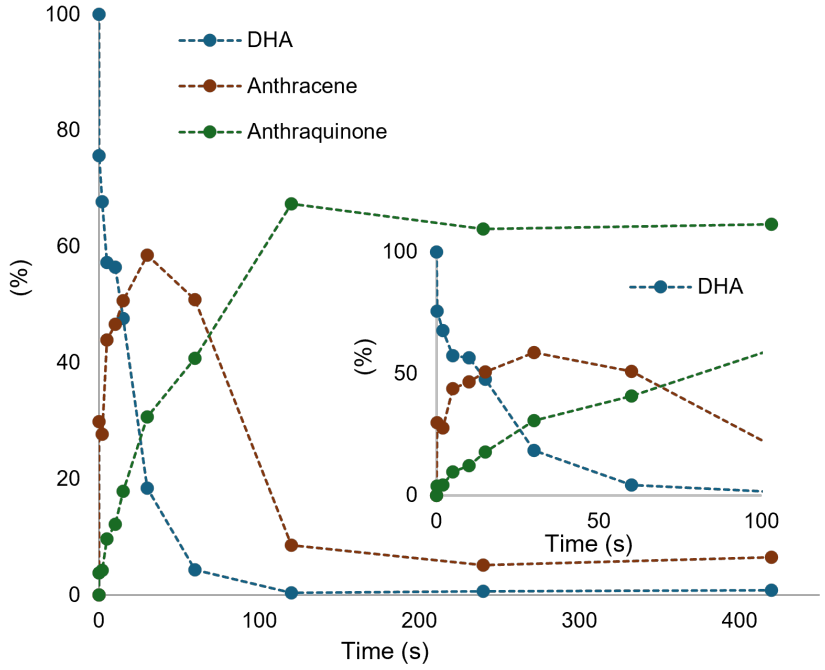

Figure S44. DHA oxidation reaction time-course catalysed with the precatalysts **3a** (2.5 mol%).

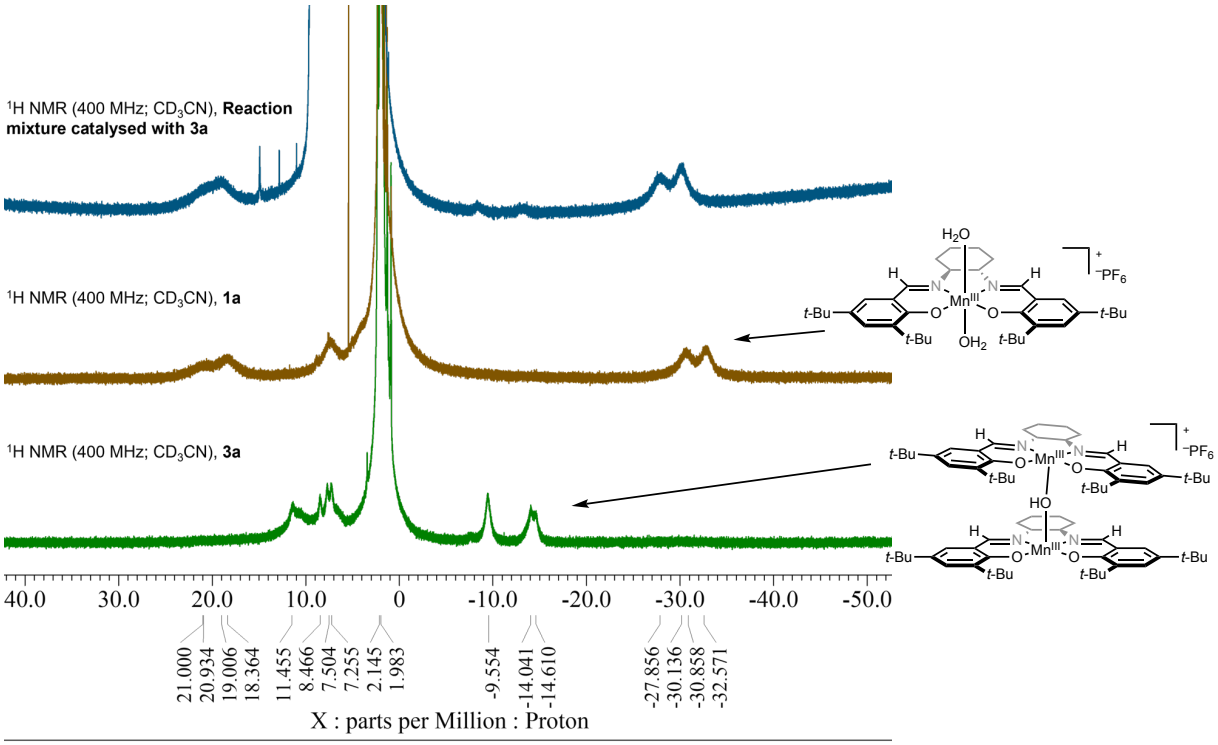

Figure S45. Crude ^{1}H NMR spectrum of the DHA oxidation reaction catalyzed by **3a** after 16 h.

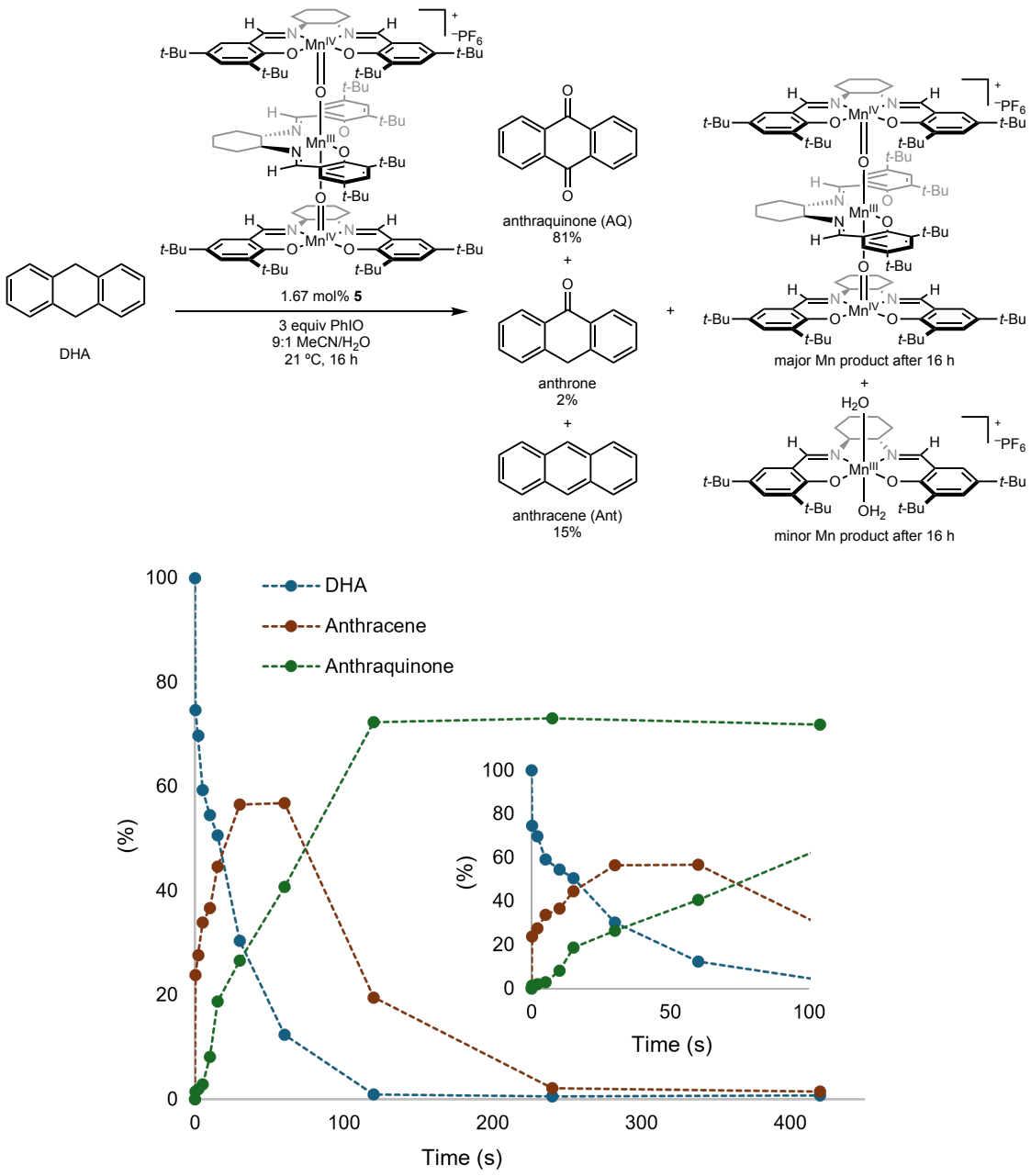

Figure S46. Time course of DHA oxidation employing precatalyst **5** (1.67 mol%). Yields determined by GC-MS.

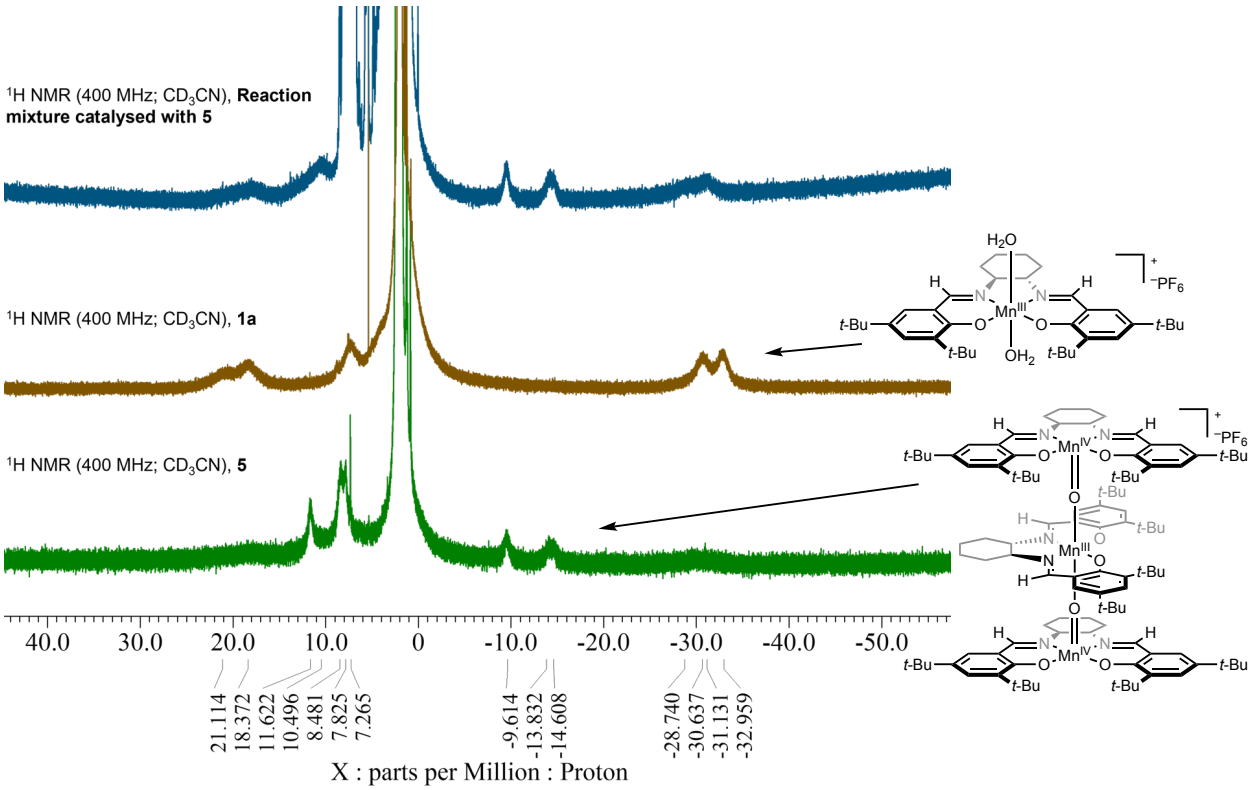

Figure S47. Crude ^{1}H NMR spectrum of the DHA oxidation reaction catalyzed by **5** after 16 h.

Procedure for (salen)manganese catalyst resting state determination: A 4.0 mL septum-capped vial with a stir bar was charged with DHA (0.14 mmol), PhIO (0.42 mmol), and metal complex (10 mol% for **1a**; 5 mol% for **3a**, and 3.3 mol% for **5**). To the vial were added MeCN (0.90 mL) and H_2O (0.10 mL), and the mixture was stirred for 5 min at ambient temperature. The solution was filtered over a pipette plug of Celite, and a 2.0 μL aliquot was diluted with MeCN (3.0 mL) and analyzed by UV-vis absorption spectroscopy.

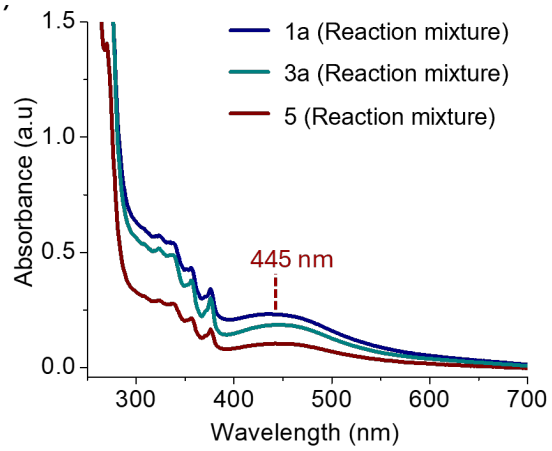

Figure S48. UV-Vis spectra of (salen)manganese-catalyzed DHA oxidation (ca. 15% conversion) initiated from 10 mol% **1a** (blue), 5 mol% **3a** (dark cyan), and 3.3 mol% **5a** (brown) in acetonitrile/water (9:1).

Table S2. Oxidation of styrene according to Mn precatalyst.

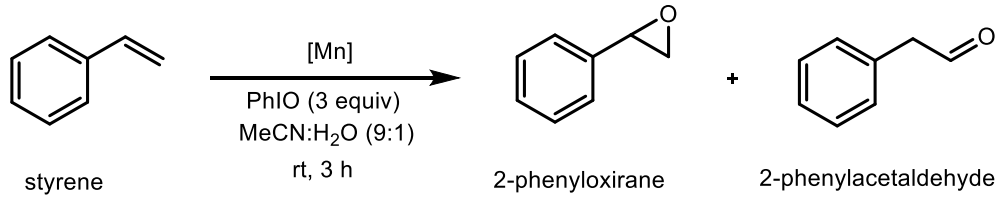

styrene — 2-phenyloxirane — 2-phenylacetaldehyde

Entry	Precatalyst	Styrene conversion	Yield styrene oxide	Yield phenylacetaldehyde
1	**1a** (10 mol%)	>99%	95%	3%
2	**1b** (10 mol%)	>99%	97%	3%
3	**2** (10 mol%)	>99%	94%	8%
4	**3a** (5 mol%)	>99%	91%	6%
5	**3b** (5 mol%)	>99%	91%	8%
6	**5** (3.3 mol%)	>99%	89%	5%

Yields determined by GC-MS calibrated against *n*-dodecane internal standard.

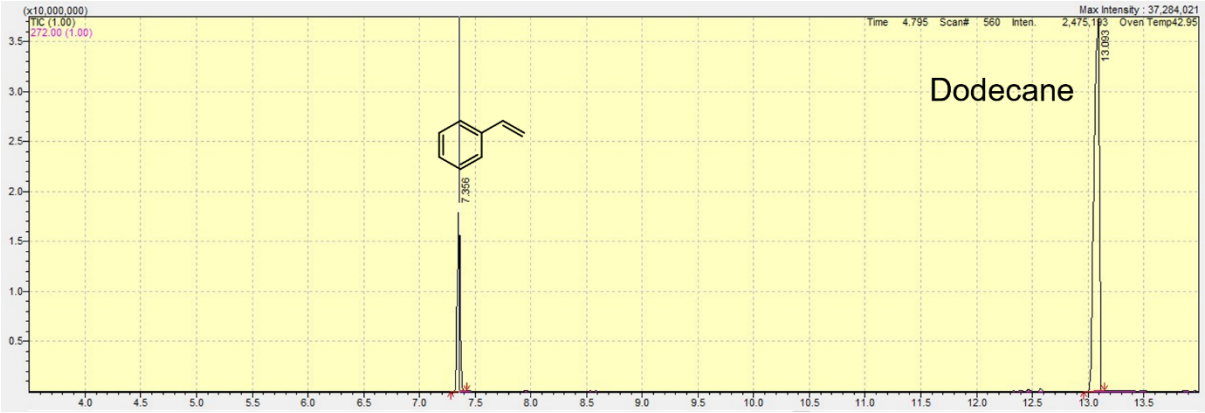

Figure S49. GC-MS chromatogram of an equimolar mixture of dodecane and styrene.

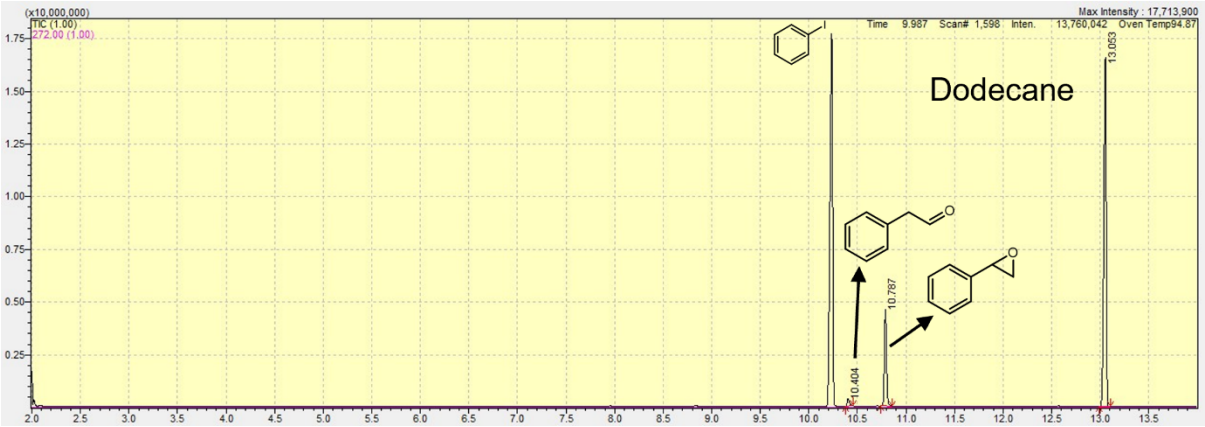

Figure S50. Crude GC-MS chromatogram demonstrating oxidation products of styrene. No styrene remained.

Table S3. Hammett competition for styrene epoxidation. Electronic trends are consistent with those previously observed.[12]

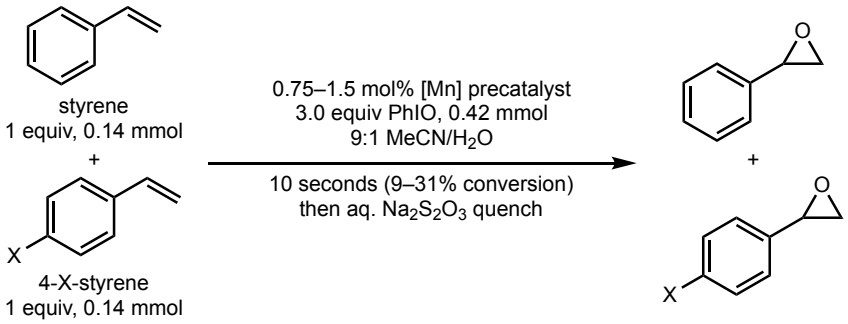

Entry	Precatalyst	X substituent	Conv. styrene	Conv. 4-X-styrene	k_X/k_H
1	**1a** (1.5 mol%)	OMe	19(4)%	31(3)%	1.6
2		*t*-Bu	9(1)%	11(1)%	1.2
3		Cl	18(1)%	16(2)%	0.89
4		CF_3	29(5)%	12(2)%	0.41
5	**3a** (0.75 mol%)	OMe	13(2)%	13(3)%	1.0
6		*t*-Bu	10(3)%	13(1)%	1.3
7		Cl	11(1)%	8(1)%	0.73
8		CF_3	19(3)%	4(1)%	0.21
9	**5** (0.75 mol%)	OMe	15(3)%	41(5)%	2.7
10		*t*-Bu	9(1)%	11(1)%	1.2
11		Cl	13(2)%	13(3)%	1.0
12		CF_3	20(5)%	6(1)%	0.30

Conversions determined by GC-MS (average of 3 trials). Error represents standard deviation.

Table S4. Oxidation of fluorene according to Mn precatalyst.

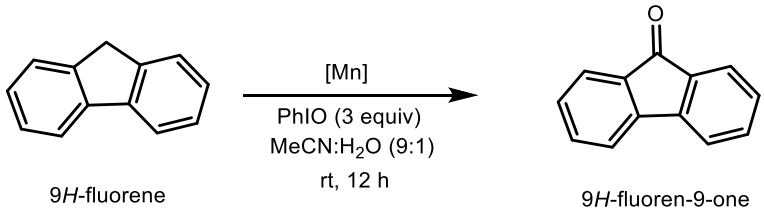

Entry	Precatalyst	fluorene conversion
1	**1a** (10 mol%)	68%
2	**1b** (10 mol%)	70%
3	**2** (10 mol%)	80%
4	**3a** (5 mol%)	52%
5	**3b** (5 mol%)	58%
6	**5** (3.3 mol%)	65%

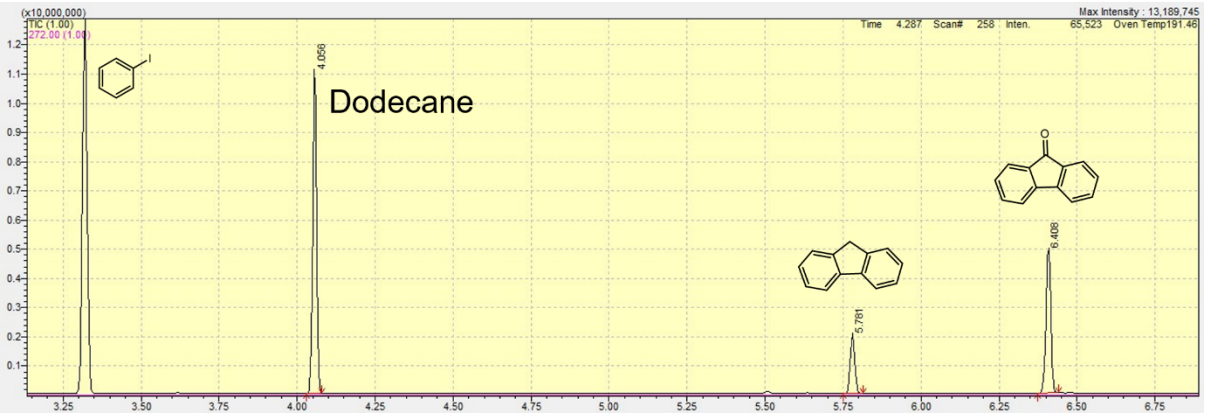

Figure S51. Representative crude GC-MS chromatogram demonstrating oxidation of fluorene.

Table S5. Oxidation of *p*-cymene according to Mn precatalyst.

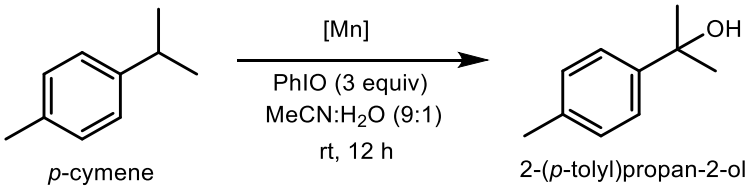

Entry	Precatalyst	cymene conversion
1	1a (10 mol%)	20%
2	1b (10 mol%)	25%
3	2 (10 mol%)	17%
4	3a (5 mol%)	19%
5	3b (5 mol%)	23%
6	5 (3.3 mol%)	20%

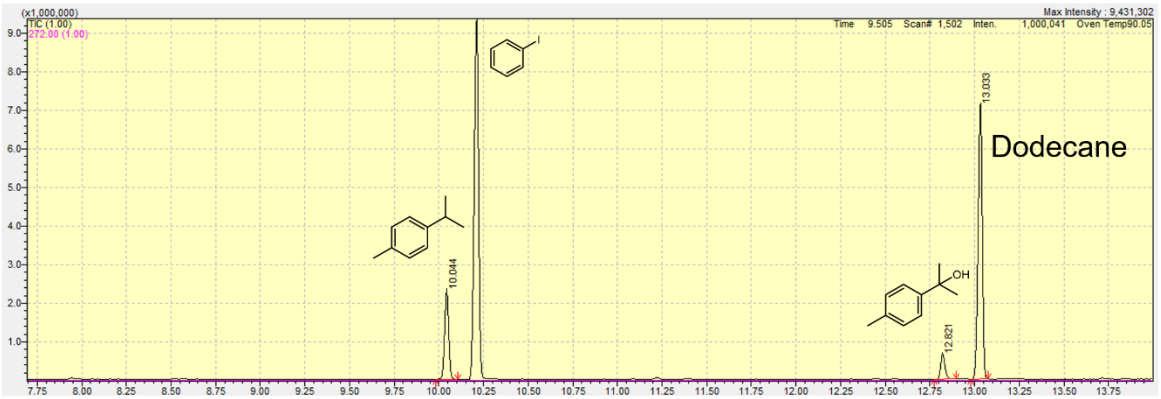

Figure S52. Crude GC-MS chromatogram demonstrating oxidation products of *p*-cymene.

Table S6. Oxidation of cyclohexylbenzene according to Mn precatalyst.

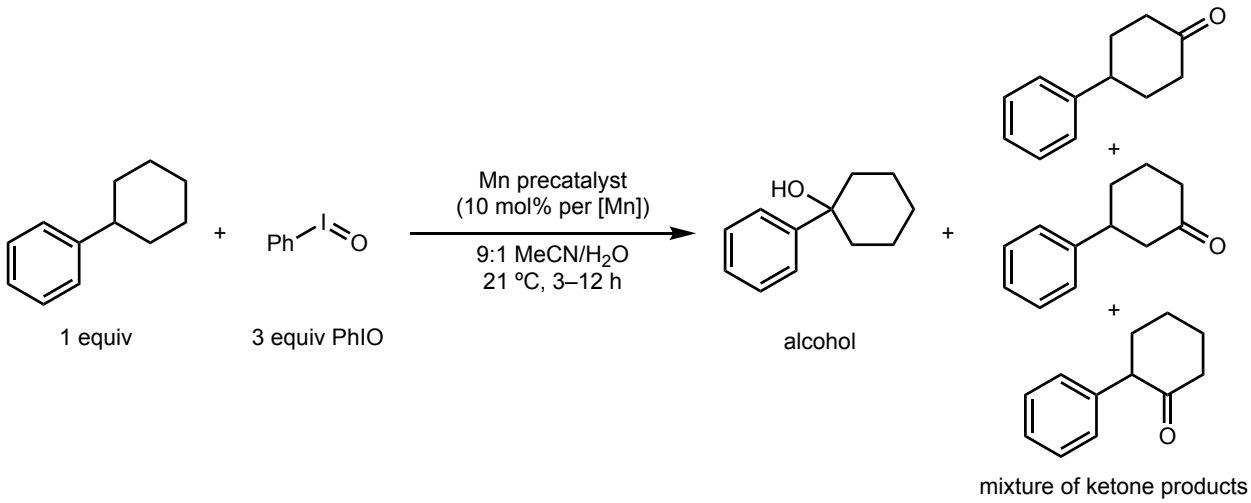

Entry	Precatalyst	Conversion	Yield alcohol	Combined yield ketone products
1	**1a** (10 mol%)	20%	12%	3%
2	**1b** (10 mol%)	22%	16%	4%
3	**2** (10 mol%)	18%	9%	3%
4	**3a** (5 mol%)	22%	13%	7%
5	**3b** (5 mol%)	23%	13%	8%
6	**5** (3.3 mol%)	18%	11%	4%

Yields determined by GC-MS calibrated against *n*-dodecane internal standard.

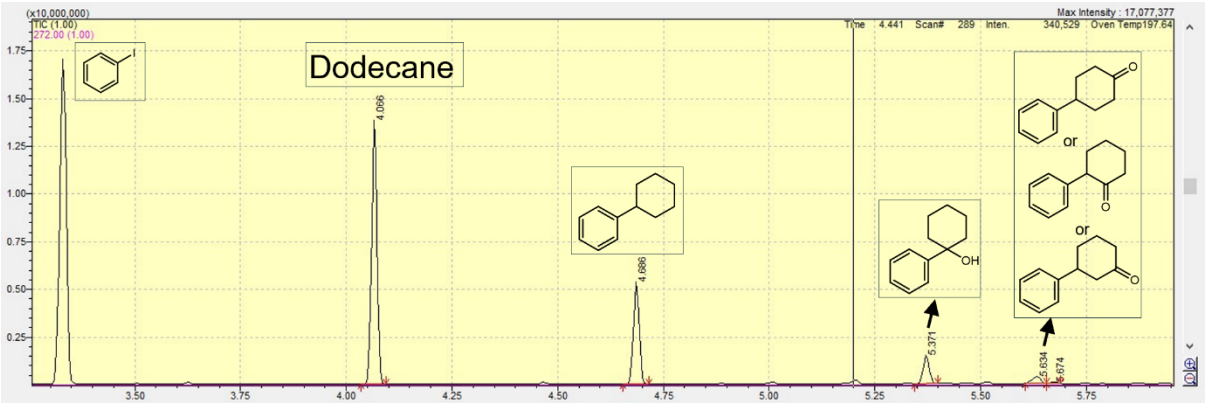

Figure S53. Crude GC-MS chromatogram demonstrating oxidation products of Phenyl cyclohexane.

V. Kinetic Experiments

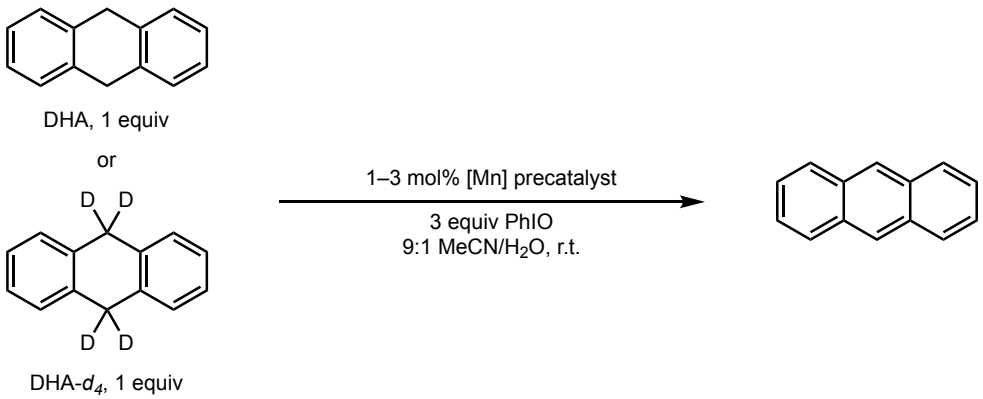

$^{1/2}$H Kinetic isotope effect determination for DHA oxidation: Reactions were performed following the General Procedure on 0.28-mmol scale employing appropriate precatalyst (**1a**, **3a**, or **5**, 1–3 mol%), DHA (50 mg, 0.28 mmol, 1.0 equiv) or DHA-d_4 (51 mg, 0.28 mmol, 1.0 equiv), PhIO (0.19 g, 0.84 mmol, 3.0 equiv), dodecane as internal standard (64 µL, 0.28 mmol, 1.0 equiv), MeCN (3.15 mL) and H_2O (0.35 mL) (total volume = 3.5 mL of a 9:1 MeCN/H_2O mixture, 0.080 M). Aliquots were taken during the initial time points and immediately quenched with sat. aq. NaS_2O_3, then extracted with 1:1 hexanes/EtOAc, filtered over a pipette plug of Celite/$MgSO_4$, and analyzed by GC-MS.

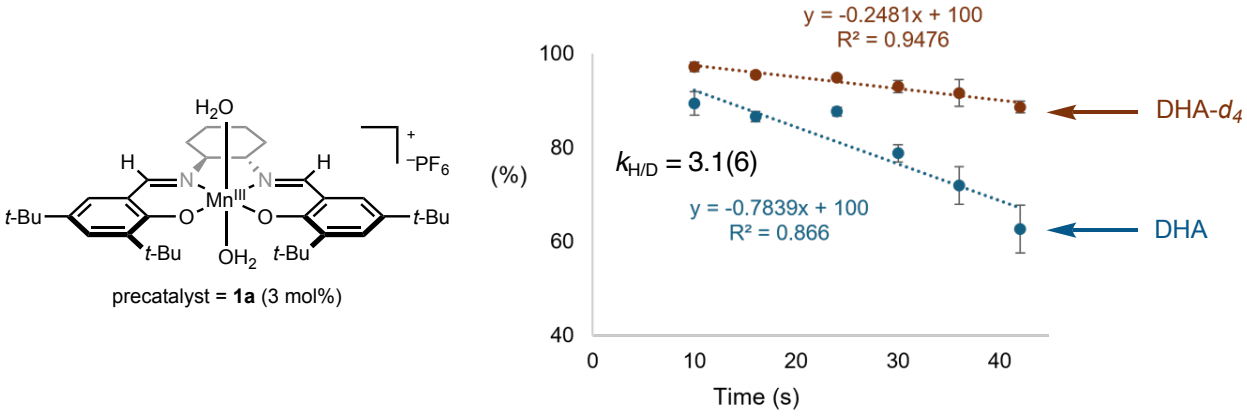

Figure S54. Initial rate of conversion of DHA vs. DHA-d_4 employing **1a** (3 mol%). Values determined by GC-MS employing dodecane as an internal standard (n = 3; error = S.D.).

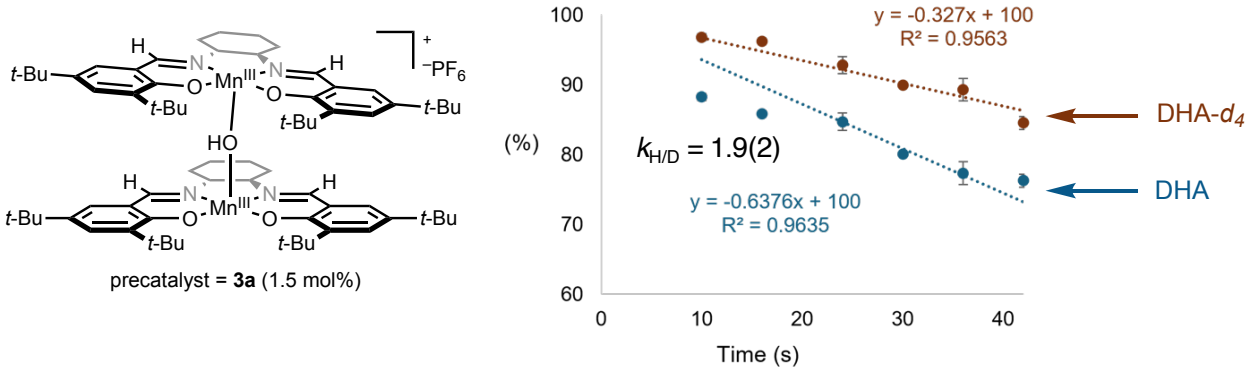

Figure S55. Initial rate of conversion of DHA vs. DHA-d_4 employing **3a** (1.5 mol%). Values determined by GC-MS employing dodecane as an internal standard (n = 5; error = S.D.).

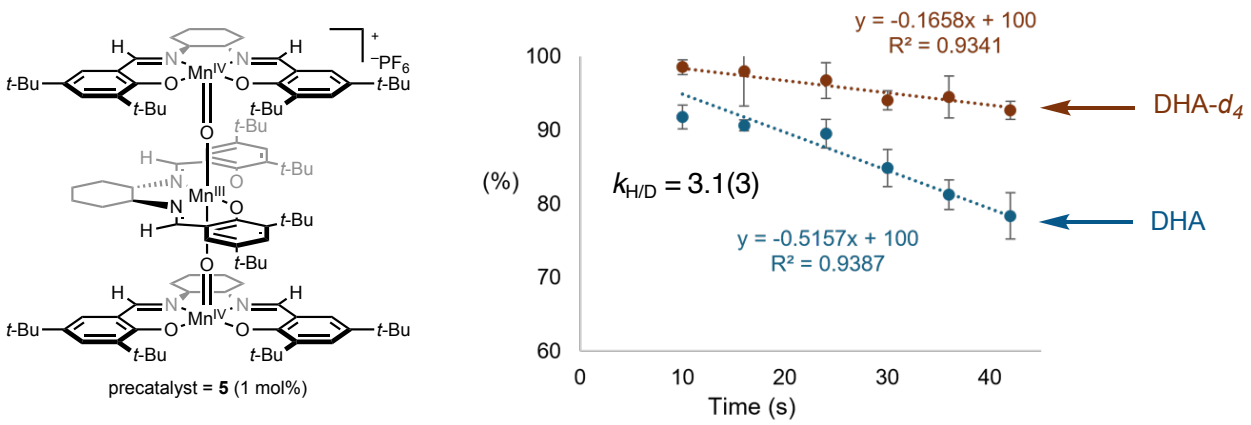

Figure S56. Initial rate of conversion of DHA vs. DHA-d_4 employing **5** (1 mol%). Values determined by GC-MS employing dodecane as an internal standard (n = 3; error = S.D.).

Scheme S1. Conditions for evaluation of order in precatalyst **1a**.

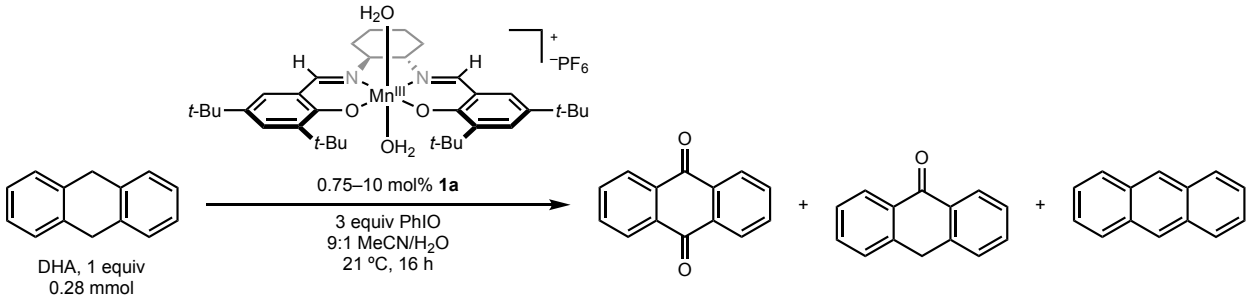

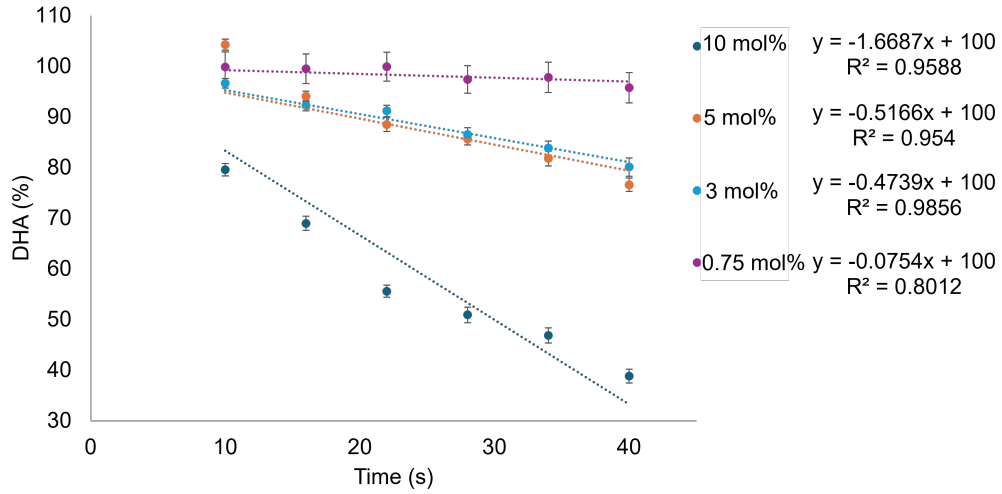

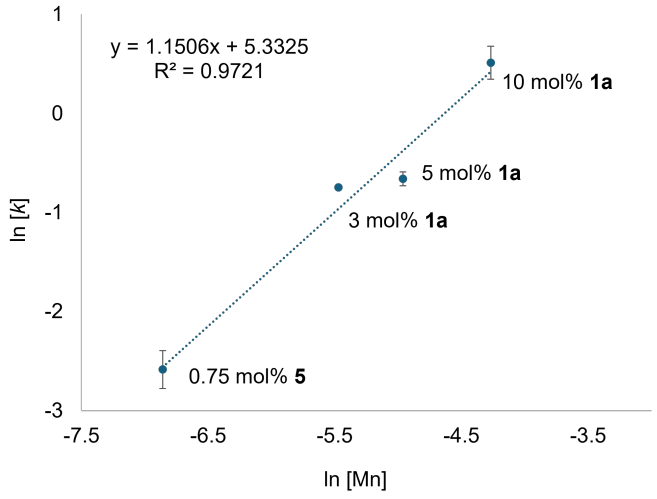

Figure S57. Determination of initial rates of DHA conversion (n = 3) by linear trendline fitting, according to concentration of **1a** precatalyst (approximate 1st order in [**1a**]). Conversion determined by GC-MS employing dodecane as internal standard.

Scheme S2. Conditions for evaluation of order dependence on dimeric precatalyst **3a** in the oxidation of DHA.

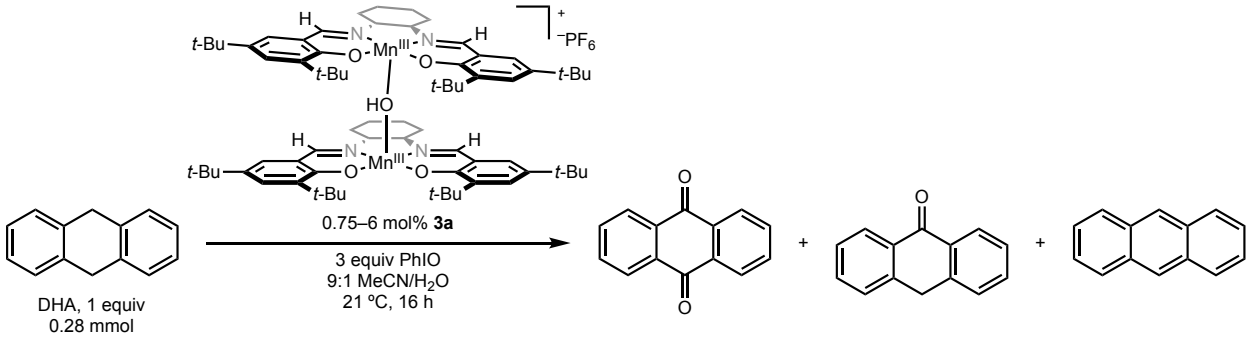

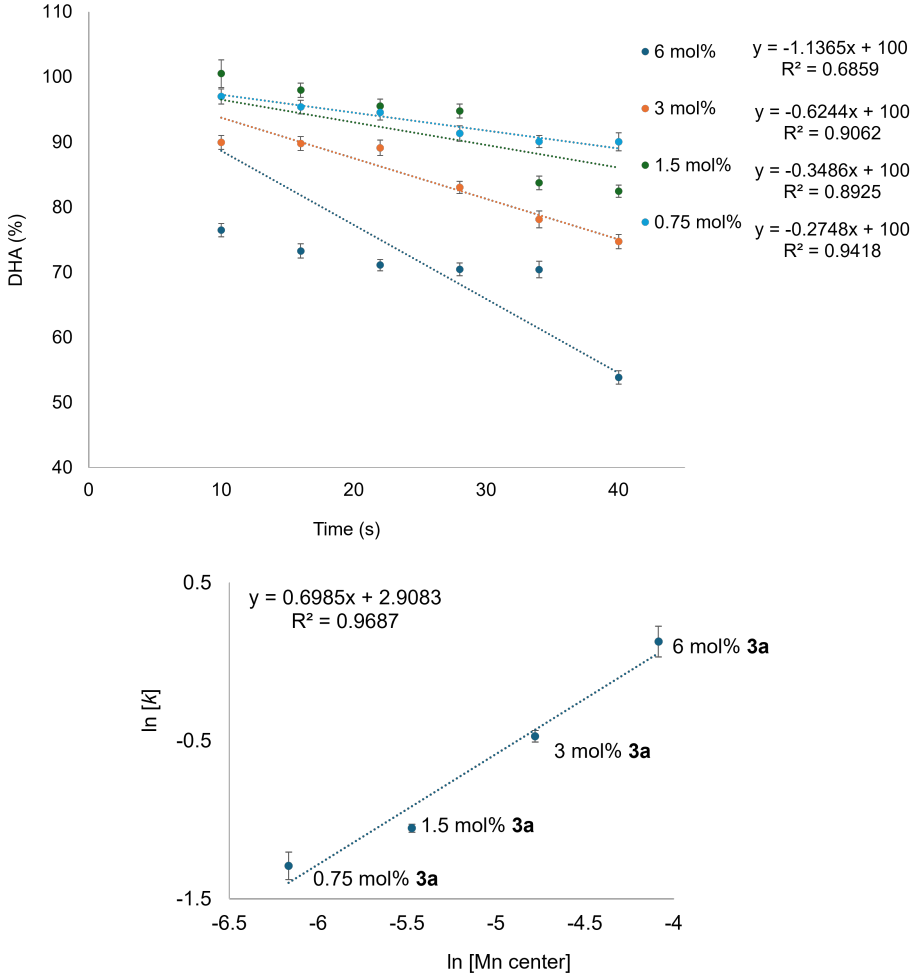

Figure S58. Determination of initial rates of DHA conversion (n = 3) by linear trendline fitting, with varying catalyst loading of **3a**. Order was determined according to concentration of [Mn] catalyst center. Partial order determination in [Mn] catalyst center was attributed to off-cycle dimerization apparent in the isolated precatalyst, with monomerization proposed preceding catalyst activation.

Scheme S3. Conditions for evaluation of order dependence on trinuclear precatalyst **5** in the oxidation of DHA.

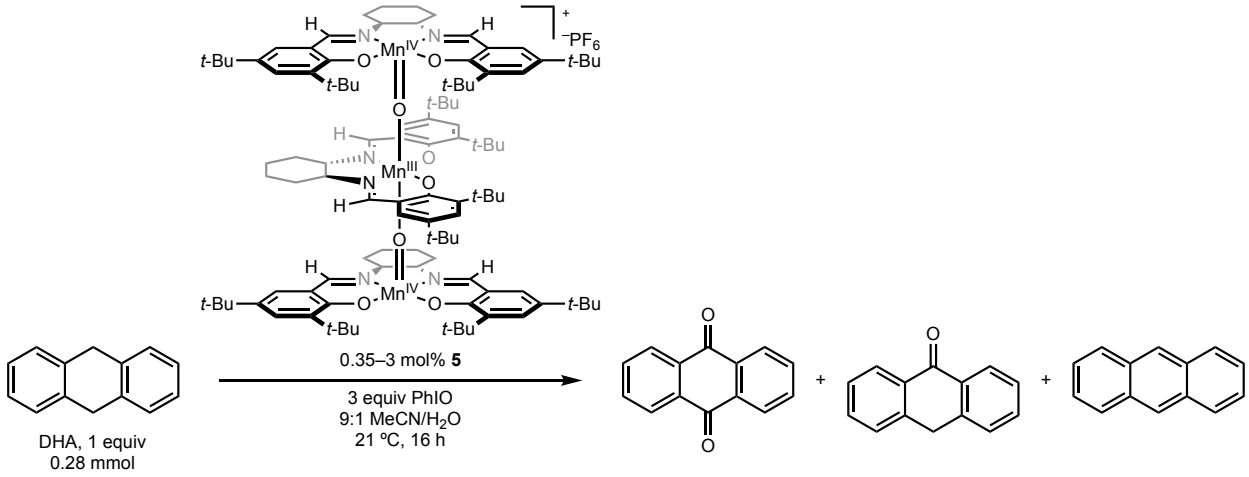

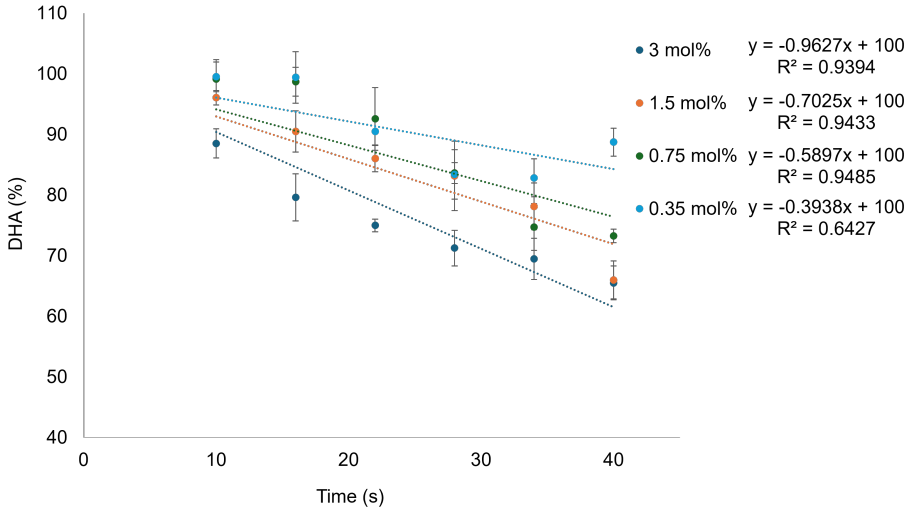

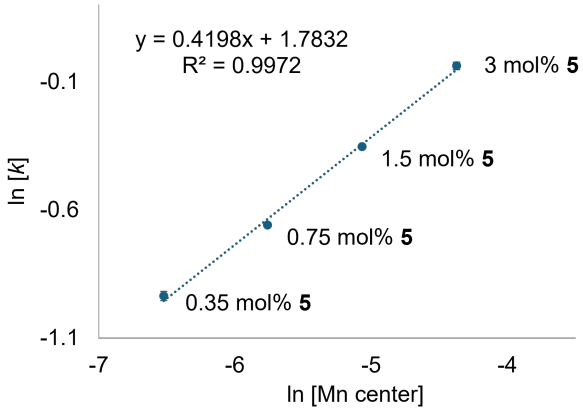

Figure S59. Determination of initial rates of DHA conversion (n = 3) employing varying concentration of **5**. Order was determined according to concentration of [Mn] catalyst center. Partial order determination in [Mn] catalyst center was consistent with slow initial dissociation of off-cycle trinuclear μ-oxo (**5**) to form on-cycle catalyst.

VI. XPS Data

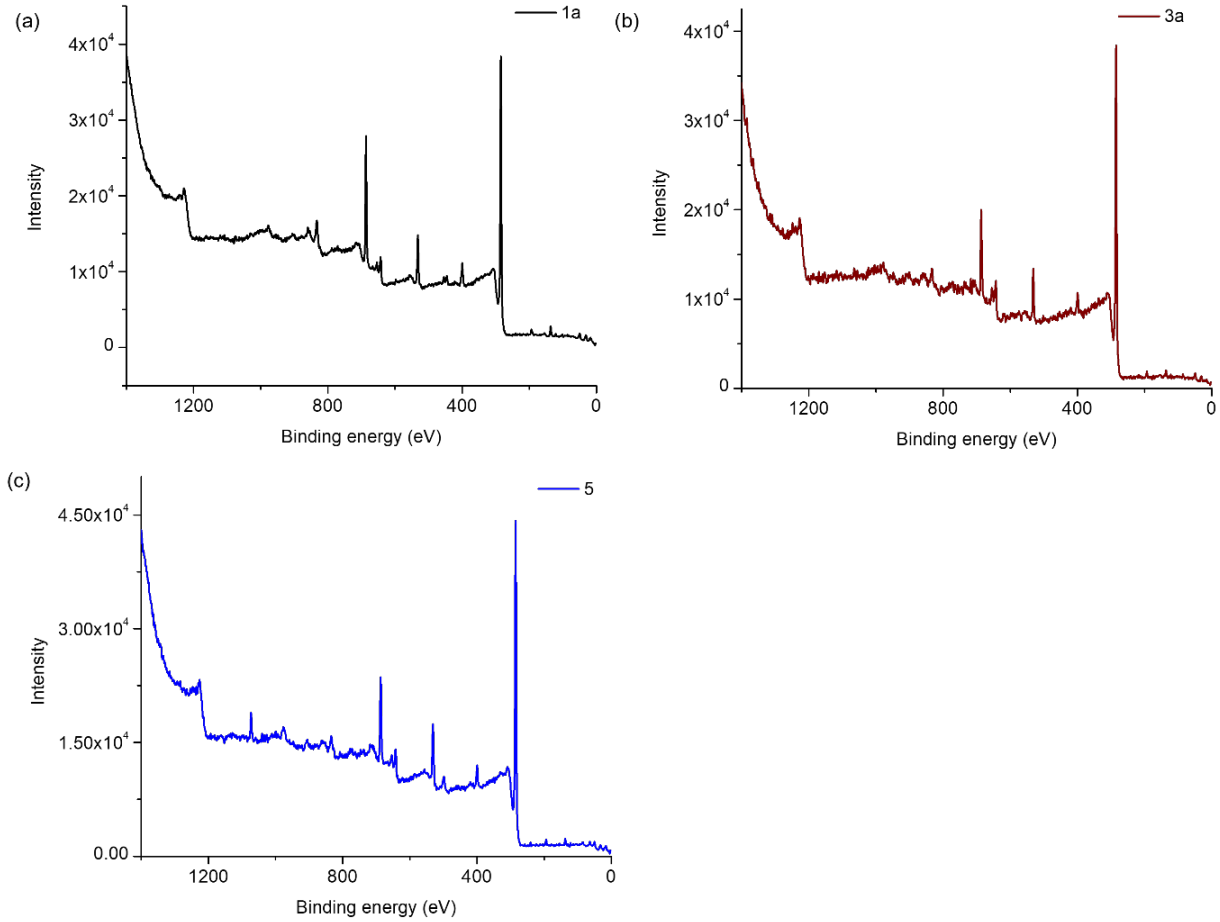

Figure S60. Full range XPS spectra for manganese complexes **1a** (a), **3a** (b), and **5** (c).

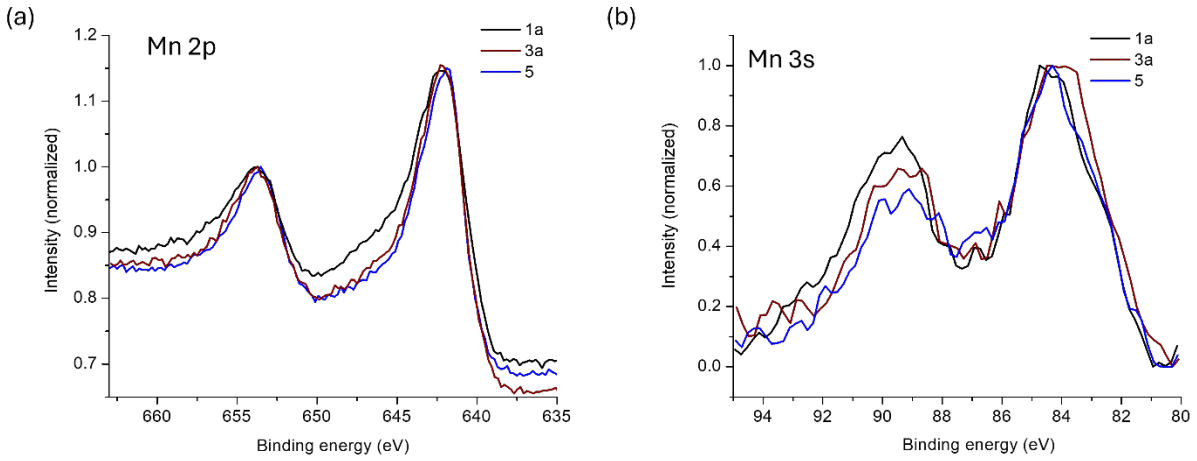

Figure S61. XPS spectra showing ionization potentials of core manganese electrons: (a) 2p spectral region, showing diagnostic 3/2 2p signature (b) 3s spectrum showing 3s electronic splitting for the manganese metal complexes **1a** (black), **3a** (brown), and **5** (blue).

Concentration in atomic %

1a

Survey spectrum

C1s	N1s	O1s	F1s	P2p	Mn2p3
75.2	**5.0**	**6.1**	**11.0**	**1.5**	**1.2**

Si trace

Binding energy $Mn2p_{3/2}$ ~ 642.1 eV

Mn3s doublet separation ΔE ~ 5.5 eV

3a

Survey spectrum

C1s	N1s	O1s	F1s	P2p	Mn2p3
81.0	**3.7**	**5.7**	**7.1**	**1.0**	**1.6**

Binding energy $Mn2p_{3/2}$ ~ 642.1 eV

Mn3s doublet separation ΔE ~ 5.3 eV

5

Survey spectrum

C1s	N1s	O1s	F1s	Na1s	P2p	Mn2p3
77.8	**4.0**	**7.0**	**7.4**	**1.9**	**0.9**	**1.0**

Binding energy $Mn2p_{3/2}$ ~ 641.8 eV

Mn3s doublet separation ΔE ~ 5.0 eV

Table S7. Mn3s multiplet splitting[13,14]

Standard/Compound	Mn3s doublet separation (eV)	Assignment
MnO	5.7(±0.01 eV)	Mn(II)
Mn_2O_3	5.3(±0.05 eV)	Mn(III)
MnO_2	4.5(±0.02 eV)	Mn(IV)
$LiMn_2O_4$	5.0 (±0.1 eV)	50% Mn(IV)/50% Mn(III)
1a	5.5	Mn(III)
3a	5.3	Mn(III)
5	5.0	Mn(IV)/Mn(III)

VII. Supplemental X-Ray Crystallographic Data

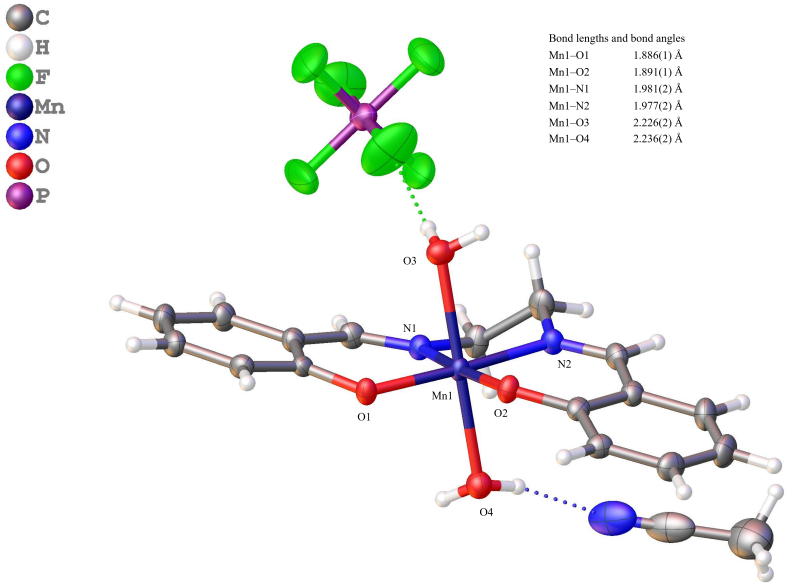

Figure S62. Single crystal X-ray diffraction structure of asymmetric unit of [(*N,N′*-bis(salicylidene)ethylenediamine)Mn(H_2O)$_2$](PF_6) (**1c**).

Table S8: Crystal data and structure refinement for [(*N,N′*-bis(salicylidene)ethylenediamine)Mn(H_2O)$_2$](PF_6) **(1c)**

Identification code	[(*N,N′*-bis(salicylidene)ethylenediamine)Mn(H_2O)$_2$](PF_6)
Empirical formula	$C_{18}H_{21}F_6MnN_3O_4P$
Formula weight	543.29
Temperature (K)	150.00
Crystal system	triclinic
Space group	*P*-1
a (Å)	6.9874(3)
b (Å)	12.2254(6)
c (Å)	13.3032(6)
α (°)	102.9360(10)
β (°)	94.3530(10)
γ (°)	91.086(2)
Volume (Å^3)	1103.62(9)
Z	2
ρ_{calc} (g cm^{-3})	1.635
μ (mm^{-1})	0.752
F(000)	552.0
Crystal size (mm)	0.24 × 0.04 × 0.02
Radiation	Mo Kα (λ = 0.71073 Å)
2Θ range for data collection (°)	4.094 to 55.19
Index ranges	$-9 \le h \le 8$, $-15 \le k \le 15$, $-16 \le l \le 17$
Reflections collected	17939
Independent reflections	5095 [R_{int} = 0.0382, R_{sigma} = 0.0472]
Data/restraints/parameters	5095/0/301
Goodness-of-fit on F^2	1.012
Final *R* indexes [$I \ge 2\sigma(I)$]	R_1 = 0.0388, wR_2 = 0.0838
Final *R* indexes [all data]	R_1 = 0.0647, wR_2 = 0.0926
Largest diff. peak/hole (e Å^{-3})	1.01/-0.46
CCDC	2483878

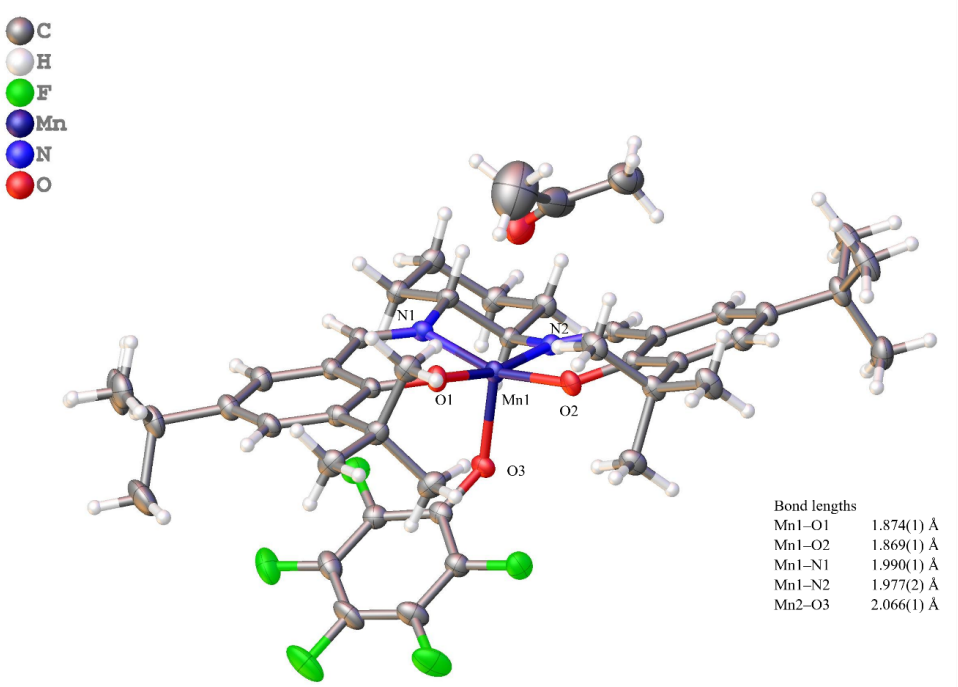

Figure S63. Single crystal X-ray diffraction structure of asymmetric unit of (salen)Mn(OC_6F_5) (**2**). The electron density corresponding to one H_2O molecules per formula unit was removed by solvent mask since it could not be modelled reliably.

Table S9: Crystal data and structure refinement for (salen)Mn(OC_6F_5) (**2**).

Identification code	(salen)Mn(OC_6F_5)
Empirical formula	$C_{45}H_{60}F_5MnN_2O_5$
Moiety formula	$C_{42}H_{52}F_5MnN_2O_3$, C_3H_6O, 1(H_2O)
Formula weight	858.89
Temperature (K)	100.00
Crystal system	triclinic
Space group	*P*-1
a (Å)	11.7342(3)
b (Å)	14.6513(4)
c (Å)	15.2022(4)
α (°)	64.452(2)
β (°)	75.527(2)
γ (°)	87.510(2)
Volume (Å^3)	2277.01(11)
Z	2
ρ_{calc} (g cm^{-3})	1.253
μ (mm^{-1})	2.902
F(000)	908.0
Crystal size (mm)	0.2 × 0.1 × 0.05
Radiation	CuK*α* (λ = 1.54178)
2*Θ* range for data collection (°)	7.11 to 136.622
Index ranges	$-12 \le h \le 14$, $-17 \le k \le 17$, $-18 \le l \le 18$
Reflections collected	23108
Independent reflections	8240 [R_{int} = 0.0470, R_{sigma} = 0.0495]
Data/restraints/parameters	8240/20/528
Goodness-of-fit on F^2	1.041
Final *R* indexes [$I \ge 2\sigma(I)$]	R_1 = 0.0440, wR_2 = 0.1141
Final *R* indexes [all data]	R_1 = 0.0535, wR_2 = 0.1204
Largest diff. peak/hole (e Å^{-3})	0.44/-0.69
CCDC	2483882

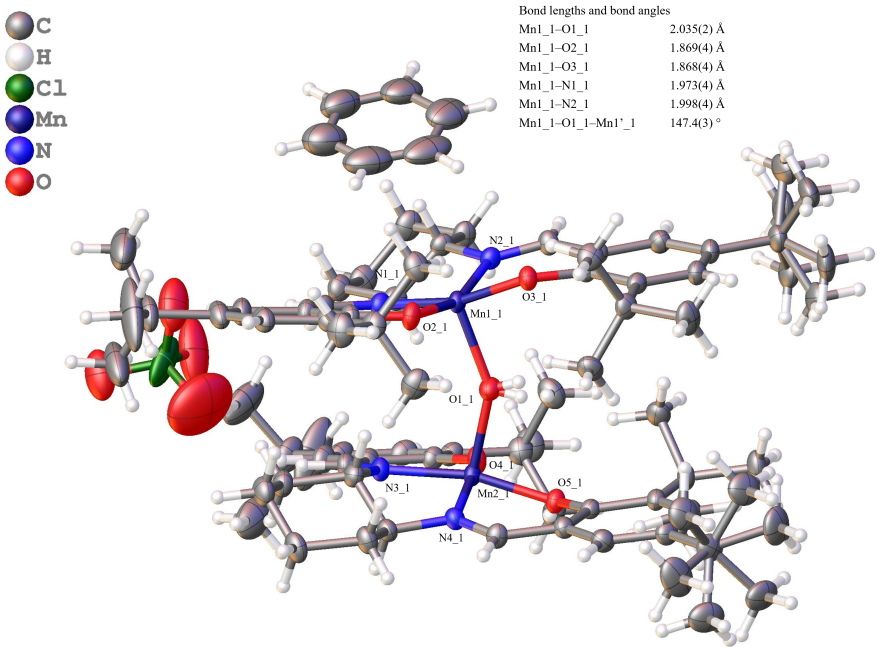

Figure S64. Single crystal X-ray diffraction structure of one molecular unit of [(salen)Mn–μ-OH–(salen)Mn](ClO$_4$) (**3a**-ClO$_4$). Several constraints and restraints (SIMU, RIGU, SADI, DFIX, ISOR) were applied during structure refinements.

Table S10. Crystal data and structure refinement for **[**(salen)Mn–μ-OH–(salen)Mn](ClO$_4$) (**3a**-ClO$_4$)

Identification code	**[(salen)Mn–μ-OH–(salen)Mn](ClO$_4$)**
Empirical formula	$C_{84}H_{118}ClMn_2N_4O_9$
Formula weight	1473.15
Temperature (K)	100.00
Crystal system	orthorhombic
Space group	$C222_1$
a (Å)	18.8329(2)
b (Å)	30.9457(4)
c (Å)	14.1235(2)
α (°)	90
β (°)	90
γ (°)	90
Volume (Å^3)	8231.14(18)
Z	4
ρ_{calc} (g cm^{-3})	1.189
μ (mm^{-1})	3.231
F(000)	3156.0
Crystal size (mm)	0.1 × 0.05 × 0.02
Radiation	Cu Kα (λ = 1.54178 Å)
2Θ range for data collection (°)	5.494 to 136.59
Index ranges	$-22 \le h \le 22$, $-37 \le k \le 36$, $-13 \le l \le 16$
Reflections collected	33393
Independent reflections	7492 [R_{int} = 0.0337, R_{sigma} = 0.0375]
Data/restraints/parameters	7492/625/522
Goodness-of-fit on F^2	1.031
Final R indexes [$I \ge 2\sigma$ (I)]	R_1 = 0.0599, wR_2 = 0.1600
Final R indexes [all data]	R_1 = 0.0621, wR_2 = 0.1617
Largest diff. peak/hole (e Å^{-3})	1.24/-0.31
Flack parameter	0.2940(13)
CCDC	2483881

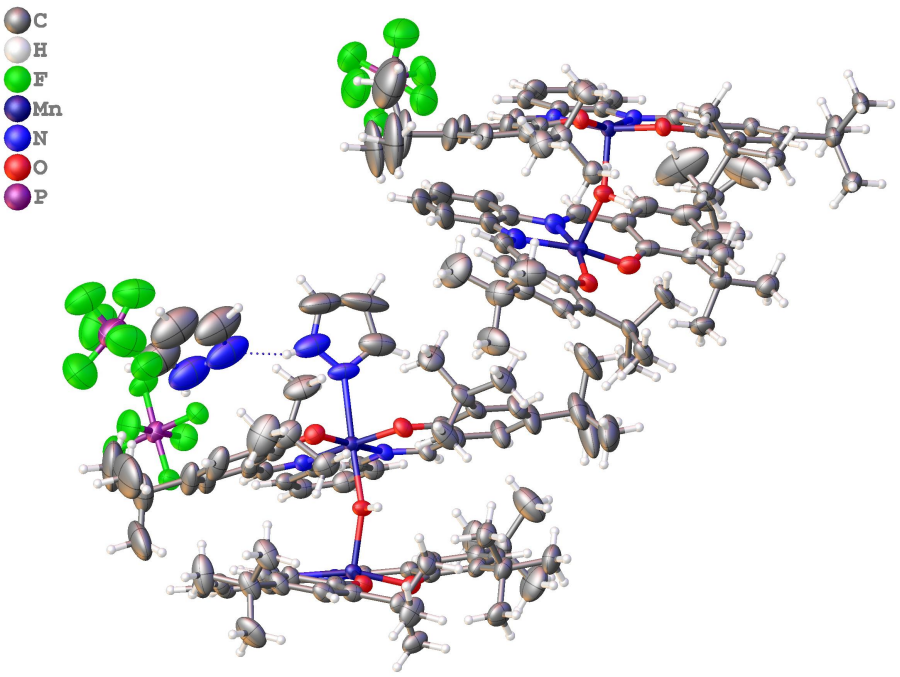

Figure S65. Single crystal X-ray diffraction structure of asymmetric unit of [(salophen)Mn–μ-OH–(salophen)Mn](PF_6) (**3b**). One PF_6 counteranion is disordered over two positions in the asymmetric unit with 50% occupancies. Several constraints and restraints (SIMU, RIGU, SADI, DFIX, ISOR) were applied during structure refinements. The electron density corresponding to two CH_3CN solvent molecules and one H_2O molecules per formula unit was removed by solvent mask since they could not be modelled reliably.

Table S11: Crystal data and structure refinement for [(salophen)Mn–μ-OH–(salophen)Mn](PF_6) (**3b**)

Identification code	**[(salophen)Mn–μ-OH–(salophen)Mn](PF_6)**
Empirical formula	$C_{154}H_{202}F_{12}Mn_4N_{14}O_{11}P_2$
Moiety formula	$C_{75}H_{97}Mn_2N_6O_5$, $C_{72}H_{93}Mn_2N_4O_5$, 2(F_6 P), $C_3H_4N_2$, 1(CH_3CN), 1(CH_3CN), 1(H_2O)
Formula weight	2934.98
Temperature (K)	100.00
Crystal system	triclinic
Space group	*P*-1
a (Å)	17.5632(4)
b (Å)	21.6143(4)
c (Å)	23.7547(5)
α (°)	105.2620(10)
β (°)	95.1030(10)
γ (°)	113.6180(10)
Volume (Å^3)	7775.7(3)
Z	2
ρ_{calc} (g cm^{-3})	1.254
μ (mm^{-1})	3.392
F(000)	3100.0
Crystal size (mm)	0.5 × 0.12 × 0.09
Radiation	Cu Kα (λ = 1.54178 Å)
2Θ range for data collection (°)	7.084 to 136.622
Index ranges	$-18 \le h \le 21$, $-26 \le k \le 26$, $-28 \le l \le 28$
Reflections collected	149365
Independent reflections	28362 [R_{int} = 0.0615, R_{sigma} = 0.0564]
Data/restraints/parameters	28362/412/1831
Goodness-of-fit on F^2	1.047
Final *R* indexes [$I \ge 2\sigma$ (*I*)]	R_1 = 0.0759, wR_2 = 0.2048
Final *R* indexes [all data]	R_1 = 0.1010, wR_2 = 0.2188
Largest diff. peak/hole (e Å^{-3})	1.34/-0.79
CCDC	2483879

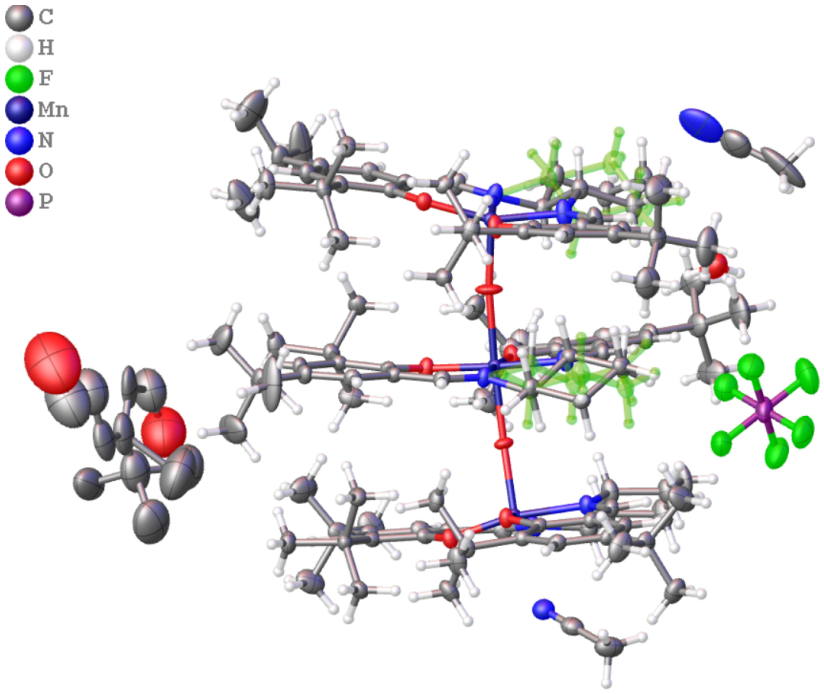

Figure S66. Single crystal X-ray diffraction structure of asymmetric unit of [(salen)Mn–μ-O–(salen)Mn–μ-O–(salen)Mn](PF_6) (**5**) The cyclohexyl moiety of two salen ligands are disordered over two conformations with 50% occupancies. The asymmetric unit contains one molecular unit 2,4-di-tert-butyl salicaldehyde, which is disordered over the inversion centre and hydrogen atoms of the 2,4-di-tert-butyl salicaldehyde molecule could not be added reliably with proper occupancies due to disordered structure. Several constraints and restraints (SIMU, RIGU, SADI, DFIX, ISOR) were applied during structure refinements. One acetonitrile molecule is also disordered over the inversion centre with 50% occupancies.

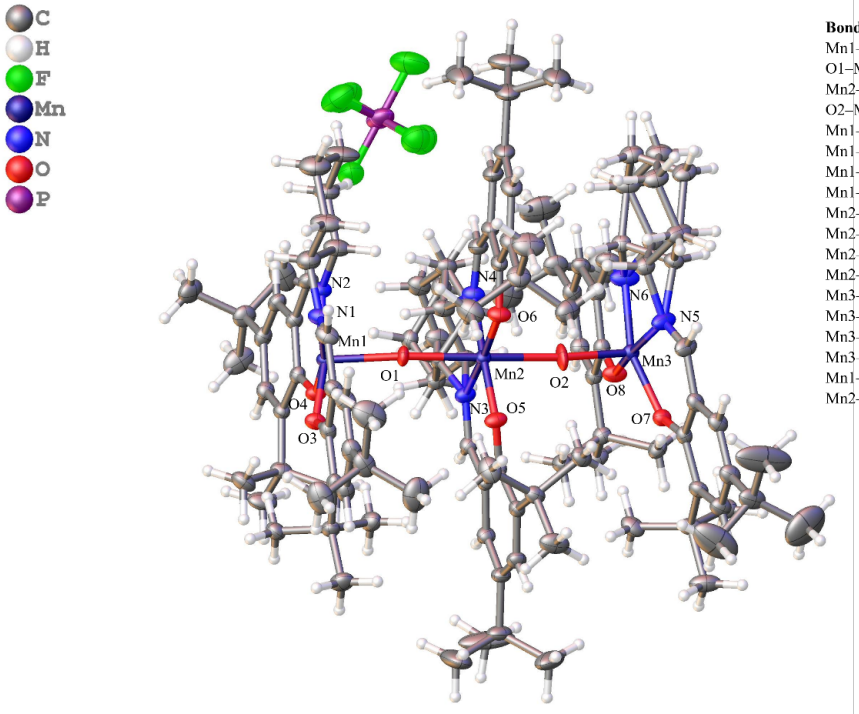

Bond lengths and bond angles

Mn1–O1	1.998(2) Å
O1–M2	2.102(2) Å
Mn2–O2	2.118(2) Å
O2–M3	1.948(2) Å
Mn1–O3	1.870(2) Å
Mn1–O4	1.879(2) Å
Mn1–N1	1.979(3) Å
Mn1–N2	1.986(3) Å
Mn2–O5	1.876(2) Å
Mn2–O6	1.892(2) Å
Mn2–N3	1.986(3) Å
Mn2–N4	1.994(3) Å
Mn3–O7	1.882(2) Å
Mn3–O8	1.866(2) Å
Mn3–N5	1.972(3) Å
Mn3–N6	1.979(3) Å
Mn1–O1–M2	166.19(1) °
Mn2–O2–M3	172.48(1) °

Figure S67. Single crystal X-ray diffraction structure of the molecular unit of [(salen)Mn–μ-O–(salen)Mn–μ-O–(salen)Mn](PF_6) (**5**).

Table S12: Crystal data and structure refinement for [(salen)Mn–μ-O–(salen)Mn–μ-O–(salen)Mn](PF$_6$) (**5**).

Identification code	**[(salen)Mn–μ-O–(salen)Mn–μ-O–(salen)Mn](PF$_6$)**
Empirical formula	$C_{122}H_{161.5}F_6Mn_3N_{7.5}O_{11}P$
Moiety formula	$C_{108}H_{158}Mn_3N_6O_8$, (H_2O), ($C_{11}O_2$), (F_6P), 1.5(CH_3CN)
Formula weight	2218.87
Temperature (K)	100.00
Crystal system	triclinic
Space group	*P*-1
a (Å)	13.8836(2)
b (Å)	19.2316(3)
c (Å)	23.6564(4)
α (°)	102.8620(10)
β (°)	98.7220(10)
γ (°)	97.8240(10)
Volume (Å^3)	5991.32(17)
Z	2
ρ_{calc} (g cm^{-3})	1.230
μ (mm^{-1})	3.217
F(000)	2356.0
Crystal size (mm)	0.1 × 0.07 × 0.05
Radiation	Cu Kα (λ = 1.54178 Å)
2Θ range for data collection (°)	6.544 to 136.754
Index ranges	$-13 \le h \le 16$, $-23 \le k \le 23$, $-28 \le l \le 28$
Reflections collected	96266
Independent reflections	21872 [R_{int} = 0.0421, R_{sigma} = 0.0308]
Data/restraints/parameters	21872/523/1446
Goodness-of-fit on F^2	1.033
Final *R* indexes [$I \ge 2\sigma(I)$]	R_1 = 0.0651, wR_2 = 0.1876
Final *R* indexes [all data]	R_1 = 0.0727, wR_2 = 0.1953
Largest diff. peak/hole (e Å^{-3})	1.31/-0.98
CCDC	2483880

Table S13. Comparison of select bond lengths (Å) of (salen) and (salen)-related complexes. For complex **5**, identical average bond lengths across M–O_{Aryl}, C–O_{Aryl}, M–N, and C_{Aryl}–C_{Aryl} are consistent with identical electronic structure of phenolates (indicates mixed valence Mn(IV/III/IV) structure).

Compound	M–O_{Aryl}	C–O_{Aryl}	M–N	C_{Aryl}–C_{Aryl}[a]
($Sal^{OMe\bullet}$)$CuSbF_6$,[15] semiquinone ring	1.944(3)	1.251(5)	1.919(4)	1.468(5), 1.354(6), 1.420(5), 1.393(6), 1.369(6), 1.461(5)
($Sal^{OMe\bullet}$)$CuSbF_6$,[15] phenolate ring	1.858(3)	1.313(5)	1.917(4)	1.431(5), 1.384(6), 1.410(5), 1.367(5), 1.421(6), 1.418(5)
(Sal^{OMe})Cu[15]	1.884(2)	1.314(2)	1.922(2)	1.437(3), 1.379(3), 1.400(3), 1.366(3), 1.408(3), 1.486(4)
($dppH_3$)$Mn(OH_2)_2(SbF_6)$[16]	1.867(7)	1.304(13)	1.956(7)	1.439(16), 1.33(2), 1.442(19), 1.399(17), 1.410(14), 1.412(15)
($dppH_3$)Mn(HOMe)[16]	1.870(3)	1.337(5)	1.956(3)	1.421(6), 1.388(6), 1.393(6), 1.373(6), 1.406(5), 1.403(5)
	1.857(3)	1.333(5)	1.963(3)	1.417(5), 1.377(5), 1.399(6), 1.370(5), 1.409(5), 1.397(6)
1a[17]	1.850(3)	1.326(4)	1.959(3)	1.426(5), 1.392(5), 1.410(4), 1.371(6), 1.413(5), 1.405(4)
	1.846(2)	1.328(4)	1.959(4)	1.427(4), 1.387(6), 1.413(6), 1.368(4), 1.419(5), 1.402(5)
3a	1.869(4)	1.330(6)	1.973(4)	1.433(7), 1.383(8), 1.406(9), 1.367(9), 1.415(7), 1.413(7)
	1.868(4)	1.335(6)	1.998(4)	1.425(7), 1.390(7), 1.409(8), 1.380(8), 1.408(7), 1.409(7)
5	1.879(2)	1.317(4)	1.986(3)	1.429(4), 1.389(5), 1.407(5), 1.375(5), 1.408(4), 1.421(4)
	1.870(2)	1.320(4)	1.979(3)	1.422(5), 1.397(5), 1.410(5), 1.368(5), 1.410(5), 1.422(5)
	1.876(2)	1.315(4)	1.986(3)	1.428(4), 1.389(5), 1.405(5), 1.375(5), 1.411(4), 1.418(4)
	1.892(2)	1.314(4)	1.994(3)	1.430(5), 1.386(5), 1.408(6), 1.371(5), 1.414(5), 1.417(5)
	1.866(2)	1.319(4)	1.979(3)	1.424(4), 1.381(5), 1.411(5), 1.365(5), 1.416(4), 1.417(4)
	1.882(2)	1.319(4)	1.972(3)	1.430(4), 1.385(5), 1.414(5), 1.369(5), 1.413(4), 1.414(4)
5 (avg)	1.877	1.317	1.983	1.427, 1.388, 1.409, 1.371, 1.412, 1.418
5 (stddev)	±0.009	±0.002	±0.008	±0.003, ±0.005, ±0.003, ±0.004, ±0.003, ±0.003

[a]C-C bond lengths listed in order (C1–C2, C2–C3, C3–C4, C4–C5, C5–C6, C6–C1):

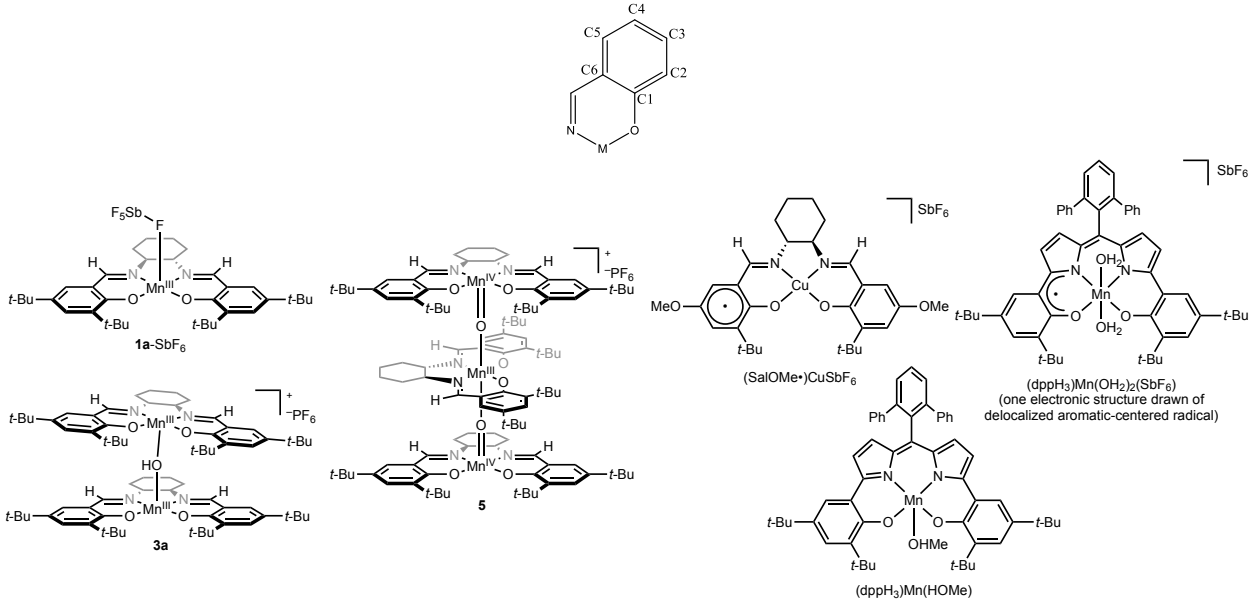

VIII. Supplemental References

1. Souilah, C., Jannuzzi, S. A. V., Becker, F. J., Demirbas, D., Jenisch, D., Ivlev, S., Xie, X., Peredkov, S., Lichtenberg, C., DeBeer, S., Casitas, A. Synthesis of Iron(IV) Alkynylide Complexes and Their Reactivity to Form 1,3-Diynes. *Angew. Chem. Int. Ed.* **2025**, *137*, e202421222.

2. Evans, D. F. The determination of the paramagnetic susceptibility of substances in solution by nuclear magnetic resonance. *J. Chem. Soc.* **1959**, *1959*, 2003–2005.

3. Sheldrick, G. M. Crystal structure refinement with SHELXL. *Acta Cryst. C Struct. Chem.* **2015**, *71*, 3.

4. Sheldrick, G. M. SHELXT - integrated space-group and crystal-structure determination. *Acta Cryst. A Found Adv.* **2015**, *71*, 3.

5. O. V. Dolomanov, L. J. Bourhis, R. J. Gildea, J. A. K. Howard, H. Puschmann. OLEX2: A complete structure solution, refinement and analysis program. *J. Appl. Cryst.* **2009**, *42*, 339.

6. Chilton, N. F.; Anderson, R. P.; Turner, L. D.; Soncini, A.; Murray, K. S. PHI: A powerful new program for the analysis of anisotropic monomeric and exchange-coupled polynuclear *d*- and *f*-block complexes. *J. Comp. Chem.* **2013**, *34*, 1164–1175.

7. Cao, M.; Wang, H.; Ma, Y.; Tung, C.-H.; Liu, L. Site- and Enantioselective Manganese-Catalyzed Benzylic C–H Azidation of Indolines. *J. Am. Chem. Soc.* **2022**, 144, 15383−15390.

8. Boucher, L. J.; Farrell, M. O. Manganese Schiff's Base Complexes—I: Synthesis and spectroscopy of some anion complexes of (4-sec-butylsalicylaldehydeethylenediiminato) manganese(III). *J. Inorg, Nucl. Chem.,* **1973**, *35*, 3731–3738.

9. Liao, S.; List, B. Asymmetric Counteranion-Directed Transition-Metal Catalysis: Enantioselective Epoxidation of Alkenes with Manganese(III) Salen Phosphate Complexes. *Angew. Chem. Int. Ed.* **2010**, *49*, 628–631.

10. Takuya Kurahashi. Reverse Catalase Reaction: Dioxygen Activation via Two-Electron Transfer from Hydroxide to Dioxygen Mediated by a Manganese(III) Salen Complex**.** *Inorganic Chemistry* **2015**, *54*, 8356-8366.

11. Takuya Kurahashi, Masahiko Hada, and Hiroshi Fujii. Di-μ-oxo Dimetal Core of Mn^{IV} and Ti^{IV} as a Linker Between Two Chiral Salen Complexes Leading to the Stereoselective Formation of Different *M*- and *P*-Helical Structures. *Inorganic Chemistry* **2014**, *53*, 1070–1079.

12. Srinivasan, K.; Michaud, P.; Kochi, J. K. Epoxidation of olefins with cationic (salen)manganese(III) complexes. The modulation of catalytic activity by substituents. *J. Am. Chem. Soc*. **1986**, *108*, 2309–2320.

13. J. M. Cerrato, M. F. Hochella, W. R. Knocke, A. M. Dietrich, T. F. Cromer, Use of XPS to Identify the Oxidation State of Mn in Solid Surfaces of Filtration Media Oxide Samples from Drinking Water Treatment Plants. *Environ. Sci. Technol.* **2010**, 44, 5881−5886.

14. M. C. Biesinger, B. P. Payne, A. P. Grosvenor, L. W. M. Lau, A. R. Gerson, R. S. C. Smart, Resolving surface chemical states in XPS analysis of first row transition metals, oxides and hydroxides: Cr, Mn, Fe, Co and Ni. *Appl. Surf. Sci.* **2011**, 257, 2717−2730.

15. M. Orio, O. Jarjayes, H. Kanso, C. Philouze, F. Neese and F. Thomas, X-Ray Structures of Copper(II) and Nickel(II) Radical Salen Complexes: The Preference of Galactose Oxidase for Copper(II). *Angew. Chem., Int. Ed.* **2010**, 49, 4989–4992.

16. L. Lecarme, L. Chiang, J. Moutet, N. Leconte, C. Philouze, O. Jarjayes, T. Storr, and F. Thomas Structure of a one-electron oxidized Mn(III)-bis(phenolate)dipyrrin Radical Complex and Oxidation Catalysis Control via Ligand-centered Redox Activity, *Dalton Trans.* **2016**,45, 16325-16334.

17. R. M. Clarke and T. Storr, Tuning Electronic Structure To Control Manganese Nitride Activation, *J. Am. Chem. Soc.* **2016**, *138*, 15299-15302.